RAS-protein activation but not mutation status is an outcome predictor and unifying therapeutic target for high-risk acute lymphoblastic leukemia

David Koschut,[1] Debleena Ray,[1] Zhenhua Li,[2] Emanuela Giarin,[3] Jürgen Groet,[4] Ivan Alić,[1,5] Shirley Kow-Yin Kham,[2] Wee Joo Chng,[6] Hany Ariffin,[7] David M. Weinstock,[8] Allen Eng-Juh Yeoh,[2,6] Giuseppe Basso,[3,9] and Dean Nižetić[1,4#]

[1]Lee Kong Chian School of Medicine, Nanyang Technological University, Singapore

[2]Department of Paediatrics, Yong Loo Lin School of Medicine, National University of Singapore, Singapore

[3]Department of Women's and Children's Health (SDB), Hematology-Oncology Laboratory, University of Padua, Italy

[4]The Blizard Institute, Barts and The London School of Medicine and Dentistry, Queen Mary University of London, United Kingdom

[5]Department of Anatomy, Histology and Embryology, Faculty of Veterinary Medicine, University of Zagreb, Croatia

[6]National University Cancer Institute, Singapore

[7]University of Malaya Medical Centre, University of Malaya, Malaysia

[8]Department of Medical Oncology, Dana-Farber Cancer Institute, Harvard Medical School, USA

[9]Italian Institute for Genomic Medicine, Italy

#Correspondence

Dean Nizetic, Lee Kong Chian School of Medicine (LKCMedicine), Nanyang Technological University (NTU), 11 Mandalay Road, Singapore 308232; Tel. +65-6904 7003; e-mail: d.nizetic@ntu.edu.sg

and

Dean Nizetic, The Blizard Institute, Barts and The London School of Medicine and Dentistry, Queen Mary University of London, 4 Newark St., London E1 2AT; e-mail: d.nizetic@qmul.ac.uk

Abstract

Leukemias are routinely sub-typed for risk/outcome prediction and therapy choice using acquired mutations and chromosomal rearrangements. Down syndrome acute lymphoblastic leukemia (DS-ALL) is characterized by high frequency of *CRLF2*-rearrangements, *JAK2*-mutations, or RAS-pathway mutations. Intriguingly, *JAK2* and *RAS*-mutations are mutually exclusive in leukemic sub-clones, causing dichotomy in therapeutic target choices. We prove in a cell model that elevated CRLF2 in combination with constitutionally active JAK2 is sufficient to activate wtRAS. On primary clinical DS-ALL samples, we show that wtRAS-activation is an obligatory consequence of mutated/hyperphosphorylated JAK2. We further prove that CRLF2-ligand TSLP boosts the direct binding of active PTPN11 to wtRAS, providing the molecular mechanism for the wtRAS activation. Pre-inhibition of RAS or PTPN11, but not of PI3K or JAK-signaling, prevented TSLP-induced RAS-GTP boost. Cytotoxicity assays on primary clinical DS-ALL samples demonstrated that, regardless of mutation status, high-risk leukemic cells could only be killed using RAS-inhibitor or PTPN11-inhibitor, but not PI3K/JAK-inhibitors, suggesting a unified treatment target for up to 80% of DS-ALL. Importantly, protein activities-based principal-component-analysis multivariate clusters analyzed for independent outcome prediction using Cox proportional-hazards model showed that protein-activity (but not mutation-status) was independently predictive of outcome, demanding a paradigm-shift in patient-stratification strategy for precision therapy in high-risk ALL.

Introduction

Acute lymphoblastic leukemia (ALL) is the most common malignancy and cancer-related cause of death at pediatric age(1, 2). Despite a considerable success rate of standard chemotherapy treatments, as many as 10-15% of children with ALL have recurrent disease (relapses)(3, 4). Patients with high-risk (HR) forms of ALL show increased incidence of relapses, poorer prognosis and lower overall 5-year survival rates following relapse(5). Recently, significant progress has been achieved in understanding the mechanistic consequences of individual pathways affected in HR-ALL, and the resulting selection of therapeutic targets leading to clinical trials using pathway-specific drugs, such as JAK/STAT inhibitors (6). Recent detailed studies of the evolution of acquired genomic changes in ALL identified certain sub-types as being particularly HR forms (7, 8). Among these are hypodiploid ALL(9), Philadelphia chromosome-like (Ph-like) type (defined as a type of ALL with the genomic profile similar to that of the Ph+ ALL)(8, 10, 11), ALL with an intrachromosomal amplification of chromosome 21 (iAMP21)(12, 13), and ALL in children with Down syndrome (DS-ALL)(14, 15).

The acquired mutations landscape does not find a unifying profile that distinguishes HR childhood ALL from non-HR childhood ALL, suggesting the need for individualized therapy approach(16) preceded by individual patient sub-type assignment based on the mutational profile analysis. While Ph-like ALL has a high incidence (60%) of genomic rearrangements leading to an increased expression of the receptor to the cytokine TSLP, CRLF2(17), and more than half of these have mutations in JAK and IL7R pathway - including constitutionally activating JAK2 mutations(11, 18, 19), less than 10% of Ph-like ALL also acquire RAS/MAPK pathway mutations. DS-ALL is distinguished by the similarly high presence of both CRLF2-rearrangements (60%) (with JAK2 mutations at 32%), with a higher proportion of RAS-MAPK pathway mutations (36%)(20, 21). Intriguingly, a near complete mutual exclusion between JAK2 and RAS mutations in diagnosis samples, or individual sub-clones of relapse samples of DS-ALL is repeatedly observable(20, 21).

We hypothesized that the reason for this mutual exclusion is that increased CRLF2-levels in combination with JAK2 activation could be sufficient to activate wild-type (wt) RAS protein in the absence of *RAS* mutations.

Materials and Methods

Cell culture and cell viability

Ba/F3 (Cat.#RCB0805), a murine IL-3 dependent pro-B cell line, was obtained from RIKEN BioResource Center (Tsukuba, Japan) and MUTZ-5 (Cat.#ACC490), a human B cell precursor leukemia cell line established at relapse, was obtained from the Leibniz Institute DSMZ (Braunschweig, Germany); authenticated via multiplex PCR of minisatellite markers. Mycoplasma-free cells were routinely passaged (passage range for shown experiments: 15-35) according to the respective cell bank recommendations. Handling of primary patient samples is described in detail in Supplementary material.

Cell count and cell viability (percentage of acridine orange-positive cells not stained by 4',6-diamidino-2-phenylindole (DAPI) were determined in an NC-250 automated cell-analyzer (ChemoMetec, Allerod, DK).

Patient samples

Surplus clinical or archived clinical material for peripheral blood/bone marrow samples of DS-ALL and non-DS ALL patients was collected by the tissue bank of the Italian Association for Paediatric Haematology-Oncology (AIEOP). In accordance with the Declaration of Helsinki, informed written consent was obtained by the tissue bank for all subjects. Samples were processed and stored in the tissue bank at The Blizard Institute, which is licensed for tissue storage and monitored by UK-Human Tissue Authority. Detailed clinical description of studied DS-ALLs and Non-DS B-ALLs is available in Supplementary-Tab.S1. Detailed cytogenetics was available in 12 cases.

MS2003/2010 cohort(22, 23) RNA-seq data was submitted to the European Genome-phenome Archive (Accession# EGAS00001001858).

RAS activity assays

Cells were left uninduced or induced with human TSLP at 37 °C. Whenever indicated, DMSO or inhibitors were added for 3 hrs before TSLP-induction. Cells were lysed on ice at 1000 cells/µL lysis buffer according to the manufacturer's protocol of the active RAS detection kit (Cat.#8821; Cell Signaling Technology). Total protein concentrations of samples were measured using a BCA protein-assay kit (Cat.#23225; ThermoFisher Scientific). 50 µg total protein was loaded per column of the active RAS detection kit for Western blot (WB). In the RAS activation assay kit for ELISA (Cat.#17-497; EMD Millipore), 12 µg total protein was used at 100 ng/µL and the RAS-GTP pull-down was measured using a Synergy H1 plate reader (BioTek, Winooski, US) in luminescent mode.

For methods on proximity ligation assay (PLA), principal-component-analysis (PCA), statistical analysis, as well as lists of antibodies/chemicals, and standard protocols for the sequencing, SDS-PAGE/WB, phospho-protein antibody-microarray, and transduction please see "Supplementary Methods".

Results

CRLF2 and JAK2mut co-expression is sufficient to activate RAS in Ba/F3 cells

We hypothesized that increased CRLF2-level in combination with a mutation in JAK2 pathway genes could be sufficient to activate wtRAS protein in the absence of RAS mutations, as a mechanism to explain the mutual exclusion of JAK2 and RAS/MAPK mutations in DS-ALL. The level of RAS activity is generally assessed using a pull-down assay whereby the (activated) RAS-GTP is captured by virtue of its high affinity to RAS-binding-domain (RBD) of RAF proteins. In order to observe the effects of elevated CRLF2 signaling on the activation of RAS, we stably integrated a human *CRLF2* overexpression construct(24) into the mouse pre-B-cell line Ba/F3. This alteration did not increase the level of pulled-down RAS-GTP (Fig.1A) and neither did the stable overexpression of $hJAK2_{R683G}$(24), the most prevalent specific activating JAK2 mutation in DS-ALL and Ph-like-ALL. However, when both of these alterations were combined, eight fold higher RAS-GTP level was measured, in the absence of cytokines (Fig.1B, post-hoc Bonferroni p-values are listed in Supplementary-Tab.S2). An independent set of Ba/F3 lines, in which *CRLF2* was transduced first, confirms that this increased RAS-activity is not due to variations in CRLF2 overexpression levels within the lines (Supplementary-Fig.S1F). Growth of Ba/F3 cells depends on IL-3 (Supplementary-Fig.S1A), which induces wtJAK2 phosphorylation(25), and interestingly we found that it also activates RAS (Supplementary-Fig.S1B). The cells with combined CRLF2 and $JAK2_{R683G}$ overexpression were the only ones in this series that grew in a cytokine-independent manner (Supplementary-Fig.S1E), as also previously observed(24). This proves that increased CRLF2-expression together with activated JAK2 is sufficient to activate wtRAS, and this coincides with the transition to cytokine-independent growth.

TSLP-inducible RAS activity in absence of RAS mutations is a feature of human CRLF2 rearranged B-ALL

In order to prove the observations from Fig.1 in human ALL cells, we selected a B-ALL cell line that harbors identical changes as our double-transfected model line in Fig.1. The B cell precursor leukemia cell line MUTZ-5 from a relapsed Philadelphia-like B-ALL patient features a *CRLF2*-translocation leading to wt CRLF2 overexpression, as well as the $JAK2_{R683G}$ mutation, and the absence of mutations in any RAS-MAPK pathway genes(26). The absence of *RAS* mutations in the MUTZ-5 cells grown in our cultures was confirmed by performing standard Sanger DNA-sequencing of PCR-amplicons from genomic DNA, encompassing all exons of *KRAS*, *NRAS* and *HRAS* genes (Supplementary-Tab.S3). We detected the presence of activated RAS in these cells by RAF-RBD pull-down of RAS-GTP (Fig.2A), which was tripled upon a 10 min induction with the CRLF2-ligand TSLP. Similar results were reproduced using an ELISA-based RAS-pull-down (Fig.2C). Both immediate upstream (PTPN11) and immediate downstream (MEK1/2, bRAF) components of the RAS/MAPK pathway were also induced by TSLP induction (Fig.2A, Fig.2B). The direct binding of activated RAS and bRAF proteins expressed in these cells (Supplementary-Fig.S2A) was further validated via PLA (Supplementary-Fig.S2B), as was RAS and phospho-PTPN11 interaction in the Ba/F3 model (Supplementary-Fig.S3B). Both KRAS and NRAS, but not HRAS, isoforms showed increased activity after TSLP-induction (Fig.2C). Interestingly, the genes for the same two isoforms (*KRAS* and *NRAS*), but not *HRAS*, acquire mutations in B-ALL(12, 20). Therefore, we conclude that the RAS isoform activity pattern of TSLP-inducibility in wtRAS leukemia cells matches the isoforms that acquire mutations in RAS-mutated leukemia cases. Furthermore, we traced TSLP-signaling throughout cellular pathways in 68 individual protein-phosphorylation sites via an antibody-based phospho-array (Supplementary-Fig.S4C). The phospho-array confirmed the increased phosphorylation observed for denatured proteins in WB for STAT5A, ERK1/2, MEK1, and JAK2 on their respective native epitopes (Supplementary-Fig.S4C) while the most statistically significant results demonstrate

additional TSLP-effects by increasing activating phosphorylations (AKT2, CDKN1A, ELK1) but also by downregulating pathway-inhibiting phosphorylations (cRAF(Ser296), GAB2, MYC, PTPN6) (Fig.2E).

RAS inhibitor can significantly block the growth of human B-ALL Ph-like wtRAS cells

We next examined to what extent the direct RAS activation in wtRAS leukemic cells affects the cell growth and viability. We tracked the cell count and cell viability of MUTZ-5 cells after treatment with pan-wtRAS-inhibitor and in comparison to treatments with other compounds that have been previously reported to induce dose-dependent cytotoxicity in MUTZ-5(27), some of which are currently in clinical trials for Ph-like ALL(6). After 4 days treatment with pan-wtRAS inhibitor the growth and viability of MUTZ-5 cells were significantly reduced (Fig.3A,B), and this was not affected by the presence of TSLP. In comparison, the dual PI3K/mTOR inhibitor also significantly reduced the growth and viability of MUTZ-5 cells, but this inhibitory effect could be partially counteracted by the TSLP-induction (Fig.3A). Both of these compounds, at the concentrations used (tested to achieve high efficacy on the respective main pathway target in WB, Fig.3C), showed a much stronger inhibitory effect on cell growth than the JAK inhibitor (Fig.3A), despite the observation that this concentration of JAK-inhibitor, which blocks almost all STAT5-signaling (Fig.3C, Fig.3E), showed the strongest inhibition of TSLP-induced phosphorylation of MEK1/2, PTPN11, ERK1/2 and rpS6 (Fig.3C, right-hand side blots). However, neither the JAK inhibitor, nor the PI3K/mTOR inhibitor could block the wtRAS activation by TSLP as shown in WB (Fig.3C, left-hand side blots) and ELISA (Fig.3D). For the JAK2 inhibitor this might be explained by its failure to reduce the direct interaction between RAS and PTPN11 in PLA (Supplementary-Fig.S2E). In contrast, the pan-wtRAS-inhibitor significantly blocked the TSLP-induced RAS-activity (Fig.3C, left-hand side blot) and ELISA (Fig.3D). Moreover, the pre-inhibition of RAS-direct interacting proteins (RAF and PTPN11) also reduced TSLP-induced wtRAS boost in human Ph-ALL cells (Fig.3C). Combined, our data suggest that TSLP-activation of RAS in the absence of RAS mutations drives B-ALL cell growth, and represents an independent drug target, in addition to the PI3K/mTOR and JAK/STAT pathway targets.

DS-ALL patients differ in the level of activity and inducibility of RAS, independently of RAS mutations

The MUTZ-5 ALL cells used in the analysis so far share the increased CRLF2 expression and mutated JAK2 with approximately a third of DS-ALL patients(20), which also have no mutations in RAS genes. We therefore analyzed primary cells from presentation samples (at primary diagnosis) of DS-ALL in RAS pull-down WB and ELISA assay measurements (+/- TSLP stimulation). The analyses were performed blinded to the mutation profile of the patient material and distinct DS-ALL patient profiles for RAS-activity and TSLP-inducibility of RAS were observed in WB (Fig.4A) and confirmed by ELISA (Fig.4B). As we see examples of RAS-mutated, wtRAS, or JAK2-mutated DS-ALL in each of the profile types (Fig.4C), with exception of low-RAS and non-inducible type, we can conclude that activity levels and TSLP-inducibility of RAS cannot be predicted on the basis of DNA-sequencing (acquired mutations) patterns.

The most important conclusion of this analysis is that RAS is active/inducible in 14/20 (70%) of primary DS-ALL samples analyzed, 8 of which had no RAS mutations, but 75% of those had either mutated or hyperphosphorylated JAK2 (Fig.4C). This means that either the RAS mutation, or the combination of high CRLF2 and hyperphosphorylated JAK2 (including mutated JAK2) can explain the mechanism for high RAS activity in 12/14 (86%) of DS-ALL with high RAS activity. Importantly, not a single wtRAS case with either mutated or hyperphosphorylated JAK2 was seen that lacked activated RAS protein (Fig.4C), suggesting that RAS activation is an obligatory consequence in wtRAS DS-ALL cases with mutated or hyperphosphorylated JAK2.

RAS activity and its TSLP inducibility correlate with outcome in DS-ALL patients

Data from primary cells analysis from n=20 presentation samples of DS-ALL for the RAS/MAPK, PI3K/mTOR, and JAK/STAT pathway activity profiles using WB (Supplementary-Fig.S5A,

Supplementary-Fig.S5B), as well as ELISA for activated RAS-pull-down (Fig.4C) were integrated with the similar data we obtained using n=7 DS-ALL relapse and n=4 DS-ALL remission samples, as well as n=4 non-DS ALL presentation samples and n=2 non-DS relapse samples. We performed a PCA using all of these integrated data on N=37 samples from n=31 individual patients, in parallel to the same readouts from the MUTZ-5 Ph-like ALL reference cell line, and the PCA result was mapped onto a coordinate system (Fig.5A) using the three principal components (PC1-3, Supplementary-Fig.S6A). Unsupervised *k*-means clustering grouped ALL samples into Clusters 1-4 (Fig.5A). This analysis grouped almost all presentation and remission samples of 9-year event-free survival patients (good outcome) together into Cluster 1 (green symbols). In contrast, out of 15 samples grouped into Cluster 2 (red symbols), 13 samples (87%) were from patients with death or subsequent relapse as outcome. Clusters 3 and 4, further along the PC1-axis, consisted of a small number of exclusively relapse samples. Using an independent mathematical approach, unsupervised hierarchical clustering of the 20 DS-ALL presentation samples (Supplementary-Fig.S6E) grouped 90% of the samples into the same groups as the PCA-mapping. The clustering revealed that presentation samples from Cluster 1 correlated with good outcome for DS-ALL patients while DS-ALL patients grouped into Cluster 2 showed a significantly increased risk of relapse (Fig.5B,C). The PCA-derived protein activity score was independently predictive of outcome (*P*=.041) (Fig.5C) when analyzed by a multivariate Cox regression model together with CRLF2 protein-expression, NCI-risk and JAK2-mutation status (or RAS-mutation status, not shown). Cluster 2 contains a subgroup of DS-ALL presentation samples that clustered closer to the MUTZ-5 sample (Cluster 3). Like MUTZ-5, these patient samples had high CRLF2-expression, high JAK2-phoshorylation, and all featured the pattern of high basal RAS-activity that is TSLP-inducible. An event-free survival analysis that treats these MUTZ-5-like DS-ALL samples as a separate subcluster indicated a lower median survival (Supplementary-Fig.S6D) but a higher number of samples is required to reach statistical significance for such subgrouping.

We restricted the further analysis only to DS-ALL primary presentation samples, and quantitatively compared those that PCA grouped into Cluster 1 (PCA-predicted standard-risk (SR)) to those in

Cluster 2 (PCA-predicted high-risk (HR)), for the basal activities (Fig.5D top row) and TSLP-induced activities (Fig.5D bottom row) of pan-RAS, JAK2, STAT5, MEK1/2, ERK1/2 and rpS6. We observed that basal and TSLP-induced activities of JAK2, ERK1/2 and rpS6 were significantly increased in HR-DS-ALL presentation samples compared to the SR group (within PCA-Cluster 1). For these proteins, correlation between risk and protein-activity/inducibility profile for our DS-ALL cohort, resembles previously reported findings for a different group of HR-ALL, the non-DS Ph-like ALL, grouped by the presence or absence of CRLF2 rearrangements(27). Additionally, (and this has, to our knowledge, never been demonstrated for any ALL before), we also observed a significant increase in basal and TSLP-induced activity of both MEK1/2 and RAS in the HR-DS-ALL group, compared to the SR group. We also looked at protein expression levels and found RAS and rpS6 levels to correlate with the high-risk DS-ALL group (Supplementary-Fig.S7A). This provided the rationale to look for differences in a larger non-DS ALL cohort (see Supplementary Results, Supplementary-Fig.S7B, Supplementary-Fig.S8A, Supplementary-Fig.S8B).

Our data on primary patient material suggest the compulsory activation of RAS whenever elevated CRLF2 is present in combination with either mutated or otherwise activated JAK2. This would eliminate the selective advantage gained by a RAS mutation, explaining the mutual exclusion, however the underlying molecular mechanism remains to be explained. We therefore sought to further characterize the molecular mechanism behind the wtRAS activation in these leukemic cells.

TSLP activates RAS directly and independently of PI3K/mTOR pathway activation

The use of inhibitors on MUTZ-5 cells (Fig.3A) suggested RAS activation to be independent from blocking of PI3K or JAK pathways. TSLP induction in high CRLF2-expressing and JAK2-mutated B-ALL is known to activate STAT5 and PI3K/mTOR pathways(27), and this insight is exploited in innovative new therapeutic approaches that are currently clinically trialed(6). We therefore first confirmed that our experimental system can reproduce these same results in WB (Supplementary-Fig.S4A). In

addition, we designed a quantitative method (PLA) to measure rpS6-phoshporylation in individual cells (Fig.6B). Similar to the TSLP-induction in MUTZ-5 cells, the Ba/F3 CRLF2+JAK2$_{R683G}$ cells also display an increased rpS6-phosphorylation in PLA compared to cells overexpressing only JAK2$_{R683G}$ (Supplementary-Fig.S3A).

Downstream effectors of the activated PI3K/mTOR pathway have been shown in some situations to cross-activate the downstream effectors of RAS-MAPK cascade, and vice versa(28, 29). However, we observed that immediately upon addition of TSLP (0 min timepoint, Fig.6A) the relative levels of activated pan-RAS, KRAS, NRAS, PTPN11, MEK1/2, and ERK1/2 were all higher than at any later timepoint, while in comparison, the activity onset of the PI3K/mTOR downstream target rpS6 was delayed (Fig.6A). This makes it less likely, at least as the initial effect of TSLP, that the activation of MEK1/2 and ERK1/2 in such leukemic cells is caused by the cross-talk from the activated PI3K pathway. As PI3K can also be an effector of RAS(30), we used an alternative biochemical approach (PLA) by which we demonstrated the ability of a chemical inhibitor of RAS (Salisarib) to block the TSLP-induced rpS6-activating phosphorylation (Fig.6B, Fig.6C), at a concentration lower than required to block EIF4EBP1 activity via mTOR-complex destabilization(31). PLA also detected a strong interaction between RAS and the RBD-containing PI3K-subunit p110α in these cells, which could be reduced using Rigosertib, a RAS-GTP mimetic that inhibits RAS by binding to the RBD of RAS-effectors (Supplementary-Fig.S2D).

Our data therefore strongly suggest that direct, wtRAS activation can precede, and to a certain extent promote, the PI3K/mTOR pathway activation in TSLP-induced human ALL cells.

CRLF2-signaling increases direct interaction between active PTPN11 and RAS

While the PTPN11-inhibitor reduced wtRAS activity in MUTZ5- cells (Fig.3C), the connection between PTPN11 and RAS in ALL as well as in CRLF2-signaling is unknown. Active PTPN11 is thought to dephosphorylate RAS to prime it for activation(32), and we found PTPN11 phosphorylation to be increased by induced CRLF2-signaling (Fig.2A). Furthermore, PTPN11 is published to be in complex

with JAK2 upon cytokine-induction in tumor cells(33). In order to confirm that the mechanism of activating RAS in JAK2-mutated B-ALL cells is regulated via PTPN11, we designed a PLA assay that specifically detects the direct interaction between RAS and phosphorylated PTPN11 (Fig.7A,C). Indeed, compared to the signal for two cytosolic proteins not expected to interact (PLA negative control (NC)), a strong PLA signal between RAS and p-PTPN11 was observed and this interaction almost doubled upon TSLP-induction (Fig.7A). Of note, Ba/F3 cells cultured with IL-3, which activated RAS (Supplementary-Fig.S1B) and JAK2-phosohorylation, also featured a higher level of RAS and p-PTPN11 interaction in PLA compared to unstimulated cells (Supplementary-Fig.S3B). PLA assays also detected interactions between SOS1 and GRB2 in these leukemic cells, as well as other direct interactions involved in RAS activation, which also showed response to CRLF2-activation (RAS and SOS1; GRB2 and p-PTPN11) (Supplementary-Fig.S2C). Remarkably, blocking PTPN11-activity via the PTPN11-inhibitor II-B08 reduced both endogenous, and TSLP-induced RAS activity in these cells (Fig.7B). The PTPN11-inhibitor did not reduce the phosphorylation marker on PTPN11 itself (Fig.7B) but disrupted the direct interaction between RAS and p-PTPN11, lowering it to levels below those in uninduced cells (Fig.7C). Furthermore, a cytotoxic assay showed leukemic cell viability to be reduced by the PTPN11-inhibitor, similarly as with the RAS-inhibitor (Fig.7D). Taken together, these results show that the mechanism of wtRAS activation by CRLF2 signaling depends on its direct interaction with catalytically active PTPN11.

Primary DS-ALL patient biopsies from high-risk sub-cohorts have a potent response to RAS-inhibition in vitro as a distinguishing feature

We used primary surplus clinical material in Fig.5 from n=31 patients. Out of these, we had enough primary diagnosis material for 13 patients (before any therapy) to measure the effects of RAS, PI3K, or JAK inhibitors on individual pathway activation status in the presence of TSLP. The efficacy of RAS inhibition on intracellular protein activity (expressed as panRAS activity ratio between inhibitor and vehicle treated samples) for primary presentation samples showed a significant difference (*P*=.021

by Fisher's exact test) between the good outcome (n=7) and poor outcome DS-ALL groups (n=6) (Fig.8A). Also, samples in which RAS can be further activated by TSLP were more sensitive to RAS inhibitor treatment (Supplementary-Fig.S9). For all poor outcome DS-ALL primary presentation samples, inhibitions of individual pathway effector activities via the RAS, PI3K, or JAK inhibitors was visualized as inverted bar graph ranging from 0% (no inhibition) to 100% (complete inhibition) (Fig.8B). As indicated by red *P*-values, PI3K inhibitor significantly inhibited rpS6 phosphorylation, whereas JAK inhibitor significantly inhibited ERK, rpS6, and STAT5 phosphorylation. Notably, these inhibitors did not have any significant effect on RAS activity, reproducing the result obtained for the MUTZ-5 Ph-like ALL cell line (Fig.3A). Only the RAS inhibitor was able to significantly block RAS activation in poor outcome DS-ALLs (Fig.8B), in addition to blocking rpS6 phosphorylation, as likewise shown for the MUTZ-5 cells (Fig.6B and Fig.3B). This suggests that only RAS-inhibitor action is capable of efficiently blocking RAS activation in cells from both Ph-like/non-DS and DS-ALL poor outcome patient samples at the point of first clinical presentation, irrespective of the presence of RAS mutation. In contrast, JAK and PI3K inhibitor treatments alone did not significantly impact RAS activity in these samples (Fig.8B).

In order to better understand the physiological/therapeutic relevance, we measured the effect of RAS-inhibition on cell viability in 6 DS-ALL primary presentation samples (Fig.8C). The competitive RAS-inhibitor Rigosertib was chosen over Salisarib as Rigosertib shows more potential in current clinical trials and still can disrupt both wtRAS and mutant-RAS signaling activity. Remarkably, after 7 days the RAS-inhibitor treatment had significantly reduced the viable cell count (almost halved compared to vehicle-control) in almost all 6 samples, independent of RAS-mutation status (Fig.8C). Only in one patient sample (DS17) the RAS inhibitor needed a combinatorial-treatment (adding JAK-inhibitor) to achieve a similar reduction of viable cells. Cells of this patient treated separately with PTPN11-inhibitor resulted in a significantly reduced viable cell count (Fig.8D).

The JAK-inhibitor alone showed no statistically significant effect in any of the DS-ALL samples, similar to what was observed for MUTZ-5 (Fig.3A). Interestingly, while the PI3K/mTOR-inhibitor and the

RAS-inhibitor both showed effective reduction of viable cells in all 3 samples (DS16, DS20, DS27) that were clustered by PCA as SR (Fig.5), only RAS-inhibition was able to reduce the viable cell count in the samples grouped by the PCA (Fig.5) as HR (DS09, DS17, DS23) (Fig.8C).

These results suggest a paradigm shift in precision-therapy approach, by identifying HR sub-groups that are unlikely to respond to PI3K- or JAK-inhibitors alone and require direct RAS-inhibition. Importantly, the data confirm the notion that wtRAS-inhibitors could provide a uniform treatment for both mutated and activated wtRAS cases (encompassing up to 80% of DS-ALL).

Discussion

Both DS-ALL and Ph-like ALL share CRLF2-rearrangements and various kinase-activating alterations as potential targets for individualized therapy using specific kinase-inhibitors(8, 34). This lead to the use of phosphorylation patterns of individual kinase signaling cascades as informative biomarkers for combinatorial therapy design(6, 16, 35).

In DS-ALL, recent studies of sub-clonal and single-cell evolution of changes in leukemic ALL blasts have identified signaling activators (CRFL2-rearrangements, JAK2 mutations, RAS-MAPK mutations and iAMP21) as frequent events in primary and relapsed leukemic blasts(20, 21, 36). In particular, JAK2 and RAS mutations were found to be both acquired and lost in relapse samples in a mutually exclusive manner(20, 21). This emphasizes the need for individualized combined-therapy approaches that have a better chance of preventing the selection of sub-clones driven by a different signaling. Our data show that elevation in CRLF2 levels combined with JAK2 activation are sufficient to activate wtRAS, and that TSLP has the potential to induce the wtRAS activity, independently of the PI3K/mTOR activity. This has implications on the choice of the combinatorial therapy design. Remarkably, our combined data from exome sequencing(20), and primary ALL cell protein signaling (presented in this study), suggest that up to 65-82% of DS-ALL cases have highly activated RAS, either constitutively, or upon TSLP induction, regardless of their mutation profiles. 12 of 14 cases with high RAS-activity featured either RAS mutations or high CRLF2/JAK2 signaling (including JAK2-mutations). The only two samples featuring high wtRAS activity in absence of high JAK2 phosphorylation levels might activate RAS via a different pathway yet to be uncovered for DS-ALL. A very recent novel patient-derived xenograft models for DS-ALL found *CBL*-mutant (wt*RAS*) cells to have as high ERK1/2-phosphorylation as *KRAS*-mutant cells(37). Interestingly in the same study, the leukemia burden in both wt*RAS*(*JAK2*-mutant) and mutant-*RAS* xenograft models was reduced via MEK-inhibitor, representing a strongly corroborating evidence to some of the conclusions of our study.

Taking RAS activity and inducibility, integrated with other protein activation patterns, we performed a multivariate analysis clustering that identified SR and HR groups for DS-ALL and showed that protein activation pattern is independently predictive of outcome using multivariate Cox regression. Ultimately, patient-specific inhibitor combinations based on analyzed pathway activities should be part of future precision medicine approaches for HR-ALL groups. Ph-like ALL patients are already being studied for the combined effects of PI3K/mTOR and JAK/STAT inhibitor treatment(6). "Supplementary Discussion" contains an expanded discussion on RAS-inhibitor strategies.

Compared to RAS, mutations in *PTPN11* are less prevalent in DS-ALL but mutations in JAK2, RAS, and PTPN11 also appear to be mutually exclusive throughout different types of childhood ALL (20, 22, 38, 39). Our data reveal that reducing RAS activity via inhibition of PTPN11 catalytical action may provide a functional alternative for ALL cells, while blocking the phosphorylation of PTPN11 via JAK inhibitors was not sufficient to prevent RAS activity, and concordantly with our mechanistic insight was also unable to block the direct interaction between PTPN11 and RAS. Our findings suggest that, depending on the patient's protein activity profile, RAS inhibition (upstream, direct, or downstream) should be considered in combination with PI3K/mTOR and/or JAK/STAT inhibitors to further augment clinical treatment. In particular in DS-ALL, RAS/MAPK-inhibition might be applicable to most HR patients, as we show that specifically samples stratified by our PCA analysis as HR seemed resistant to treatment with PI3K/mTOR or JAK inhibitors alone while only RAS-inhibition slashed the viable cell count in half. However, based on our data, the focus should not lie on targeting mutant-RAS alone but also the inhibition of overstimulated wtRAS pathway activity in absence of RAS mutations.

Childhood leukemia in DS is distinguished by a relatively specific pattern of acquired mutation changes, for both AML(40-45) and ALL(20, 21, 46), and the reasons for this are not fully explained. More generally, people with DS have an unusual epidemiological pattern of malignancy: increased incidence and mortality for childhood leukemias of all types, but much decreased childhood and adult solid tumors(47, 48). Functional consequences of an increased dose of some chromosome 21

genes may play important roles(48), and this is discussed in greater detail in "Supplementary Discussion". It will be important to unravel the mechanisms behind the actions of these chromosome 21 genes, as their specific inhibition may be an additional component to consider in combinatorial therapy approaches(37, 49). This is highlighted by very frequent observations of extra copies of chromosome 21 as acquired changes in DS and non-DS ALL, both at diagnosis, and at relapse(20, 50).

In conclusion, our data show that activation of RAS protein is a common feature of up to 80% of DS-ALL, suggesting inhibition of overstimulated RAS pathway activity should be a unifying therapeutic strategy, even in the absence of RAS mutations. Importantly, our data indicate that patient pre-stratification for therapy optimization should assess RAS/MAPK protein activation status.

Acknowledgements

Singapore Ministry of Education Academic Research Funds Tier 2 grants (2015-T2-2-119 and 2015-T2-1-023) to D.N.; AIRC IG 19186 and Fondazione Cariparo 17/07 to G.B.

Competing interests

The authors declare that they have no competing interests.

References

1. Inaba H, Greaves M, Mullighan CG. Acute lymphoblastic leukaemia. Lancet. 2013;381(9881):1943-55.
2. Pui CH, Robison LL, Look AT. Acute lymphoblastic leukaemia. Lancet. 2008;371(9617):1030-43.
3. Nguyen K, Devidas M, Cheng SC, La M, Raetz EA, Carroll WL, et al. Factors influencing survival after relapse from acute lymphoblastic leukemia: a Children's Oncology Group study. Leukemia. 2008;22(12):2142-50.
4. Pui CH, Yang JJ, Hunger SP, Pieters R, Schrappe M, Biondi A, et al. Childhood Acute Lymphoblastic Leukemia: Progress Through Collaboration. J Clin Oncol. 2015;33(27):2938-48.
5. Bhojwani D, Pui CH. Relapsed childhood acute lymphoblastic leukaemia. Lancet Oncol. 2013;14(6):e205-17.
6. Tasian SK, Teachey DT, Li Y, Shen F, Harvey RC, Chen IM, et al. Potent efficacy of combined PI3K/mTOR and JAK or ABL inhibition in murine xenograft models of Ph-like acute lymphoblastic leukemia. Blood. 2017;129(2):177-87.
7. Hunger SP, Mullighan CG. Redefining ALL classification: toward detecting high-risk ALL and implementing precision medicine. Blood. 2015;125(26):3977.
8. Tasian SK, Loh ML, Hunger SP. Philadelphia chromosome–like acute lymphoblastic leukemia. Blood. 2017;130(19):2064-72.
9. Holmfeldt L, Wei L, Diaz-Flores E, Walsh M, Zhang J, Ding L, et al. The genomic landscape of hypodiploid acute lymphoblastic leukemia. Nature genetics. 2013;45(3):242-52.
10. Den Boer ML, van Slegtenhorst M, De Menezes RX, Cheok MH, Buijs-Gladdines JG, Peters ST, et al. A subtype of childhood acute lymphoblastic leukaemia with poor treatment outcome: a genome-wide classification study. Lancet Oncol. 2009;10(2):125-34.
11. Mullighan CG, Su X, Zhang J, Radtke I, Phillips LA, Miller CB, et al. Deletion of IKZF1 and prognosis in acute lymphoblastic leukemia. The New England journal of medicine. 2009;360(5):470-80.
12. Knight T, Irving JAE. Ras/Raf/MEK/ERK Pathway Activation in Childhood Acute Lymphoblastic Leukemia and Its Therapeutic Targeting. Frontiers in Oncology. 2014;4.
13. Ryan SL, Matheson E, Grossmann V, Sinclair P, Bashton M, Schwab C, et al. The role of the RAS pathway in iAMP21-ALL. Leukemia. 2016;30(9):1824-31.
14. Buitenkamp TD, Izraeli S, Zimmermann M, Forestier E, Heerema NA, van den Heuvel-Eibrink MM, et al. Acute lymphoblastic leukemia in children with Down syndrome: a retrospective analysis from the Ponte di Legno study group. Blood. 2014;123(1):70-7.
15. Lee P, Bhansali R, Izraeli S, Hijiya N, Crispino JD. The biology, pathogenesis and clinical aspects of acute lymphoblastic leukemia in children with Down syndrome. Leukemia. 2016;30(9):1816-23.
16. Harrison CJ. Targeting signaling pathways in acute lymphoblastic leukemia: new insights. Hematology / the Education Program of the American Society of Hematology American Society of Hematology Education Program. 2013;2013:118-25.
17. Russell LJ, Capasso M, Vater I, Akasaka T, Bernard OA, Calasanz MJ, et al. Deregulated expression of cytokine receptor gene, CRLF2, is involved in lymphoid transformation in B-cell precursor acute lymphoblastic leukemia. Blood. 2009;114(13):2688-98.
18. Roberts KG, Morin RD, Zhang J, Hirst M, Zhao Y, Su X, et al. Genetic alterations activating kinase and cytokine receptor signaling in high-risk acute lymphoblastic leukemia. Cancer cell. 2012;22(2):153-66.
19. Roberts KG, Mullighan CG. Genomics in acute lymphoblastic leukaemia: insights and treatment implications. Nat Rev Clin Oncol. 2015;12(6):344-57.

20. Nikolaev SI, Garieri M, Santoni F, Falconnet E, Ribaux P, Guipponi M, et al. Frequent cases of RAS-mutated Down syndrome acute lymphoblastic leukaemia lack JAK2 mutations. Nature communications. 2014;5:4654.
21. Schwartzman O, Savino AM, Gombert M, Palmi C, Cario G, Schrappe M, et al. Suppressors and activators of JAK-STAT signaling at diagnosis and relapse of acute lymphoblastic leukemia in Down syndrome. Proc Natl Acad Sci U S A. 2017;114(20):E4030-E9.
22. Yeoh AE, Ariffin H, Chai EL, Kwok CS, Chan YH, Ponnudurai K, et al. Minimal residual disease-guided treatment deintensification for children with acute lymphoblastic leukemia: results from the Malaysia-Singapore acute lymphoblastic leukemia 2003 study. J Clin Oncol. 2012;30(19):2384-92.
23. Yeoh AEJ, Lu Y, Chin WHN, Chiew EKH, Lim EH, Li Z, et al. Intensifying Treatment of Childhood B-Lymphoblastic Leukemia With IKZF1 Deletion Reduces Relapse and Improves Overall Survival: Results of Malaysia-Singapore ALL 2010 Study. J Clin Oncol. 2018;36(26):2726-35.
24. Yoda A, Yoda Y, Chiaretti S, Bar-Natan M, Mani K, Rodig SJ, et al. Functional screening identifies CRLF2 in precursor B-cell acute lymphoblastic leukemia. Proc Natl Acad Sci U S A. 2010;107(1):252-7.
25. Mohi MG, Arai K, Watanabe S. Activation and functional analysis of Janus kinase 2 in BA/F3 cells using the coumermycin/gyrase B system. Molecular biology of the cell. 1998;9(12):3299-308.
26. Barretina J, Caponigro G, Stransky N, Venkatesan K, Margolin AA, Kim S, et al. The Cancer Cell Line Encyclopedia enables predictive modelling of anticancer drug sensitivity. Nature. 2012;483(7391):603-7.
27. Tasian SK, Doral MY, Borowitz MJ, Wood BL, Chen IM, Harvey RC, et al. Aberrant STAT5 and PI3K/mTOR pathway signaling occurs in human CRLF2-rearranged B-precursor acute lymphoblastic leukemia. Blood. 2012;120(4):833-42.
28. Castellano E, Downward J. RAS Interaction with PI3K: More Than Just Another Effector Pathway. Genes Cancer. 2011;2(3):261-74.
29. Mendoza MC, Er EE, Blenis J. The Ras-ERK and PI3K-mTOR Pathways: Cross-talk and Compensation. Trends in biochemical sciences. 2011;36(6):320.
30. Hobbs GA, Der CJ, Rossman KL. RAS isoforms and mutations in cancer at a glance. J Cell Sci. 2016;129(7):1287-92.
31. McMahon LP, Yue W, Santen RJ, Lawrence JC, Jr. Farnesylthiosalicylic acid inhibits mammalian target of rapamycin (mTOR) activity both in cells and in vitro by promoting dissociation of the mTOR-raptor complex. Molecular endocrinology. 2005;19(1):175-83.
32. Bunda S, Burrell K, Heir P, Zeng L, Alamsahebpour A, Kano Y, et al. Inhibition of SHP2-mediated dephosphorylation of Ras suppresses oncogenesis. Nature communications. 2015;6:8859.
33. Schaper F, Gendo C, Eck M, Schmitz J, Grimm C, Anhuf D, et al. Activation of the protein tyrosine phosphatase SHP2 via the interleukin-6 signal transducing receptor protein gp130 requires tyrosine kinase Jak1 and limits acute-phase protein expression. The Biochemical journal. 1998;335 (Pt 3):557-65.
34. Roberts KG. Why and how to treat Ph-like ALL? Best Pract Res Clin Haematol. 2018;31(4):351-6.
35. Roberts KG, Yang YL, Payne-Turner D, Lin W, Files JK, Dickerson K, et al. Oncogenic role and therapeutic targeting of ABL-class and JAK-STAT activating kinase alterations in Ph-like ALL. Blood Adv. 2017;1(20):1657-71.
36. Potter N, Jones L, Blair H, Strehl S, Harrison CJ, Greaves M, et al. Single-cell analysis identifies CRLF2 rearrangements as both early and late events in Down syndrome and non-Down syndrome acute lymphoblastic leukaemia. Leukemia. 2018:1.
37. Laurent AP, Siret A, Ignacimouttou C, Panchal K, Diop M, Jenni S, et al. Constitutive Activation of RAS/MAPK Pathway Cooperates with Trisomy 21 and Is Therapeutically Exploitable in Down Syndrome B-cell Leukemia. Clin Cancer Res. 2020.

528 38. Paulsson K, Horvat A, Strombeck B, Nilsson F, Heldrup J, Behrendtz M, et al. Mutations of
529 FLT3, NRAS, KRAS, and PTPN11 are frequent and possibly mutually exclusive in high hyperdiploid
530 childhood acute lymphoblastic leukemia. Genes Chromosomes Cancer. 2008;47(1):26-33.
531 39. Yamamoto T, Isomura M, Xu Y, Liang J, Yagasaki H, Kamachi Y, et al. PTPN11, RAS and FLT3
532 mutations in childhood acute lymphoblastic leukemia. Leukemia research. 2006;30(9):1085-9.
533 40. De Vita S, Mulligan C, McElwaine S, Dagna-Bricarelli F, Spinelli M, Basso G, et al. Loss-of-
534 function JAK3 mutations in TMD and AMKL of Down syndrome. Br J Haematol. 2007;137(4):337-41.
535 41. Groet J, McElwaine S, Spinelli M, Rinaldi A, Burtscher I, Mulligan C, et al. Acquired mutations
536 in GATA1 in neonates with Down's syndrome with transient myeloid disorder. Lancet.
537 2003;361(9369):1617-20.
538 42. Nikolaev SI, Santoni F, Vannier A, Falconnet E, Giarin E, Basso G, et al. Exome sequencing
539 identifies putative drivers of progression of transient myeloproliferative disorder to AMKL in infants
540 with Down syndrome. Blood. 2013;122(4):554-61.
541 43. Norton A, Fisher C, Liu H, Wen Q, Mundschau G, Fuster JL, et al. Analysis of JAK3, JAK2, and
542 C-MPL mutations in transient myeloproliferative disorder and myeloid leukemia of Down syndrome
543 blasts in children with Down syndrome. Blood. 2007;110(3):1077-9.
544 44. Vyas P, Roberts I. Down myeloid disorders: a paradigm for childhood preleukaemia and
545 leukaemia and insights into normal megakaryopoiesis. Early Hum Dev. 2006;82(12):767-73.
546 45. Wechsler J, Greene M, McDevitt MA, Anastasi J, Karp JE, Le Beau MM, et al. Acquired
547 mutations in GATA1 in the megakaryoblastic leukemia of Down syndrome. Nature genetics.
548 2002;32(1):148-52.
549 46. Bercovich D, Ganmore I, Scott LM, Wainreb G, Birger Y, Elimelech A, et al. Mutations of JAK2
550 in acute lymphoblastic leukaemias associated with Down's syndrome. Lancet. 2008;372(9648):1484-
551 92.
552 47. Hasle H, Friedman JM, Olsen JH, Rasmussen SA. Low risk of solid tumors in persons with
553 Down syndrome. Genetics in medicine : official journal of the American College of Medical Genetics.
554 2016;18(11):1151-7.
555 48. Nizetic D, Groet J. Tumorigenesis in Down's syndrome: big lessons from a small
556 chromosome. Nat Rev Cancer. 2012;12(10):721-32.
557 49. Thompson BJ, Bhansali R, Diebold L, Cook DE, Stolzenburg L, Casagrande AS, et al. DYRK1A
558 controls the transition from proliferation to quiescence during lymphoid development by
559 destabilizing Cyclin D3. J Exp Med. 2015;212(6):953-70.
560 50. Berger R. Acute lymphoblastic leukemia and chromosome 21. Cancer Genet Cytogenet.
561 1997;94(1):8-12.

562

Fig.1) Combination of CRLF2 overexpression and constitutively active JAK2 is sufficient for wt RAS activation. WB analysis of the murine pro B cell line Ba/F3. Cells were stably transfected with human $JAK2_{R683G}$ and/or human CRLF2 (see Supplementary-Fig.S1C and Supplementary-Fig.S1D) and cultured in IL-3-containing medium. All cells were then starved from IL-3 and cells were lysed. Each cell lysate was split up for analysis in RAS-GTP pull-down assay and for total proteins. An SDS-PAGE followed by WB was performed.

(A) Left-hand side blot shows the RAS-GTP (activated RAS) pull-down while the right-hand side blots show whole cell lysates of the same samples. Antibody-targets are labeled on the right side of each image with black arrows marking the respective protein band; the antibody against HA-tag shows the expression of the human JAK2 construct. The experiment was repeated 4 times independently.

(B) Quantification of (A) for active RAS (RAS-GTP) normalized to its level in untransfected cells. Error bars are SD and *P*-values were determined in one-way ANOVA and post-hoc Bonferroni multiple comparison.

Fig.2) Human Ph-like B-ALL (spontaneous CRLF2-rearrangment and JAK2R683G-mutation) cells activate wtRAS and RAS-interacting proteins upon TSLP-induction. MUTZ-5 cells were stimulated with 20 ng/mL hTSLP (maximal effective TSLP-concentration, Supplementary-Fig.S4B) for 10 min before lysis. Each lysate was split up for analysis in RAS-GTP pull-down assay and for WB.

(A) An SDS-PAGE followed by WB was performed. To assess the total protein and phosphorylated protein amounts on the same PVDF-membrane, each membrane part was stripped and reprobed with new antibodies. RAS-GTP pull-down blots are on the left side while the right-hand side blots show whole cell lysates of the same samples. The grey arrow shows the unspecific signal of the GST-RAS binding domain (RBD) used in the active RAS pull-down assay acting as a loading control. The experiment was repeated 5 times independently and the graphs show the quantification for active RAS (RAS-GTP), phospho-MEK1/2, phospho-JAK2, and phosho-PTPN11. Beta-actin and total protein signals were used as a loading control to normalize samples.

(B) A blot separate from (A) demonstrates the TSLP-inducibility of RAS-effector bRAF.

(C) Quantification of 5 independent ELISA experiments in which RAS-GTP in MUTZ-5 cells was measured using a different, ELISA-specific active-RAS pull-down assay.

(D) MUTZ-5 cells were probed for the activation of KRAS-GTP, HRAS-GTP, or NRAS-GTP isoforms (left side). The blots on the right show the total expression of the respective RAS proteins and the graphs show the average signal fold-change for KRAS-GTP, HRAS-GTP and NRAS-GTP (N=4, means ±SD). *P*-values were calculated using Student's T-test and adjusted with a Bonferroni-correction for sequential multiple-comparison.

(E) Whole, non-denatured lysate from uninduced or TSLP-induced MUTZ-5 cells was subjected to an antibody-microarray. The graph shows relevant, most statistically significant changes in protein-phosphorylations, a heatmap-overview for all analyzed protein-phosphorylations can be found in Supplementary-Fig.S4C. (N=6, means±SD). *P*-values were calculated using Student's T-test (Bonferroni-correction for sequential multiple comparison can be found in Supplementary-Tab.S2).

Fig.3) Inhibition of RAS stops wt-RAS sequence Philadelphia-like ALL cell growth in the presence of TSLP. (A) MUTZ-5 cells were seeded at 6.5×10^5/mL density and cultured over 4 days with either 0.5% DMSO (vehicle control), 50 µM Salirasib (indirect Pan-RAS inh.), 10 µM PI-103 (PI3K/mTOR dual inh.), or 5 µM Ruxolitinib (JAK inh.), each in absence or presence of 20 ng/mL human TSLP. Cell count and viability was determined in an NC-250 automated cell counter daily. The stacked-bar graph on the left side shows the growth rate after the 90 hrs timepoint, averaged from 2 independent experiments, each with triplicate wells. Red error bars are SD from the dead cell fraction while the black error bars show the SD of the viable cells. *P*-values were calculated in one-way ANOVA from the total cell growth rate and adjusted in a post-hoc Bonferroni multiple comparison. Only relevant *P*-values are shown in the graph, for a complete list see Supplementary-Tab.S2.

(B) The graph shows the cell viability of the experiment in (A) over time.

(C) MUTZ-5 cells were pre-treated for 2 hrs with either 0.5% DMSO (vehicle control), 10 µM PI-103 (PI3K/mTOR dual inh.), 50 µM Salirasib (indirect pan-RAS inh.), 5 µM Ruxolitinib (JAK inh.), 50 µM Vemurafenib (Pan-Raf inh.), or 25 µM II-B08 (PTPN11 inh.), and then stimulated with 20 ng/mL human TSLP for 10 min followed by cell lysis. Each lysate sample was split up for analysis in RAS-GTP pull-down assay and for total protein signal. RAS-GTP pull-down (left) and lysate samples (right) were loaded on separate gels. An SDS-PAGE followed by WB was performed. To assess the total protein and phosphorylated protein amounts on the same PVDF-membrane, membranes were stripped and reprobed with new antibodies. Antibody-targets are labeled on the right side of each image with black arrows indicating the respective protein band.

(D) MUTZ-5 cells were treated with 50 µM Salirasib (pan-RAS-inhibitor), 10 µM PI-103 (PI3K/mTOR dual inhibitor), or 5 µM Ruxolitinib (JAK-inhibitor) like in (C) after which the RAS-GTP levels were measured in ELISA. N=3 independent experiments, bar graph shows means±SD.

(E) MUTZ-5 cells were treated as in (D) and STAT5 activity was determined via Western blot. N=3 independent experiments, bar graph shows means±SD. *P*-values for (D, E) were calculated in one-way ANOVA and post-hoc Bonferroni multiple comparison.

Fig.4) 70% of primary DS-ALL presentation samples show activated and/or TSLP-inducible RAS, regardless of mutation-status. Primary presentation samples of DS-ALL patients were cultured for 2 days (detailed in Supplementary-Fig.S5A-legend) and then induced for 10 min with 20 ng/mL TSLP (or uninduced) in serum-reduced medium.

(A) Each lysate was split up for RAS-GTP pull-down assay (left blot) and for standard WB (right blot). Grey arrow shows the loading of the GST-RBD in the pull-down assay.

(B) The RAS activity pattern in the patient samples from (A) was confirmed via ELISA measurement of RAS-activity in aliquots that were independently thawed and processed.

(C) Overview of the ELISA-measured RAS activity for the DS-ALL cohort at diagnosis (not enough cell material was available for DS26, DS29, and DS30). The RAS-GTP pull-down ELISA was performed on lysates (100 ng/µL total-protein) from cells at minimum 75% viability. Brackets on top indicate the four RAS activity patterns presented in (A, B). For visualization purposes only in this graph, basal RAS-activity over 0.5 (median of all patient samples) MUTZ-5 basal RAS activity was grouped as high RAS activity while an increase by at least 10% RAS-GTP in TSLP-stimulated samples over uninduced samples in ELISA was classed as TSLP-inducible RAS. For visualization, JAK2-phosphorylation levels measured in WB were categorized as –(negative)=0.00-0.05; +=0.05-0.50; ++=0.50-1.00; +++=1.00-2.00, and CRLF2 protein-levels were categorized as –(negative)=0.00-0.05; +=0.05-0.20; ++=0.20-0.50; +++=0.50-1.50. None of these arbitrary threshold-groupings were used in the clustering analysis (Fig.5). Known CRLF2-rearrangements are marked (R). All values are normalized to those measured for uninduced MUTZ-5 cells processed in parallel to patient cells. Table boxes: Outcome of leukemia (white = good outcome, black = poor outcome), *RAS* mutations (=blue) or *JAK2* mutations (=red) (grey=unsequenced). For patient/sample groups other than DS-ALL-diagnosis (Non-DS (NDS) at presentation, DS complete remission (CR), and DS/NDS at relapse) only averages are shown. For an overview of the WB data and analyzed protein expression/phosphorylation of all individual samples, see Supplementary-Fig.S5.

Fig.5) Sub-stratification of DS-ALL patients based on primary cells: RAS-activation and downstream signaling in relation to standard-therapy outcomes. (A) A PCA was performed on the quantified data of Fig.4 (data was given as continuous variables; no cutoffs nor pre-groupings were used) for the DS-ALL cohort at diagnosis, and (where available) at remission, and relapse, as well as presentation and relapse samples from Non-DS ALL patients. Top view of the PCA-mapping for all 6 analyzed protein-activities (basal and TSLP-induced) as well as CRLF2-protein expression of all samples along the calculated principal components (see also Supplementary-Fig.S6A). *K*-means unsupervised clustering (with *k* set to 4 to achieve minimal class-class deviation, Supplementary-Fig.S6B) grouped samples into clusters 1 to 4 (listed in Supplementary-Fig.S6C).

(B) PCA Clusters 1 and 2 contain all samples of the DS-ALL diagnosis cohort and were analyzed according to their outcome: A Fisher's exact test determined the *P*-value between the number of good and poor outcomes between the two clusters (bar graph).

(C) Kaplan–Meier curves of cluster 1 (SR = standard risk) and cluster 2 (HR = high risk) DS-ALL patients. Table show a Cox proportional-hazards model for protein activity score (PCA-derived principal component from all quantified protein activities at basal and TSLP-induced level) together with CRLF2-protein expression level (for CRLF2+ samples), NCI risk groups (SR: age at diagnosis 1-10 yrs and WBC < 50.000/µL; HR = children age > 10 yrs and/or WBC > 50.000/µL; or unknown), and presence of activating JAK2-mutations. Reverse Kaplan-Meier median follow-up for N=20 DS-ALL was 18.4 years. Patient numbers at risk for each year are given in the table.

(D) The means of all analyzed basal or TSLP-induced protein activities are compared between the SR group (DS-ALL patients in PCA cluster 1) and the HR group (DS-ALL patients in PCA cluster 2). All error bars are SD; *P*-values were calculated using Student's T-test and are adjusted with a Bonferroni-correction for sequential multiple comparison.

Fig.6) Direct wtRAS-activation can precede PI3K/mTOR-pathway activation and resulting PI3K-downstream signaling activity was blocked by RAS inhibitor. (A) Effect of TSLP induction over time. MUTZ-5 cells were incubated with 20 ng/mL human TSLP at 37 °C for the indicated time points (0 min to 18 hrs) before cell lysis. Due to the centrifugation step the TSLP can act for 5 min before lysis at timepoint 0. Each cell lysate was split up for RAS-GTP pull-down assay and WB. RAS-GTP pull-down elutions are on the left side while the right-hand side blots show whole cell lysates of the same samples. Antibody-targets are labeled on the right side of each image with black arrows indicating the respective protein band.

(B) Activation of PI3K/mTOR downstream target rpS6 protein was monitored via PLA in high-throughput microscopy. MUTZ-5 cells were either not induced or induced with 20 ng/mL TSLP for 10 min. Where indicated, cells were pre-treated for 3 hrs with either DMSO (vehicle control), RAS inhibitor, or JAK inhibitor. Cells were fixed and permeabilized in a 96 well plate. After blocking, antibodies against phosphorylated rpS6 and total rpS6 were used in conjunction with PLA rabbit and mouse probes to allow specific readout of rpS6 activation in single cells in a high-throughput manner. Histograms show the distribution for a single experiment of the number of PLA spots in cells with at least 1 PLA spot (assay control is only shown in the bar graph). A minimum of 600 cells were analyzed per sample. Non-linear Gaussian fitting curves were plotted. Fluorescent microscope images show examples of PLA spots in MUTZ-5 cells for the respective treatment; white scale bars are 20 µm long.

(C) The bar graph summarizes the average PLA spot counts of 3 independent experiments. Error bars are SD and *P*-values were determined in one-way ANOVA and post-hoc Bonferroni multiple comparison.

Fig.7) CRLF2-signaling induces direct interaction between activated PTPN11 and RAS, and PTPN11-activity is required for ALL cell growth. (A) Direct interaction between RAS and phosphorylated PTPN11 was monitored via PLA using high-content microscopy. Serum-starved MUTZ-5 cells were induced (or not) with 20 ng/mL TSLP for 10 min. Cells were fixed and permeabilized in a 96 well plate. Antibodies against phosphorylated PTPN11 and pan-RAS were used in conjunction with PLA-probes to allow the amplification and staining of interaction-specific PLA-spots. The negative control (NC) are two cytosolic proteins not expected to interact. Fluorescent-microscopy images show examples of PLA-spots (scale bars = 20 µm). At least 250 cells per well were analyzed using Operetta-CLS automated high-content microscopy platform. The bar-graph shows the averages of 3 independent experiments (each performed in triplicates). Error bars are SD and *P*-values were determined in one-way ANOVA and post-hoc Bonferroni multiple comparison.

(B) MUTZ-5 cells were pre-incubated with DMSO or 25 µM II-B08 (PTPN11 inhibitor) for 2 hrs and then stimulated or not with 20 ng/mL TSLP for 10 min before cell lysis. Each cell lysate was split up for RAS-GTP pull-down assay and for WB (whole-cell lysates).

(C) MUTZ-5 cells were treated as in (B) before fixation. A PLA described in (A) was performed.

(D) MUTZ-5 cells were seeded at 1.6×10^5/mL density and cultured for 7 days with either 0.5% DMSO (vehicle control), 50 µM Salirasib (indirect pan-RAS inhibitor), 25 µM II-B08, 50 µM Vemurafenib (pan-Raf inhibitor), 1 µM PD0325901 (MEK1/2-inhibitor), or 5 µM Ruxolitinib (JAK-inhibitor), in presence of 20 ng/mL TSLP. Percentage of viable cells was determined in an NC-250 automated cell counter.

Fig.8) RAS-inhibitor blocks RAS-activity with greater efficiency in primary, poor outcome DS-ALL patient samples, prior to relapse.

(A) Efficacy of RAS-inhibitor on ELISA-measured RAS-activity in DS-ALL, compared by outcome. Primary presentation DS-ALL samples were cultured for 2 days (detailed in Supplementary-Fig.S5A-legend). Samples with sufficient cell count were treated with 0.5% DMSO (vehicle-control), or 50 µM Salirasib (indirect pan-RAS-inhibitor) for 3 hrs, and then induced for 10 min with 20 ng/mL TSLP in serum-reduced medium. Cells were lysed for RAS-GTP pull-down assay and whole-lysate WB (Supplementary-Fig.S5A). Protein-activities of inhibitor-treated TSLP-induced samples were normalized to the activity-level of the respective vehicle-treated TSLP-induced samples. If inhibitor-treatment reduced the RAS-activity by over 10% compared to vehicle-control (dashed-line), the sample was tallied as successful RAS-blocking. A Fisher's exact test was performed between the groups. Good outcome: N=7 (3 *RAS*-mutations, 1 *JAK2*-mutation); poor outcome: N=6 (1 *JAK2*-mutation).

(B) Waterfall-plot shows the mean efficacies of 50 µM Salirasib, 10 µM PI-103 (PI3K/mTOR dual-inhibitor), or 5 µM Ruxolitinib (JAK-inhibitor) on pathway components (0%=no effect, 100%=full block of TSLP-induced protein-activation); tested on primary presentation samples from poor outcome DS-ALL patients in (A). Error bars are SD; black *P*-values were determined in one-way ANOVA with post-hoc Bonferroni multiple-comparison. The red *P*-values (Bonferroni-corrected for sequential multiple-comparison) indicate if each inhibitor on average significantly reduced the respective protein-activity in these samples (only $P < 0.05$ shown; Supplementary-Tab.S2 lists all *P*-values).

(C) Cell-toxicity effect of inhibitors in DS-ALL. Samples from 6 patients were cultured for 2 days like in (A) before seeding 8×10^5 viable cells/mL in IMDM-complete medium (without IL-3/IL-7 but containing 20 ng/mL TSLP) together with 0.5% DMSO, 30 µM Rigosertib (non-ATP competitive RAS-GTP inhibitor), 10 µM PI-103, 5 µM Ruxolitinib, or Rigosertib&Ruxolitinib (DS23 cell count was insufficient). After 7 days, cell count and viability were measured (N=3, means±SD); vehicle-control

cell numbers reduced to 1-4×10^5/mL, 70-90% viability. *P*-values were determined in one-way ANOVA with post-hoc Dunnett's multiple-comparison (all treatments compared to DMSO-control).

E) 8×10^5 viable cells/mL of patient-DS17 were handled like in (C) and treated with 0.5% DMSO, or 25 µM II-B08. After 7 days, cell count and viability were measured (N=3, means±SD); average vehicle-control viability: 74% (II-B08: 66%).

Fig.1

A)

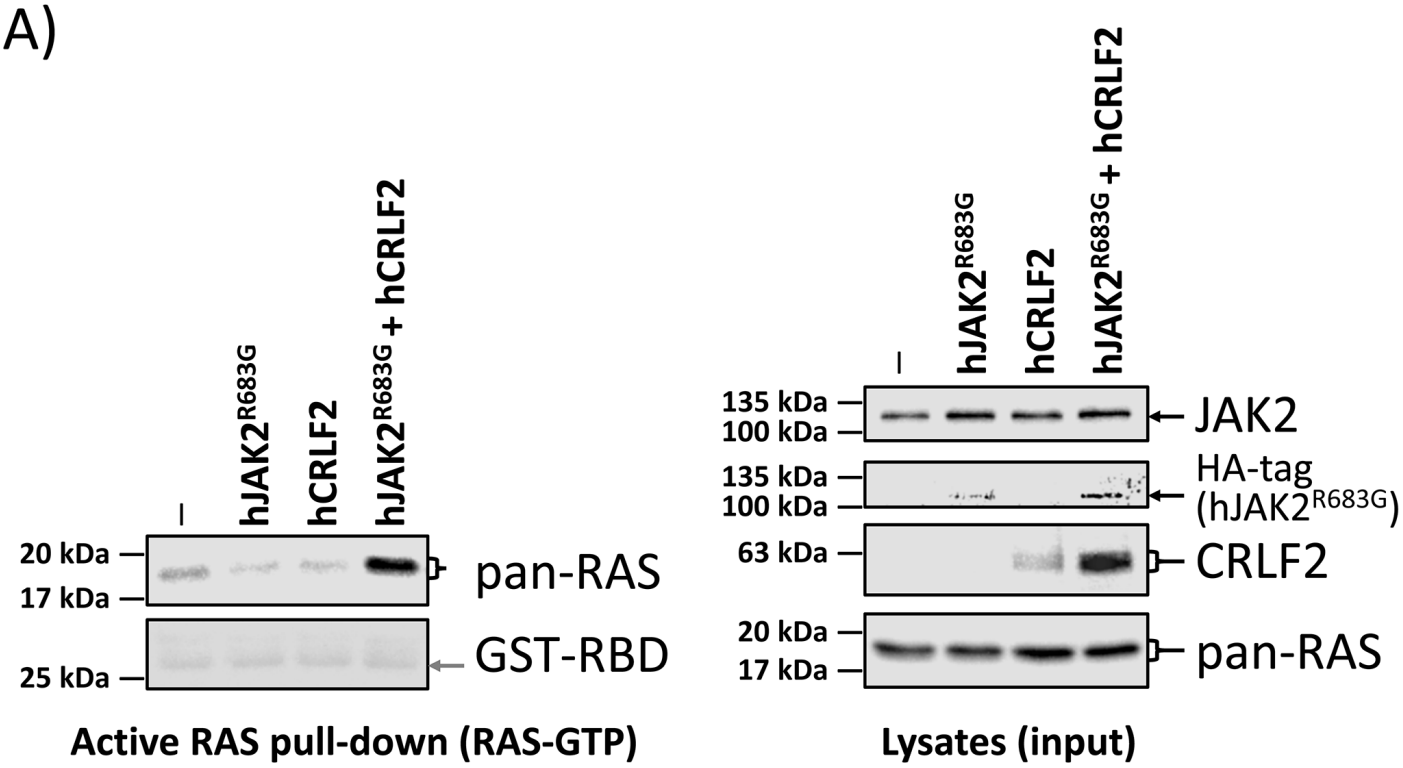
–
hJAK2R683G
hCRLF2
hJAK2R683G + hCRLF2
20 kDa
17 kDa
pan-RAS
25 kDa
GST-RBD
Active RAS pull-down (RAS-GTP)
135 kDa
100 kDa
JAK2
HA-tag
(hJAK2R683G)
63 kDa
CRLF2
pan-RAS
Lysates (input)

B)

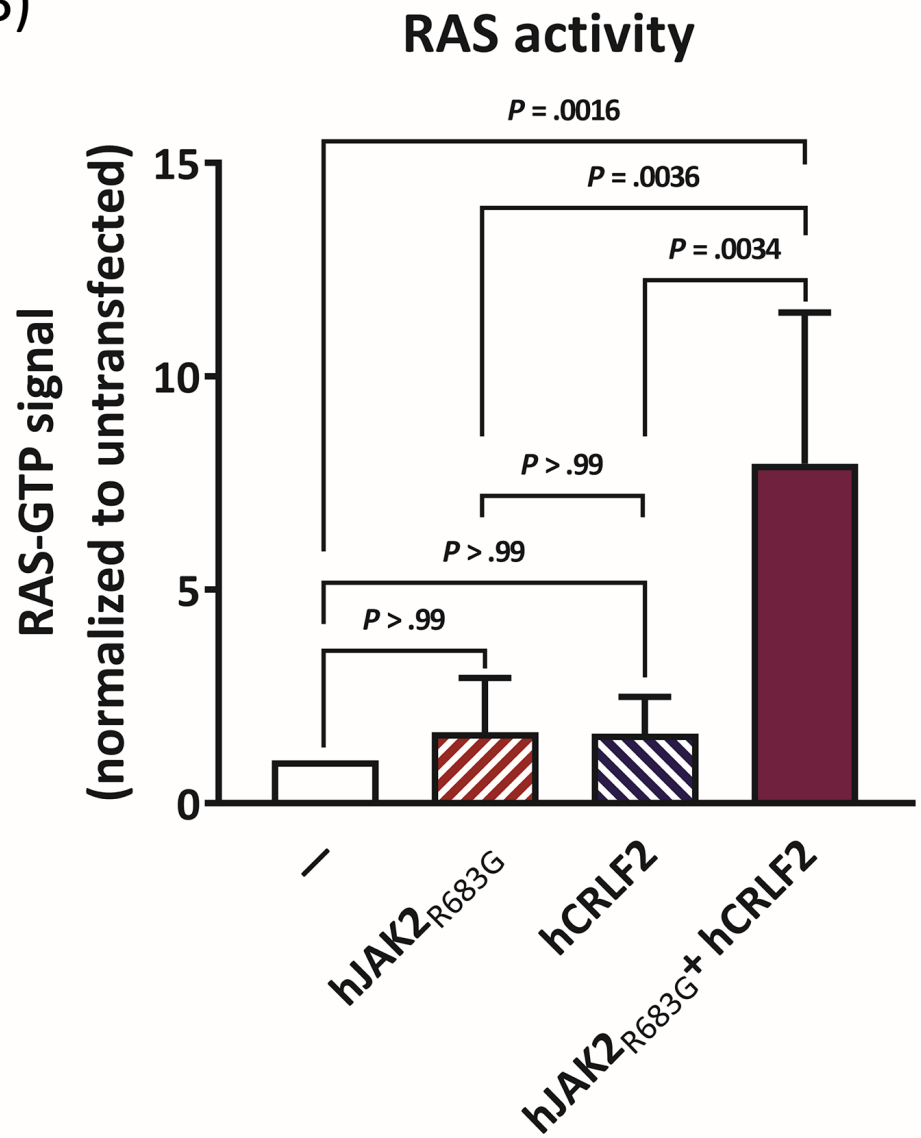
RAS activity
RAS-GTP signal
(normalized to untransfected)
15
10
5
0
P = .0016
P = .0036
P = .0034
P > .99
P > .99
P > .99
–
hJAK2R683G
hCRLF2
hJAK2R683G + hCRLF2

Fig.2

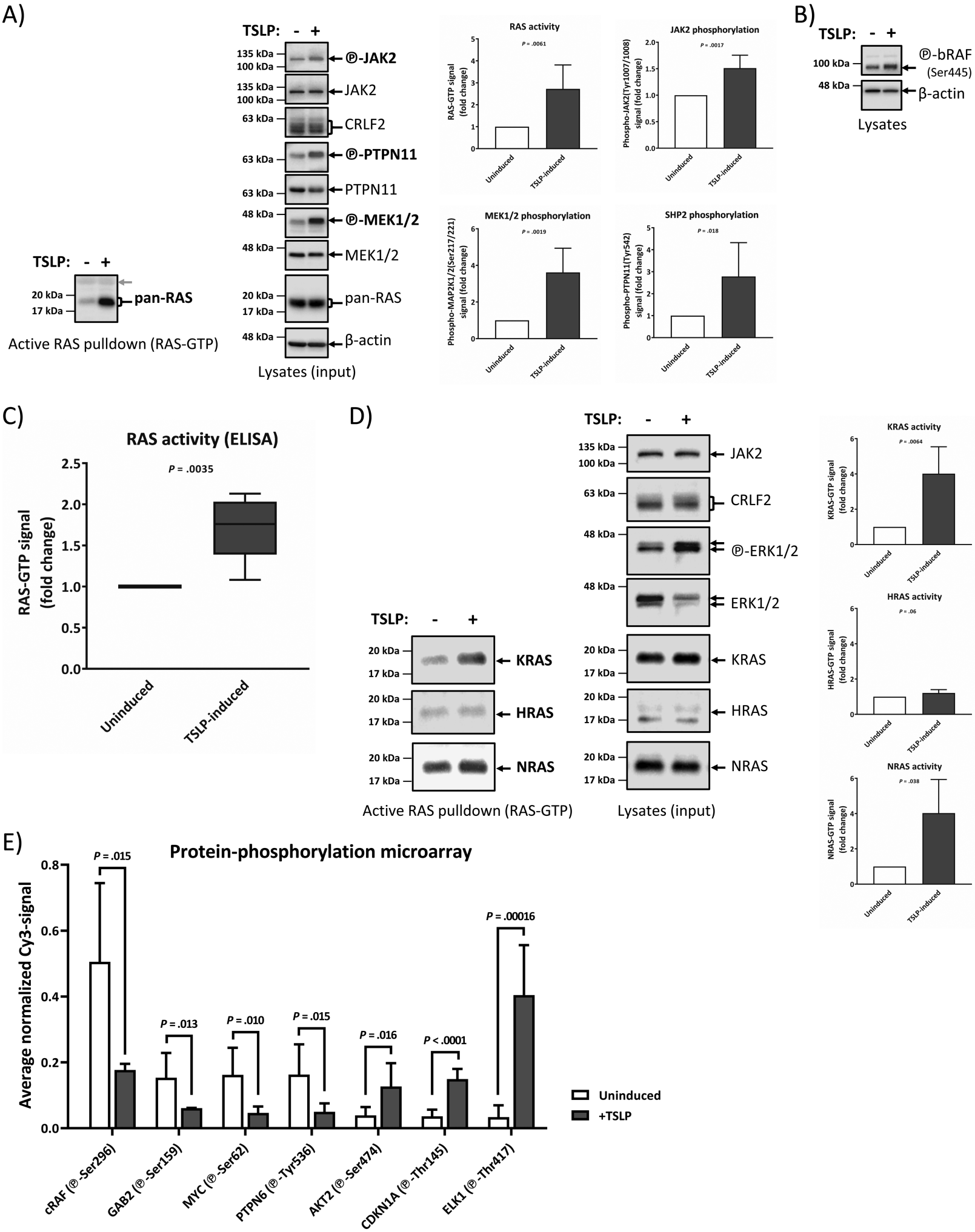
A)
TSLP: - +
135 kDa
100 kDa
Ⓟ-JAK2
JAK2
63 kDa
CRLF2
Ⓟ-PTPN11
PTPN11
48 kDa
Ⓟ-MEK1/2
MEK1/2
20 kDa
17 kDa
pan-RAS
β-actin
Lysates (input)
TSLP: - +
20 kDa
17 kDa
pan-RAS
Active RAS pulldown (RAS-GTP)
RAS activity
P = .0061
RAS-GTP signal (fold change)
JAK2 phosphorylation
P = .0017
Phospho-JAK2(Tyr1007/1008) signal (fold change)
MEK1/2 phosphorylation
P = .0019
Phospho-MAP2K1/2(Ser217/221) signal (fold change)
SHP2 phosphorylation
P = .018
Phospho-PTPN11(Tyr542) signal (fold change)
Uninduced
TSLP-induced
B)
TSLP: - +
100 kDa
Ⓟ-bRAF (Ser445)
48 kDa
β-actin
Lysates
C)
RAS activity (ELISA)
P = .0035
RAS-GTP signal (fold change)
Uninduced
TSLP-induced
D)
TSLP: - +
135 kDa
100 kDa
JAK2
63 kDa
CRLF2
48 kDa
Ⓟ-ERK1/2
ERK1/2
20 kDa
17 kDa
KRAS
HRAS
NRAS
Active RAS pulldown (RAS-GTP)
Lysates (input)
KRAS activity
P = .0064
HRAS activity
P = .06
NRAS activity
P = .038
KRAS-GTP signal (fold change)
HRAS-GTP signal (fold change)
NRAS-GTP signal (fold change)
E)
Protein-phosphorylation microarray
Average normalized Cy3-signal
P = .015
P = .013
P = .010
P = .015
P = .016
P < .0001
P = .00016
Uninduced
+TSLP
cRAF (Ⓟ-Ser296)
GAB2 (Ⓟ-Ser159)
MYC (Ⓟ-Ser62)
PTPN6 (Ⓟ-Tyr536)
AKT2 (Ⓟ-Ser474)
CDKN1A (Ⓟ-Thr145)
ELK1 (Ⓟ-Thr417)

Fig.3

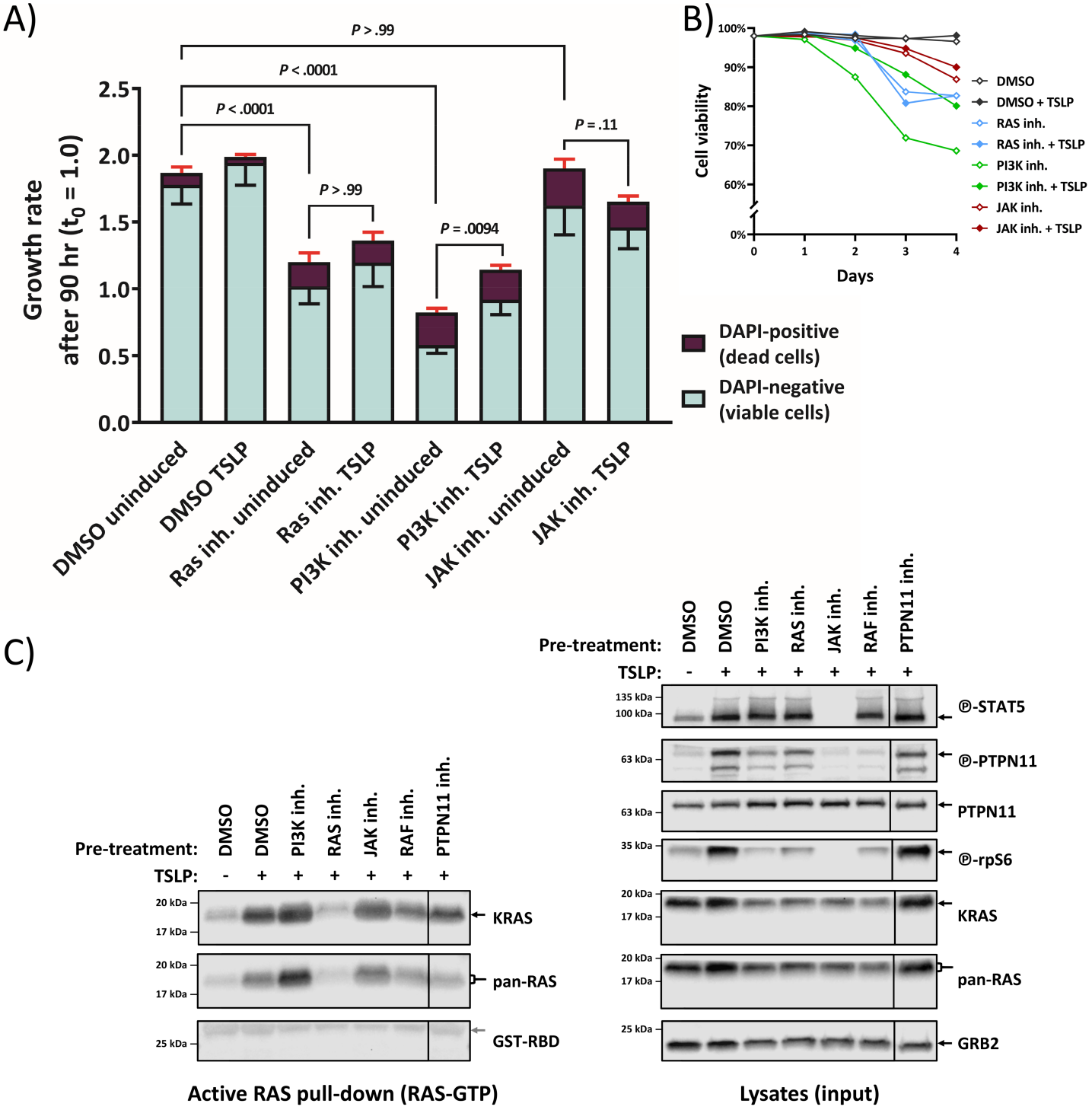
A)
P > .99
P < .0001
P < .0001
P = .11
P > .99
P = .0094
Growth rate after 90 hr (t_0 = 1.0)
2.5
2.0
1.5
1.0
0.5
0.0
DMSO uninduced
DMSO TSLP
Ras inh. uninduced
Ras inh. TSLP
PI3K inh. uninduced
PI3K inh. TSLP
JAK inh. uninduced
JAK inh. TSLP
B)
Cell viability
100%
90%
80%
70%
60%
0%
0
1
2
3
4
Days
DMSO
DMSO + TSLP
RAS inh.
RAS inh. + TSLP
PI3K inh.
PI3K inh. + TSLP
JAK inh.
JAK inh. + TSLP
DAPI-positive (dead cells)
DAPI-negative (viable cells)
C)
Pre-treatment:
DMSO
DMSO
PI3K inh.
RAS inh.
JAK inh.
RAF inh.
PTPN11 inh.
TSLP:
- + + + + + +
20 kDa
17 kDa
KRAS
20 kDa
17 kDa
pan-RAS
25 kDa
GST-RBD
Active RAS pull-down (RAS-GTP)
135 kDa
100 kDa
Ⓟ-STAT5
63 kDa
Ⓟ-PTPN11
63 kDa
PTPN11
35 kDa
Ⓟ-rpS6
20 kDa
17 kDa
KRAS
20 kDa
17 kDa
pan-RAS
25 kDa
GRB2
Lysates (input)
D)
RAS-activity (ELISA)
Protein activity level in MUTZ-5 (normalized to vehicle control)
1.5
1.0
0.5
0.0
P=.68
P>.99
P=.022
DMSO + TSLP
pan-RAS(wt) ind. inh. + TSLP
PI3K/mTOR dual inh. + TSLP
JAK inh. + TSLP
E)
STAT5 activity (WB)
Protein activity level in MUTZ-5 (normalized to vehicle control)
1.5
1.0
0.5
0.0
P=.0017
P=.43
P>.99
DMSO + TSLP
pan-RAS(wt) ind. inh. + TSLP
PI3K/mTOR dual inh. + TSLP
JAK inh. + TSLP

Fig.4

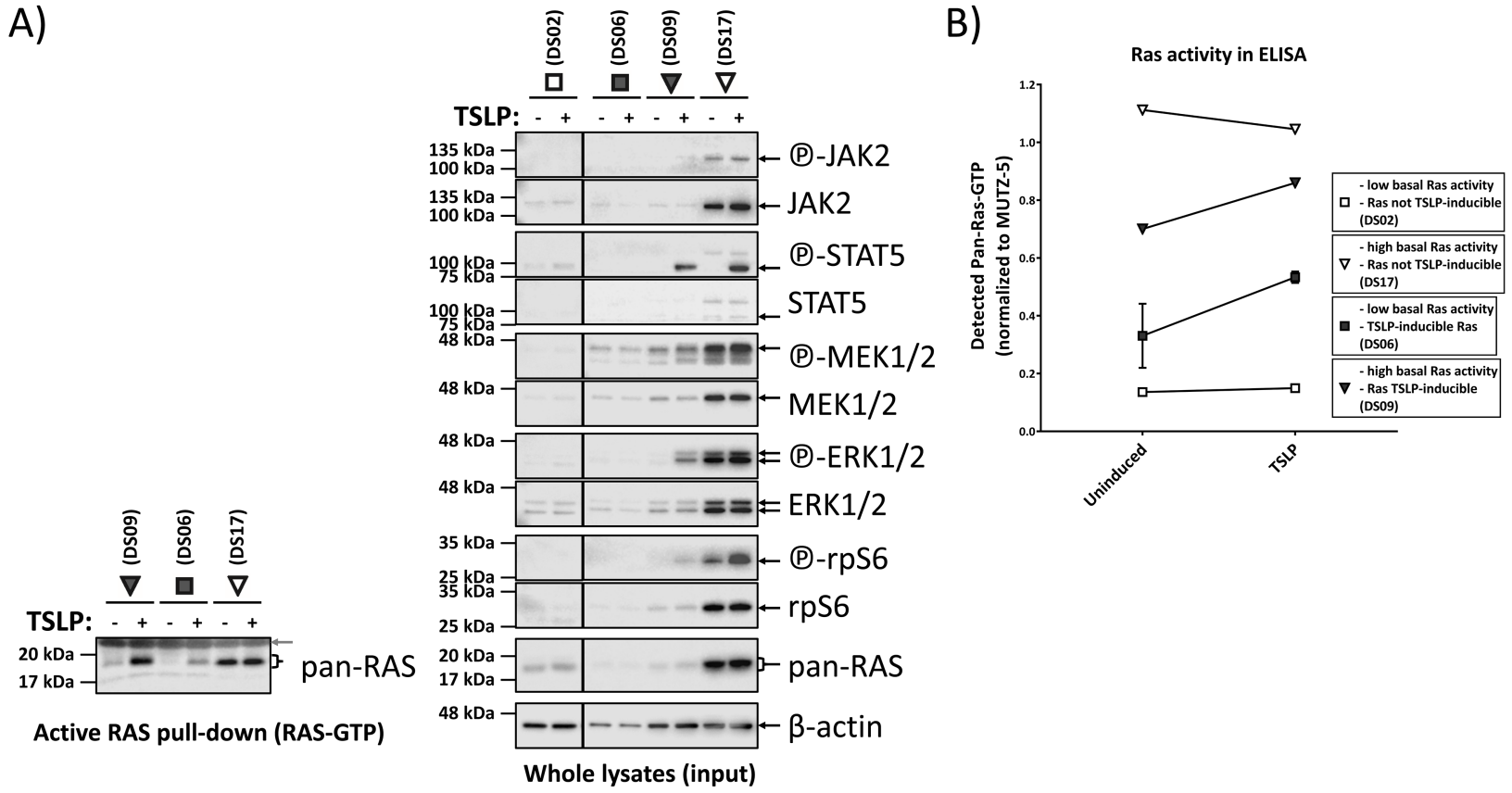
A)
(DS02)
(DS06)
(DS09)
(DS17)
TSLP: - + - + - + - +
135 kDa
100 kDa
Ⓟ-JAK2
JAK2
Ⓟ-STAT5
STAT5
75 kDa
48 kDa
Ⓟ-MEK1/2
MEK1/2
Ⓟ-ERK1/2
ERK1/2
35 kDa
25 kDa
Ⓟ-rpS6
rpS6
20 kDa
17 kDa
pan-RAS
β-actin
Whole lysates (input)
(DS09)
(DS06)
(DS17)
TSLP: - + - + - +
20 kDa
17 kDa
pan-RAS
Active RAS pull-down (RAS-GTP)
B)
Ras activity in ELISA
Detected Pan-Ras-GTP (normalized to MUTZ-5)
1.2
1.0
0.8
0.6
0.4
0.2
0.0
Uninduced
TSLP
- low basal Ras activity
- Ras not TSLP-inducible
(DS02)
- high basal Ras activity
- Ras not TSLP-inducible
(DS17)
- low basal Ras activity
- TSLP-inducible Ras
(DS06)
- high basal Ras activity
- Ras TSLP-inducible
(DS09)

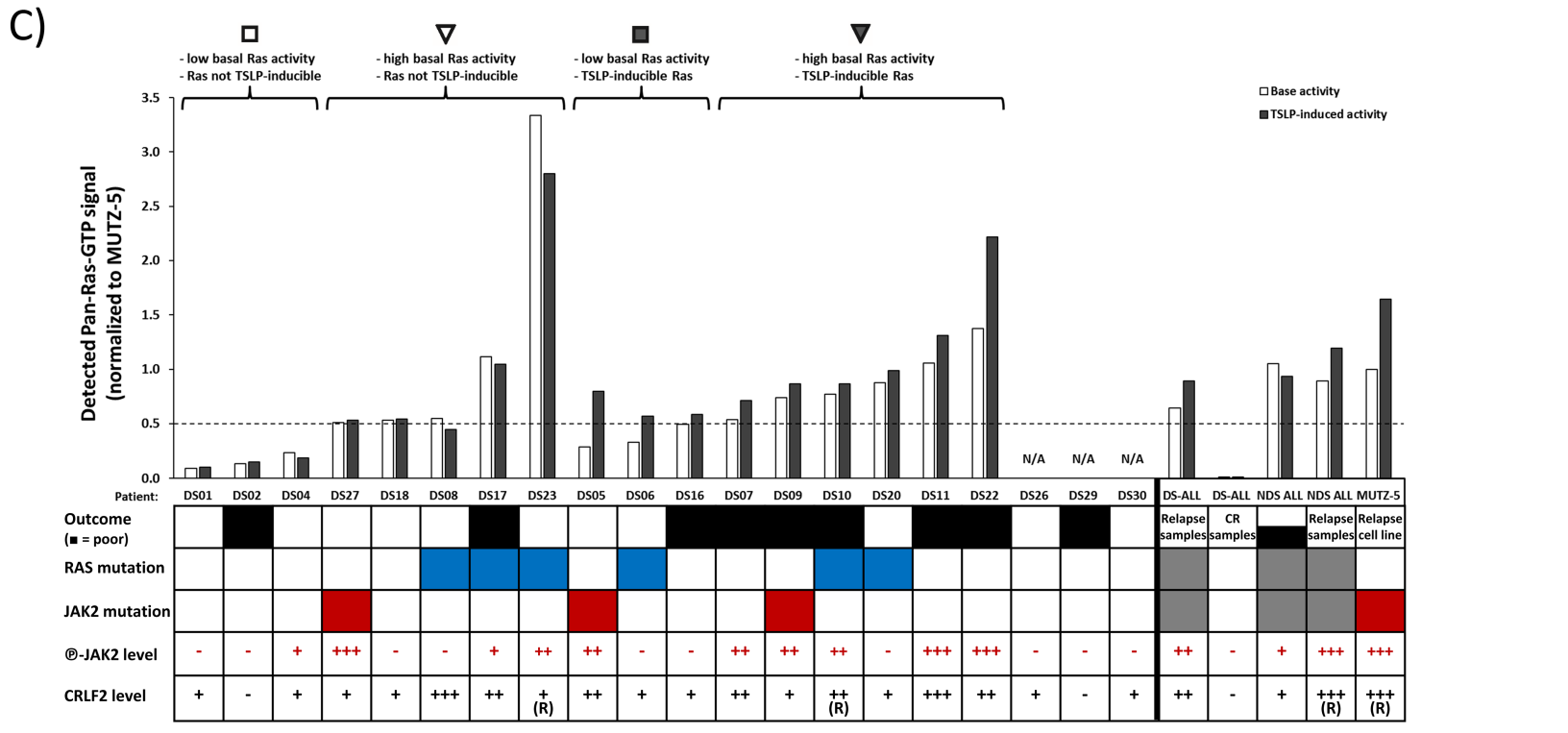
C)
- low basal Ras activity
- Ras not TSLP-inducible
- high basal Ras activity
- Ras not TSLP-inducible
- low basal Ras activity
- TSLP-inducible Ras
- high basal Ras activity
- TSLP-inducible Ras
Base activity
TSLP-induced activity
Detected Pan-Ras-GTP signal (normalized to MUTZ-5)
3.5
3.0
2.5
2.0
1.5
1.0
0.5
0.0
N/A
N/A
N/A
Patient:
DS01 DS02 DS04 DS27 DS18 DS08 DS17 DS23 DS05 DS06 DS16 DS07 DS09 DS10 DS20 DS11 DS22 DS26 DS29 DS30 DS-ALL DS-ALL NDS ALL NDS ALL MUTZ-5
Outcome (■ = poor)
Relapse samples
CR samples
Relapse samples
Relapse cell line
RAS mutation
JAK2 mutation
Ⓟ-JAK2 level
- - + +++ - - + ++ ++ - - ++ ++ ++ - +++ +++ - - - ++ - + +++ +++
CRLF2 level
+ - + + + +++ ++ + (R) ++ + + ++ + ++ (R) + +++ ++ + - + ++ - + +++ (R) +++ (R)

Fig.5

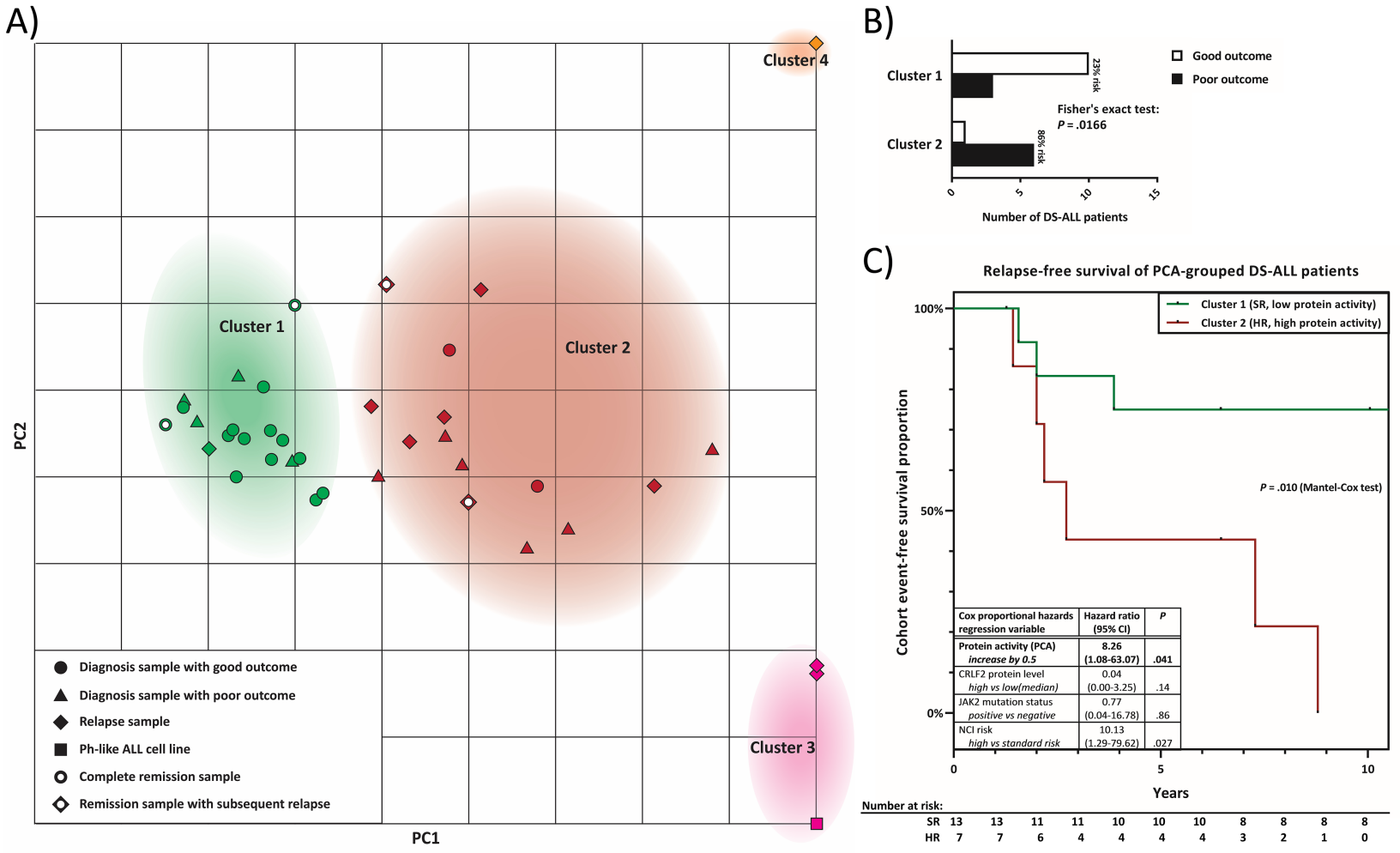
A)
Cluster 4
Cluster 1
Cluster 2
Cluster 3
PC2
PC1
Diagnosis sample with good outcome
Diagnosis sample with poor outcome
Relapse sample
Ph-like ALL cell line
Complete remission sample
Remission sample with subsequent relapse
B)
Cluster 1
Cluster 2
23% risk
86% risk
Good outcome
Poor outcome
Fisher's exact test:
P = .0166
0
5
10
15
Number of DS-ALL patients
C)
Relapse-free survival of PCA-grouped DS-ALL patients
Cluster 1 (SR, low protein activity)
Cluster 2 (HR, high protein activity)
100%
50%
0%
Cohort event-free survival proportion
P = .010 (Mantel-Cox test)
Cox proportional hazards regression variable
Hazard ratio (95% CI)
P
Protein activity (PCA) increase by 0.5
8.26 (1.08-63.07)
.041
CRLF2 protein level high vs low(median)
0.04 (0.00-3.25)
.14
JAK2 mutation status positive vs negative
0.77 (0.04-16.78)
.86
NCI risk high vs standard risk
10.13 (1.29-79.62)
.027
0
5
10
Years
Number at risk:
SR 13 13 11 11 10 10 10 8 8 8 8
HR 7 7 6 4 4 4 4 3 2 1 0
D)
Ras basal activity
JAK2 basal activity
STAT5 basal activity
MEK1/2 basal activity
ERK1/2 basal activity
rpS6 basal activity
Ras activity with TSLP
JAK2 activity with TSLP
STAT5 activity with TSLP
MEK1/2 activity with TSLP
ERK1/2 activity with TSLP
rpS6 activity with TSLP
Detected Pan-Ras-GTP (normalized to MUTZ-5)
Phospho-JAK2(Tyr1007/1008) signal (normalized to MUTZ-5)
Phospho-STAT5(Tyr694) signal (normalized to MUTZ-5)
Phospho-MAP2K1/2(Ser217/221) signal (normalized to MUTZ-5)
Phospho-MAPK1/3(Thr202/Tyr204) signal (normalized to MUTZ-5)
Phospho-RPS6(Ser235/236) signal (normalized to MUTZ-5)
DS-ALL Standard risk
DS-ALL High risk

Fig.6

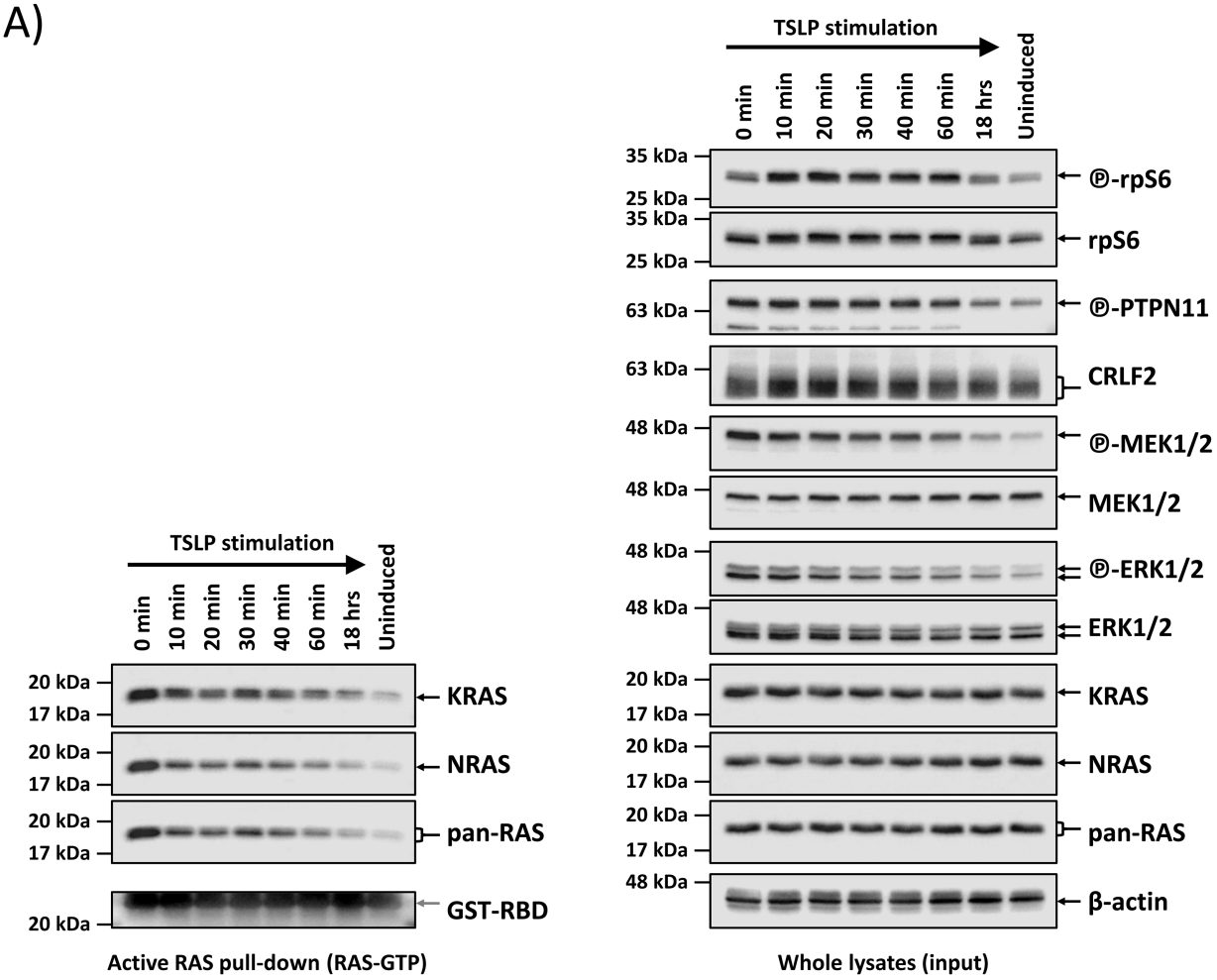
A)
TSLP stimulation
0 min
10 min
20 min
30 min
40 min
60 min
18 hrs
Uninduced
35 kDa
25 kDa
Ⓟ-rpS6
rpS6
63 kDa
Ⓟ-PTPN11
CRLF2
48 kDa
Ⓟ-MEK1/2
MEK1/2
Ⓟ-ERK1/2
ERK1/2
20 kDa
17 kDa
KRAS
NRAS
pan-RAS
β-actin
GST-RBD
Active RAS pull-down (RAS-GTP)
Whole lysates (input)

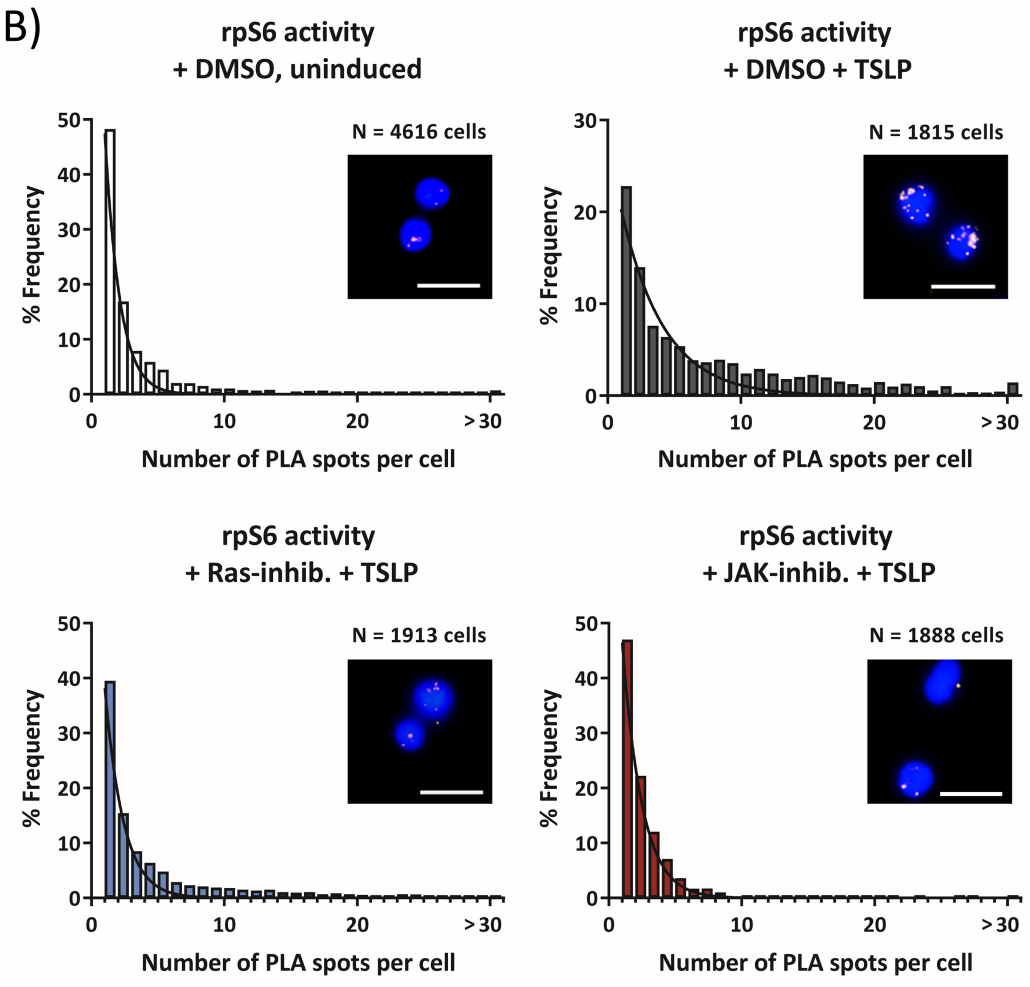
B)
rpS6 activity
+ DMSO, uninduced
N = 4616 cells
rpS6 activity
+ DMSO + TSLP
N = 1815 cells
rpS6 activity
+ Ras-inhib. + TSLP
N = 1913 cells
rpS6 activity
+ JAK-inhib. + TSLP
N = 1888 cells
% Frequency
Number of PLA spots per cell
0
10
20
>30

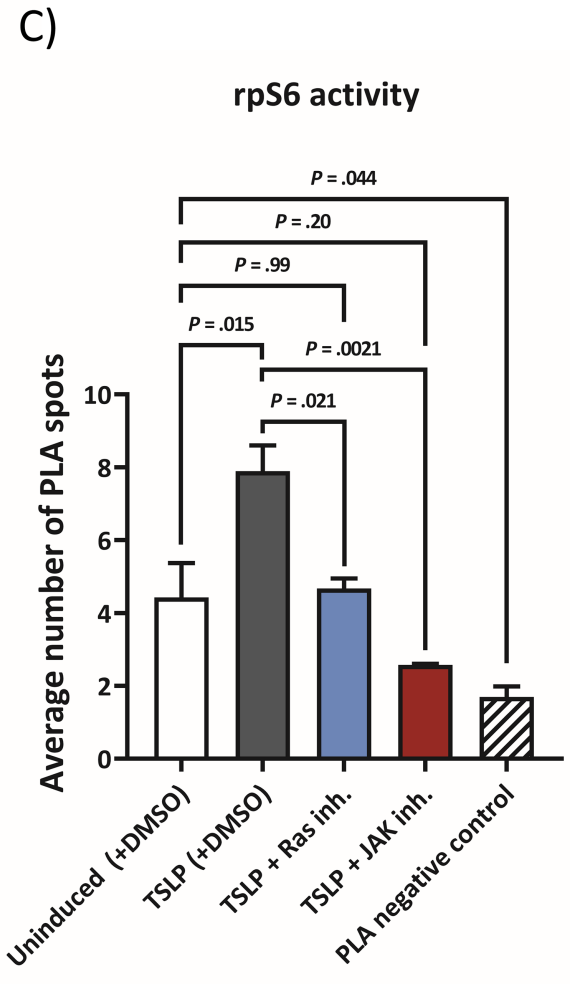
C)
rpS6 activity
P = .044
P = .20
P = .99
P = .015
P = .0021
P = .021
Average number of PLA spots
0
2
4
6
8
10
Uninduced (+DMSO)
TSLP (+DMSO)
TSLP + Ras inh.
TSLP + JAK inh.
PLA negative control

Fig.7

A)

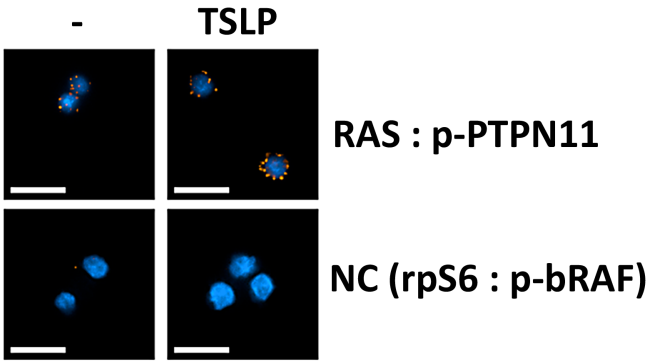

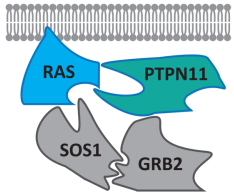

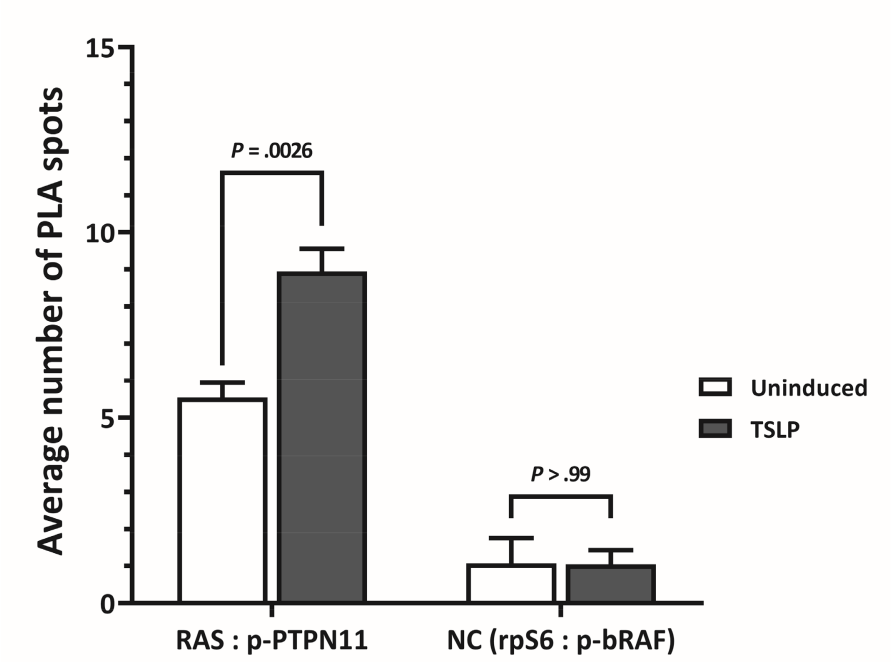

B)

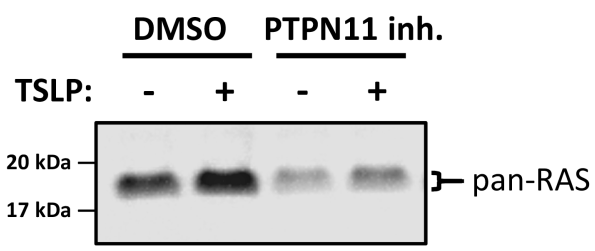

Active RAS pulldown (RAS-GTP)

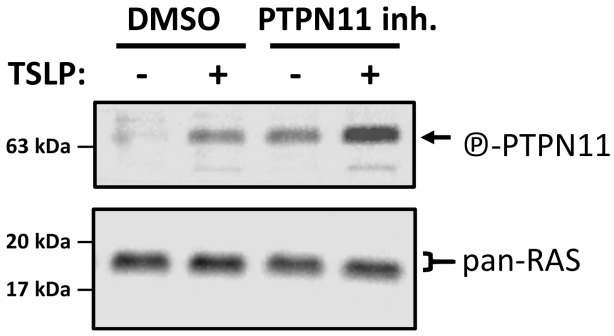

Lysates (input)

C)

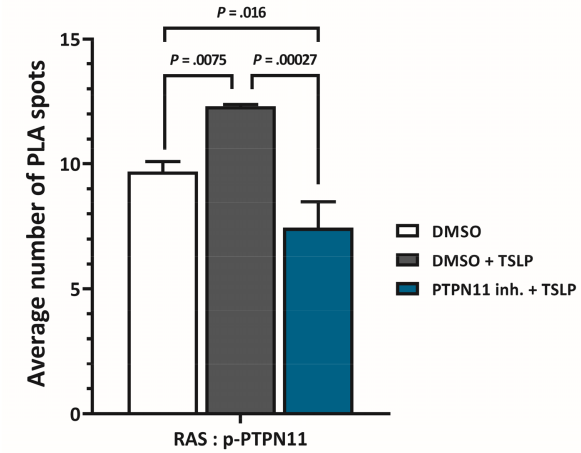

D)

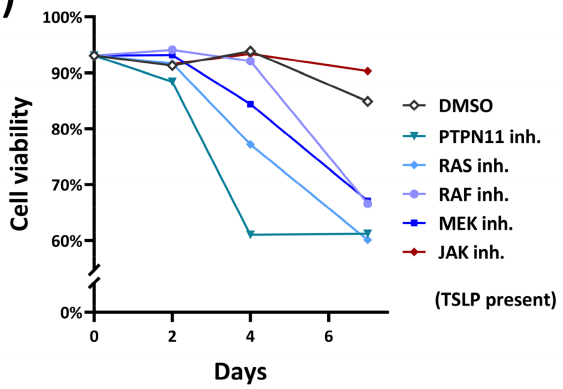

Fig.8

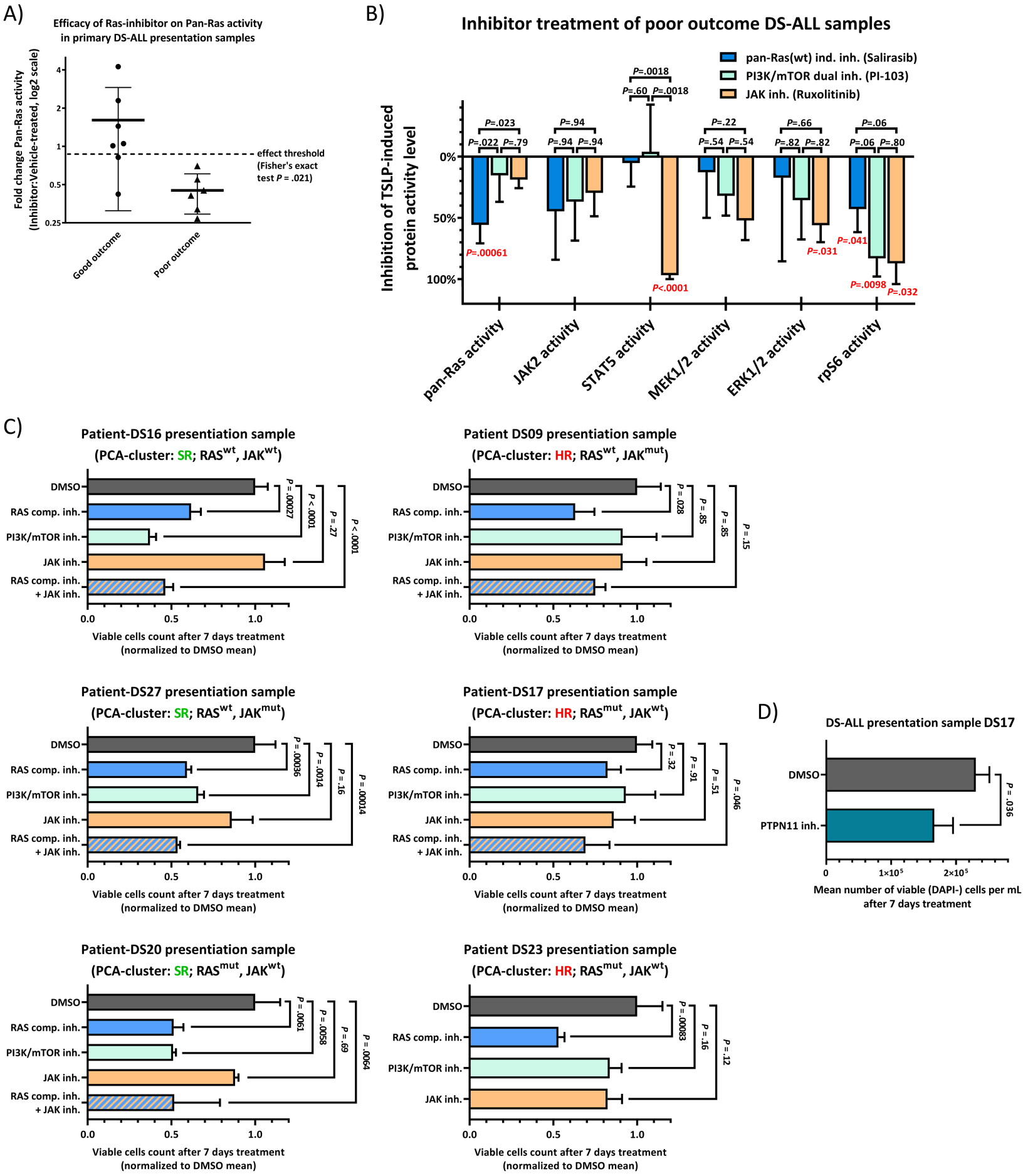
A)
Efficacy of Ras-inhibitor on Pan-Ras activity
in primary DS-ALL presentation samples
Fold change Pan-Ras activity
(Inhibitor:Vehicle-treated, log2 scale)
4
2
1
0.5
0.25
effect threshold
(Fisher's exact
test P = .021)
Good outcome
Poor outcome
B)
Inhibitor treatment of poor outcome DS-ALL samples
pan-Ras(wt) ind. inh. (Salirasib)
PI3K/mTOR dual inh. (PI-103)
JAK inh. (Ruxolitinib)
Inhibition of TSLP-induced
protein activity level
0%
50%
100%
P=.023
P=.022
P=.79
P=.94
P=.94
P=.94
P=.0018
P=.60
P=.0018
P=.22
P=.54
P=.54
P=.66
P=.82
P=.82
P=.06
P=.06
P=.80
P=.00061
P<.0001
P=.041
P=.031
P=.0098
P=.032
pan-Ras activity
JAK2 activity
STAT5 activity
MEK1/2 activity
ERK1/2 activity
rpS6 activity
C)
Patient-DS16 presentiation sample
(PCA-cluster: SR; RASwt, JAKwt)
DMSO
RAS comp. inh.
PI3K/mTOR inh.
JAK inh.
RAS comp. inh.
+ JAK inh.
P = .00027
P < .0001
P = .27
P < .0001
0.0
0.5
1.0
Viable cells count after 7 days treatment
(normalized to DMSO mean)
Patient DS09 presentiation sample
(PCA-cluster: HR; RASwt, JAKmut)
DMSO
RAS comp. inh.
PI3K/mTOR inh.
JAK inh.
RAS comp. inh.
+ JAK inh.
P = .028
P = .85
P = .85
P = .15
0.0
0.5
1.0
Viable cells count after 7 days treatment
(normalized to DMSO mean)
Patient-DS27 presentiation sample
(PCA-cluster: SR; RASwt, JAKmut)
DMSO
RAS comp. inh.
PI3K/mTOR inh.
JAK inh.
RAS comp. inh.
+ JAK inh.
P = .00036
P = .0014
P = .16
P = .00014
0.0
0.5
1.0
Viable cells count after 7 days treatment
(normalized to DMSO mean)
Patient-DS17 presentiation sample
(PCA-cluster: HR; RASmut, JAKwt)
DMSO
RAS comp. inh.
PI3K/mTOR inh.
JAK inh.
RAS comp. inh.
+ JAK inh.
P = .32
P = .91
P = .51
P = .046
0.0
0.5
1.0
Viable cells count after 7 days treatment
(normalized to DMSO mean)
D)
DS-ALL presentation sample DS17
DMSO
PTPN11 inh.
P = .036
0
1×10^5
2×10^5
Mean number of viable (DAPI-) cells per mL
after 7 days treatment
Patient-DS20 presentiation sample
(PCA-cluster: SR; RASmut, JAKwt)
DMSO
RAS comp. inh.
PI3K/mTOR inh.
JAK inh.
RAS comp. inh.
+ JAK inh.
P = .0061
P = .0058
P = .69
P = .0064
0.0
0.5
1.0
Viable cells count after 7 days treatment
(normalized to DMSO mean)
Patient DS23 presentiation sample
(PCA-cluster: HR; RASmut, JAKwt)
DMSO
RAS comp. inh.
PI3K/mTOR inh.
JAK inh.
P = .00083
P = .16
P = .12
0.0
0.5
1.0
Viable cells count after 7 days treatment
(normalized to DMSO mean)

Supplemental material for:

RAS-protein activation but not mutation status is an outcome predictor and unifying therapeutic target for high-risk acute lymphoblastic leukemia

David Koschut,[1] Debleena Ray,[1] Zhenhua Li,[2] Emanuela Giarin,[3] Jürgen Groet,[4] Ivan Alić,[1,5] Shirley Kow-Yin Kham,[2] Wee Joo Chng,[6] Hany Ariffin,[7] David M. Weinstock,[8] Allen Eng-Juh Yeoh,[2,6] Giuseppe Basso,[3,9] and Dean Nižetić[1,4]

[1]Lee Kong Chian School of Medicine, Nanyang Technological University, Singapore

[2]Department of Paediatrics, Yong Loo Lin School of Medicine, National University of Singapore, Singapore

[3]Department of Women's and Children's Health (SDB), Hematology-Oncology Laboratory, University of Padua, Italy

[4]The Blizard Institute, Barts and The London School of Medicine and Dentistry, Queen Mary University of London, United Kingdom

[5]Department of Anatomy, Histology and Embryology, Faculty of Veterinary Medicine, University of Zagreb, Croatia

[6]National University Cancer Institute, Singapore

[7]University of Malaya Medical Centre, University of Malaya, Malaysia

[8]Department of Medical Oncology, Dana-Farber Cancer Institute, Harvard Medical School, USA

[9]Italian Institute for Genomic Medicine, Italy

Materials included:

Supplementary Material and Methods

Supplementary Results

Supplementary Discussion (including additional references)

Supplementary tables: Supplementary-Tab.S1-S3

Supplementary figures (and legends): Supplementary-Fig.S1-S9

Supplementary Material and Methods

Antibodies, inhibitors, and cytokines

The primary antibodies against β-actin (Cat.#ab8227; WB (WB)1:10,000) and GRB2 (Cat.#ab86713; PLA 1:100) were purchased from Abcam (Cambridge, UK); the antibody against CRLF2 (Cat.#AF981; WB 1 µg/mL) was purchased from R&D Systems (Minneapolis, US). The primary antibodies against pan-RAS (Cat.#8832; WB1:200), phospho-bRAF (Cat.#2696; WB1:1,000, PLA1:100), JAK2 (Cat.#3230; WB1:900), HA-tag (Cat.#2367; WB1:1,000), MEK1/2 (Cat.#8727; WB1:1,000), phospho-MEK1/2 (Cat.#9154; WB1:1,000), RPS6 (Cat.#2317; PLA1:50, WB1:1,000) and phospho-STAT5 (Cat.#4322; WB1:1,000), phospho-JAK2 (Cat.#3771; WB1:1,000), ERK1/2 (Cat.#9102; WB1:1,000), phospho-ERK1/2 (Cat.#9101; WB1:1,500), GRB2 (Cat.#3972; WB1:1,500), phospho-RPS6 (Cat.#2211; PLA1:50, WB1:1,000), PI3Kp110α (Cat.#4249; PLA 1:100), SOS1 (Cat.#5890; PLA 1:100), PTPN11 (Cat.#3752; WB1:1,000, PLA1:100), phospho-PTPN11 (Cat.#3751; WB1:1,000, PLA1:100), and STAT5 (Cat.#9363; WB1:1,000) were purchased from Cell Signaling Technology (Danvers, US). The primary antibodies raised against KRAS (Cat.#sc-30; WB1:180), NRAS (Cat.#sc-31; WB1:160) and HRAS (WB1:170) were bought from Santa Cruz Biotechnology (Dallas, US). The primary antibodies used in immunofluorescence against pan-RAS (Cat.#MA1-012; IF1:100, PLA1:100) and bRAF (Cat.#PA5-14926; IF1:50, PLA1:50, WB1:1,000) were purchased from ThermoFisher Scientific (Waltham, US), as was SOS1 (Cat.#MA5-17234; PLA1:100).

Secondary HRP-conjugated antibodies against mouse (Cat.#ab97023; WB1:8,000), rabbit (Cat.#ab97051; WB1:9,000), or goat (Cat.#ab97100; WB1:7,000) IgG species were obtained from Abcam. The secondary fluorescent antibodies anti-mouse IgG Alexa Fluor 488 (Cat.#A11029) and anti-rabbit IgG Alexa Fluor 594 (Cat.#A11037) were purchased from ThermoFisher Scientific.

The small molecule inhibitors PI-103 (PI3K/mTOR-inh.; Cat.#S1038), Ruxolitinib (JAK-inh.; Cat.#S1378), Salirasib (RAS-inh.; Cat.#S7684), Rigosertib (RAS-signaling-inh.; Cat.# S1362), PD0325901 (MEK1/2-inh.; Cat.#: S7684), and Vemurafenib (RAF-inh.; Cat.#S1267) were purchased from Selleck Chemicals

(Houston, US). Additionally, the PTP inhibitor XXXI/II-B08 (PTPN11-inh.; Cat.#565852; EMD Millipore, Burlington, US) was purchased. All inhibitors were reconstituted in dimethyl sulfoxide (DMSO; Cat.#D2650; Sigma-Aldrich, St. Louis, US).

The cytokine used for Ba/F3 culturing was 10 ng/mL murine IL-3 (Cat.#31310-03-10; Gold Biotechnology, St Louis, US).

SDS-PAGE and WB

Protein lysates (see "RAS activity assays") were mixed with 4×Laemmli buffer (Cat.#161-0747; Bio-Rad Laboratories, Hercules, US) containing fresh 200 mM DL-Dithiothreitol (Cat.#3483-12-3; Sigma-Aldrich). For most samples 5 µg total protein could be loaded. SDS-PAGE with 11%-resolving/5%-stacking acrylamide gels, and WB on PVDF-membrane (Cat.#88518; ThermoFisher Scientific) were performed according to the standard protocol of the equipment-manufacturer (Bio-Rad Laboratories). Each PVDF-membrane piece (per antibody) was separately imaged via the auto-exposure function of the ChemiDoc-MP imaging system (Bio-Rad Laboratories). Supplementary-Fig.S5B legend describes the WB-signal quantification in detail. PVDF membranes were stripped from antibodies using the Restore WB-Stripping buffer (Cat.#21059; ThermoFisher Scientific).

Proximity ligation assay (PLA)

MUTZ-5 cells at 1×10^6 cells/mL density were either not induced or induced with 20 ng/mL TSLP for 10 min. Where indicated, cells were pre-treated with either DMSO (vehicle control), RAS inhibitor, or JAK inhibitor for 3 hrs. Cells were fixed in 4% PFA in a 96-well plate for 15 min during which the plate was centrifuged at 400×g. Cells were permeabilized with methanol at -20 °C for 5 min. After blocking with 5% FBS, primary antibodies were incubated over night at 4 °C. On the next day, rabbit and mouse probes from the Duolink In Situ Orange kit (Cat.#DUO92102; Sigma-Aldrich) or the Duolink flowPLA Orange kit (Cat.#DUO94003; Sigma-Aldrich) were used and the PLA was performed according to the manufacturer's protocol.

Operetta CLS high-content screening microscope (PerkinElmer, Waltham, US) were used to detect and count the fluorescent PLA spots in at least 600 single cells for each well and condition. Spot distribution histograms and non-linear Gaussian fitting curves were plotted in Prism v8.1 (GraphPad Software, San Diego, US).

Principal component analysis (PCA)

ELISA and quantified WB data for all 38 samples successfully analyzed for this study were fed into the multidimensional vectoral data visualization software ViDaExpert v1.2(1). The 13 variables included for the PCA calculations were: pan-RAS, JAK2, STAT5, MEK1/2, ERK1/2, and rpS6 activity levels in absence or presence of TSLP as well as CRLF2 protein expression. Eigenvector-based multivariate analysis was performed and the contributions of the principal components 1-3 (PC1-3) of each original variable were calculated (Supplementary-Fig.S6A). Data was transformed to a new 3D coordinate system using the projection of PC1-3. For the *k*-means clustering of the patient samples, *k* was set to 4 after identifying the smallest, significantly different class-class deviation for *k* (Supplementary-Fig.S6B). The resulting coordinate system was loaded into Adobe Illustrator software for presentation. The heatmap was generated in R-software 3.6.0 (The R Foundation, Vienna, AT) by performing unsupervised hierarchical Ward's clustering algorithm on the DS-ALL presentation samples (using the same variables of the PCA), with correlation coefficient as distance metric.

Statistical analysis

For all multiple comparison analysis, one-way ANOVA and post-hoc Bonferroni calculations were performed in Prism v8.1. When only two samples were compared, a two-tailed, unpaired student t-test was performed. For each series of experiments that are not independent, an additional Holm-Bonferroni correction was carried out to adjust the *P*-values for sequential multiple comparison. All replicate experiments were handled and measured independently.

Kaplan–Meier survival estimator plots and multivariate analysis using Cox proportional-hazards model were calculated in R-software 3.6.0, for details on the used factors see the respective figure legends. Variable/category candidates stated in the respective figures were included because they were either the respective analyzed protein/mutation/activity or are known general ALL prognostic markers.

Phospho-protein antibody-microarray

MUTZ-5 cells were serum-starved for 16 hrs at 1×10^6 cells/mL density before being induced with 20 ng/mL TSLP (or uninduced) for 10 min at 37 °C. 8×10^6 cells per condition were lysed in 110 µL Extraction Buffer from the microarray assay kit (Cat.#KAS02; FullMoon BioSystems, Sunnyvale, USA). The antibody-microarray assay was performed according to the manufacturer's protocol and the native, Cy3-labeled proteins were allowed to bind to the antibody-microarray slides (Cat.#PJS202; FullMoon BioSystems). The slides were scanned using the Operetta CLS microscope and the spots for the 202 individual antibodies were analyzed using Protein Array Analyzer software v1.1.c in ImageJ. Each signal was normalized to the Cy3-control present on each microarray slide. To exclude changes that are due to epitope-obstruction from bound protein partners, the signal for phosphorylation-site-specific antibodies was normalized to the signal from each corresponding total antibody raised against the same (unphosphorylated) peptide sequence. Background was set as the average signal from BSA-spots (empty).

Ba/F3 cells transduction

Ba/F3 cells were nucleofected using a Nucleofector 2b (Lonza, Basel, CH) using Cell Line Nucleofector Kit V (Lonza) according to the manufacturer's protocol. The plasmids used for Ba/F3 transfection were MSCVpuromycinR-hCRLF2 (human wt CRLF2) and MSCVneomycinR-hJAK2RG (human $JAK2_{R683G}$ mutant)(2). In order to select for stably transfected cells, MSCVpuromycinR-hCRLF2-transfected cells were cultured with 1 µg/mL puromycin (Cat.#P8833; Sigma-Aldrich), MSCVneomycinR-hJAK2RG-transfected cells were cultured with 1.8 mg/mL G418 (Cat.#108321-42-2; Sigma-Aldrich), and co-

transfected cells were cultured with both antibiotics together. Cells transfected with the plasmid pMax-EGFP (Lonza) were used as control.

DNA- and RNA-sequencing of primary patient material

Patient samples were either whole exome-sequenced previously(3) or amplicons of *JAK2*, *KRAS* and *NRAS* (in addition, *HRAS* of MUTZ-5 cells) were amplified from genomic DNA and sent for Sanger sequencing (1st BASE, Singapore, SG) in both orientations and screened for mutations in Mutation Surveyor v5.0.1 (Softgenetics, State College, US). Oligonucleotides (Supplementary-Tab.S3) were designed to cover known activating mutation hotspots.

RNA sequencing was performed for patients of the MS2003/2010 studies(4, 5) using TruSeq Stranded mRNA Library Prep kit (Illumina, San Diego, US); sequenced on HiSeq2000/2500 or NextSeq500 (Illumina). Reads were aligned to hg19-reference genome using Tophat2(6). The number of reads mapped to each gene were counted using featureCounts(7) and gene expression level was calculated as fragments per kilobase of transcript per million mapped reads (FPKM). GATK best practices was performed for variant calling on RNAseq(8). Data was submitted to the European Genome-phenome Archive (Accession-number EGAS00001001858).

Immunofluorescence

MUTZ-5 cells were fixated with 4% paraformaldehyde (PFA; Cat.#30525-89-4/158127; Sigma-Aldrich), permeabilized with methanol (Cat.#67-56-1; Sigma-Aldrich) at -20 °C and then stained with primary antibodies against either pan-RAS or bRAF. Secondary antibodies, labeled with either Alexa-488 (green) or Alexa-594 (red), specific to the respective primary antibody species were used to visualize the spatial organization of RAS (mostly at plasma membrane) and RAF (mostly in cytoplasma) proteins in a LSM800 inverted confocal microscope with Airyscan, 63×/NA1.20W objective (Carl Zeiss, Oberkochen, DE) at room temperature. Cell nuclei were stained with DAPI. Images were captured using ZEN software (Carl Zeiss) and processed in ImageJ.

Quantitative PCR

Quantitative PCR was performed using a StepOnePlus Real-Time PCR system (Applied Biosystems, Foster City, USA) with Power SYBR Green PCR master mix (Applied Biosystems) according to the standard manufacturer's protocol. The expression of human CRLF2 or human JAK2 was standardized against the expression of mouse GAPDH in each sample. The qPCR oligonucleotides are listed in Supplementary-Tab.S3.

Supplementary Results

(Expanded results description) Higher levels of RAS protein and mRNA correlate with poor outcome in DS-ALL and non-DS childhood ALL

The entire analysis shown so far was based on differences in activity of proteins targets. We also wanted to address protein expression levels in DS-ALL SR and HR groups. Based on individual protein expression levels (Supplementary-Fig.S7A), we found that overall levels of both RAS and rpS6 positively correlated with HR, but levels of CRLF2, STAT5, JAK2, MEK1/2, or ERK1/2 did not. In order to examine similar correlations in non-DS ALL, the material availability only permitted us to look for differences in mRNA transcript levels of the same genes within the whole transcriptome RNA-seq data of the MS2003/2010 cohort (N=346 non-DS ALL cases; median follow-up via reverse Kaplan-Meier = 7.64 years)(4, 5). *CRLF2* mRNA expression (Supplementary-Fig.S7B) and Cox regression hazard ratio (Supplementary-Fig.S8A) were significantly increased in the poor first event samples (n=47). We focused all further analysis on non-DS B-ALL samples with high-risk genetics: Moderate or high *CRLF2* expression (log2(FPKM+1)>0.7) and excluded ALL-subtypes that are considered to confer favorable outcomes (ETV6-RUNX1, Hyperdiploid, TCF3-PBX1, DUX4 and ZNF384). Within the resulting HR sub-cohort (n=91; median follow-up = 6.95 years) KRAS mRNA-expression was independently predictive of outcome (*P*=.030) when included in a multivariate analysis using Cox proportional hazards regression model together with Ph-like status, RAS mutation status, sex, and NCI risk (Supplementary-Fig.S8B). Of all analyzed genes, exclusively KRAS and JAK2 mRNA expression correlated with poor outcome (Supplementary-Fig.S7B). However, only high KRAS mRNA-levels were also significant in Kaplan–Meier survival estimator (Supplementary-Fig.S8B).

The combined data suggest that a large scale analysis on a non-DS ALL cohort is warranted for protein activation patterns of RAS, MEK1/2, and other pathway components activation readouts as this could potentially significantly inform the patient sub-stratification for outcome. This provides just a hint of a trend compatible with conclusions reached for the general role of RAS (irrespective of its mutational

status) as a biomarker in childhood ALL, but emphasizes the need to examine the protein-activation and inducibility parameters on a much larger cohort of non-DS ALL patients for a more accurate risk-prediction sub-stratification.

Supplementary Discussion

Case example: RAS activation explains the clonal evolution from presentation to relapse

DS-ALL patient DS09 highlights the need for an even deeper understanding of the driving mechanisms, and the need to block wtRAS activation as part of the combinatorial treatment design. Exome sequencing found at presentation a *JAK2*-mutation (and no *RAS*-mutation). These DS09 blast cells were highly TSLP-inducible for RAS activity, which could be blocked very efficiently using RAS-inhibitor Salisarib, but not using JAK or PI3K inhibitors in vitro. Concordantly in the experiment in Fig.8C, only RAS-inhibition using Rigosertib significantly reduced viable cell numbers in the DS09-sample. The same patient relapsed two years after standard chemotherapy regimen, and the relapse sample contained no JAK2 mutations anymore, but the main blast had gained an NRAS mutation (sequenced as sample 4-1036101-T2(3)). Interestingly, this relapse sample with constitutively activated NRAS shows no rpS6 activity any longer (with or without TSLP-induction) and TSLP could only induce moderate levels of STAT5 activity compared to the presentation sample (Supplementary-Fig.S5A).

(Expanded) RAS inhibition strategies

The importance of identifying RAS activity for the patient outcome relies on the availability of effective RAS-treatments. RAS has been commonly deemed to be 'undruggable', a term describing the lack of RAS inhibitors that perform well pharmacologically. The RAS inhibitor Salirasib, a Farnesyl Thiosalicylic Acid (FTS) acts non-direct, as a mimetic of RAS for binding to RAS-escort proteins which selectively disrupts the association of RAS to the plasma membrane. It showed no effect in clinical trials on solid cancers trials(9) and requires relatively high dosage. We chose this RAS inhibitor for being able to use a single inhibitor that can block RAS activity of all the main RAS isoforms and most importantly can also block wtRas activity independent of RAS mutations. A new generation of RAS inhibitors are on the horizon(10) such as mutant-specific inhibitors of KRAS(G12C)(11). However,

based on our data, the focus should not lie on targeting mutant-RAS alone but also the inhibition of overstimulated activity in absence of RAS mutations.

The RAS inhibitor Salirasib used in our study disrupts the spatiotemporal localization of active RAS but requires relatively high concentrations, thus rendering it ineffective in Phase II clinical trials(12). Newer RAS-inhibitors like the RAS-mimetic Rigosertib, which blocks the RBD in RAS-effectors, as seen for bRAF and p110αPI3K in our PLA analysis on MUTZ-5 cells, allowing the block of both wt and mutant RAS-activity. Rigosertib was effective in reducing the viable cell count in our DS-ALL samples, irrespective of mutation status, and is currently being evaluated in a Phase III study for MDS/AML(13).

Treatments involving the inhibition of activated RAS, independent of mutation status, that block the activation of multiple RAS-effector pathways, could help to cripple the cancer cells' ability to adapt.

(Expanded) Potential roles of chromosome 21 genes relevant to leukemogenesis

Increased propensity for early hematopoietic (both myeloid and lymphoid) cell fate can be influenced by trisomy of *RUNX1*(14, 15), whereas *ERG* trisomy is linked to skewing of cell fate towards megakaryocytic lineage (the most frequent AML form in DS)(16). Increased *HGMN1*-dose through trisomy 21 directly enhanced the early B-lymphocyte precursors, and could play a role as one of the initiating events in ALL leukemogenesis(17), whereas *CHAF1B* trisomy may increase the risk of AML(18). One of the most dose sensitive chromosome 21 genes known for multiple pathway de-regulations when copy number is increased, is *DYRK1A*. Increased *DYRK1A*-dose could promote both AML and ALL pathogenesis(19, 20). Interestingly, both *DYRK1A*, and another chromosome 21 gene *ITSN* also play a role in activating RAS, in specific cellular contexts(21, 22).

Supplementary references

1. Gorban AN, Pitenko, A., Zinovyev, A. ViDaExpert: user-friendly tool for non-linear visualization and analysis of multidimensional vectorial data. 2014(28 May 2019).

2. van Bodegom D, Zhong J, Kopp N, Dutta C, Kim MS, Bird L, et al. Differences in signaling through the B-cell leukemia oncoprotein CRLF2 in response to TSLP and through mutant JAK2. Blood. 2012;120(14):2853-63.

3. Nikolaev SI, Garieri M, Santoni F, Falconnet E, Ribaux P, Guipponi M, et al. Frequent cases of RAS-mutated Down syndrome acute lymphoblastic leukaemia lack JAK2 mutations. Nature communications. 2014;5:4654.

4. Yeoh AE, Ariffin H, Chai EL, Kwok CS, Chan YH, Ponnudurai K, et al. Minimal residual disease-guided treatment deintensification for children with acute lymphoblastic leukemia: results from the Malaysia-Singapore acute lymphoblastic leukemia 2003 study. J Clin Oncol. 2012;30(19):2384-92.

5. Yeoh AEJ, Lu Y, Chin WHN, Chiew EKH, Lim EH, Li Z, et al. Intensifying Treatment of Childhood B-Lymphoblastic Leukemia With IKZF1 Deletion Reduces Relapse and Improves Overall Survival: Results of Malaysia-Singapore ALL 2010 Study. J Clin Oncol. 2018;36(26):2726-35.

6. Kim D, Pertea G, Trapnell C, Pimentel H, Kelley R, Salzberg SL. TopHat2: accurate alignment of transcriptomes in the presence of insertions, deletions and gene fusions. Genome Biol. 2013;14(4):R36.

7. Liao Y, Smyth GK, Shi W. featureCounts: an efficient general purpose program for assigning sequence reads to genomic features. Bioinformatics. 2014;30(7):923-30.

8. Van der Auwera GA, Carneiro MO, Hartl C, Poplin R, Del Angel G, Levy-Moonshine A, et al. From FastQ data to high confidence variant calls: the Genome Analysis Toolkit best practices pipeline. Curr Protoc Bioinformatics. 2013;43:11 0 1-33.

9. Riely GJ, Johnson ML, Medina C, Rizvi NA, Miller VA, Kris MG, et al. A phase II trial of Salirasib in patients with lung adenocarcinomas with KRAS mutations. Journal of Thoracic Oncology: Official Publication of the International Association for the Study of Lung Cancer. 2011;6(8):1435-7.

10. Dang CV, Reddy EP, Shokat KM, Soucek L. Drugging the 'undruggable' cancer targets. Nat Rev Cancer. 2017;17(8):502-8.

11. Patricelli MP, Janes MR, Li LS, Hansen R, Peters U, Kessler LV, et al. Selective Inhibition of Oncogenic KRAS Output with Small Molecules Targeting the Inactive State. Cancer discovery. 2016;6(3):316-29.

12. Riely GJ, Johnson ML, Medina C, Rizvi NA, Miller VA, Kris MG, et al. A phase II trial of Salirasib in patients with lung adenocarcinomas with KRAS mutations. J Thorac Oncol. 2011;6(8):1435-7.

13. Navada SC, Fruchtman SM, Odchimar-Reissig R, Demakos EP, Petrone ME, Zbyszewski PS, et al. A phase 1/2 study of rigosertib in patients with myelodysplastic syndromes (MDS) and MDS progressed to acute myeloid leukemia. Leukemia research. 2018;64:10-6.

14. De Vita S, Canzonetta C, Mulligan C, Delom F, Groet J, Baldo C, et al. Trisomic dose of several chromosome 21 genes perturbs haematopoietic stem and progenitor cell differentiation in Down's syndrome. Oncogene. 2010;29(46):6102-14.

15. Lie ALM, Marinopoulou E, Lilly AJ, Challinor M, Patel R, Lancrin C, et al. Regulation of RUNX1 dosage is crucial for efficient blood formation from hemogenic endothelium. Development. 2018;145(5).

16. Salek-Ardakani S, Smooha G, de Boer J, Sebire NJ, Morrow M, Rainis L, et al. ERG is a megakaryocytic oncogene. Cancer Res. 2009;69(11):4665-73.

17. Lane AA, Chapuy B, Lin CY, Tivey T, Li H, Townsend EC, et al. Triplication of a 21q22 region contributes to B cell transformation through HMGN1 overexpression and loss of histone H3 Lys27 trimethylation. Nature genetics. 2014;46(6):618-23.

18. Volk A, Liang K, Suraneni P, Li X, Zhao J, Bulic M, et al. A CHAF1B-Dependent Molecular Switch in Hematopoiesis and Leukemia Pathogenesis. Cancer cell. 2018;34(5):707-23 e7.

19. Malinge S, Bliss-Moreau M, Kirsammer G, Diebold L, Chlon T, Gurbuxani S, et al. Increased dosage of the chromosome 21 ortholog Dyrk1a promotes megakaryoblastic leukemia in a murine model of Down syndrome. J Clin Invest. 2012;122(3):948-62.

20. Thompson BJ, Bhansali R, Diebold L, Cook DE, Stolzenburg L, Casagrande AS, et al. DYRK1A controls the transition from proliferation to quiescence during lymphoid development by destabilizing Cyclin D3. J Exp Med. 2015;212(6):953-70.

21. Kelly PA, Rahmani Z. DYRK1A enhances the mitogen-activated protein kinase cascade in PC12 cells by forming a complex with Ras, B-Raf, and MEK1. Molecular biology of the cell. 2005;16(8):3562-73.

22. Mohney RP, Das M, Bivona TG, Hanes R, Adams AG, Philips MR, et al. Intersectin activates Ras but stimulates transcription through an independent pathway involving JNK. J Biol Chem. 2003;278(47):47038-45.

23. Yoda A, Yoda Y, Chiaretti S, Bar-Natan M, Mani K, Rodig SJ, et al. Functional screening identifies CRLF2 in precursor B-cell acute lymphoblastic leukemia. Proc Natl Acad Sci U S A. 2010;107(1):252-7.

Supplementary-Tab.S1) Clinical and biological characteristics of the leukemia samples

DS-ALL Sample ID	Presentation / Relapse	BM/PB	AIEOP-BFM subclassification	Blasts %	WBC	Diagnosis	Karyotype	Gender	NCI	Poor outcome (death or relapse)	Sample ID in: https://doi-org.ezlibproxy1.ntu.edu.sg/10.1038/ncomms5654	
DS01	Presentation	BM	B-II	65.0	N/A	ALL	N.D.	M	N/A	N	4-23-T1	
DS02	Presentation	BM	B-II	90.0	122800	ALL	N.D.	M	HR	Y		
DS04	Presentation	BM	B-II	95.0	N/A	ALL	47,XY,+21c	M	SR	N	4-1030604-T1	
DS05	Presentation	BM	B-II	95.0	N/A	ALL	N.D.	M	HR	N		
DS06	Presentation	BM	B-III	91.6	323000	ALL	N.D.	F	HR	N	4-37-T1	
DS07	Presentation	BM	B-II	87.0	86400	ALL	N.D.	F	HR	Y		
DS08	Presentation	BM	B-II	85.0	N/A	ALL	N.D.	F	SR	N		
DS09	Presentation	BM	B-II	70.0	18780	ALL	47,XY,+21c	M	SR	Y	4-1036101-T1	
DS10	Presentation	BM	B-II	62.0	35400	ALL	47,XY,+21c	M	HR	Y	4-1036272-T1	
DS11	Presentation	BM	B-III	91.0	N/A	ALL	48,XY,+X,+21	M	SR	Y		
DS16	Presentation	BM	B-II	90.0	2400	ALL	N.D.	M	HR	Y	4-44-T1	
DS17	Presentation	BM	B-II	90.0	44600	ALL	47,XY,+21c[1	M	HR	Y	4-03-T1	
DS18	Presentation	BM	B-II	86.0	23530	ALL	N.D.	M	SR	N	4-02-T1	
DS20	Presentation	BM	B-II	80.0	11500	ALL	47,XX,t(8;14	F	SR	N	4-29-T1	also Remission sample tested
DS22	Presentation	BM	B-II	97.0	N/A	ALL	N.D.	F	NA	Y		
DS23	Presentation	BM	B-II	88.0	27400	ALL	47,XX,+21c	F	SR	N	4-1044929-T1	
DS26	Presentation	BM	B-II	88.0	N/A	ALL	47,XX,+21c[1	F	N/A	N		
DS27	Presentation	N/A	N/A	N/A	N/A	ALL	N/A	M	N/A	N		also Remission sample tested
DS29	Presentation	BM	B-II	87.0	55000	ALL	47,XY,+21c[1	M	HR	Y		
DS30	Presentation	PB	B-II	82.0	206000	ALL	N.D.	F	HR	N		
DS09R	Relapse	BM	B-II	47.0	12200	ALL	47,XY,+21c	M			4-1036101-T2	
DS12R	Relapse	BM	B-II	79.0	17000	ALL	N.D.	M				
DS16R	Relapse	BM	B-II	90.0	N/A	ALL	N.D.	M			4-44-T2	
DS19R	Relapse	BM	B-II	88.0	221400	ALL	N.D.	M				
DS22R	Relapse	BM	B-III	87.0	46000	ALL	N.D.	F			4-29-T2	
DS28R	Relapse	BM	B-II	83.0	98400	ALL	N.D.	M				
DS29R	Relapse	BM	B-II	83.0	39800	ALL	N.D.	M				
DS24m	Remission	BM	N/A	N/A	N/A	N/A	N.D.	M		Y		
DS25m	Remission	BM	N/A	N/A	N/A	N/A	N.D.	F		Y		

Non-DS ALL Sample ID	Presentation / Relapse	BM/PB	AIEOP-BFM subclassification	Blasts %	WBC	Diagnosis	Karyotype	Gender	NCI	Poor outcome (death or relapse)
NDS03	Presentation	N/A	N/A	N/A	N/A	ALL	N/A	F	N/A	N
NDS04	Presentation	BM	B-II	93	97800	ALL	N.D.	M	HR	N
NDS05	Presentation	BM	B-II	82.8	56000	ALL	46,XX	F	HR	Y
NDS06	Presentation	BM	B-II	89	80000	ALL	46,XX	F	HR	N

NDS01R	Relapse	BM	B-II	44.1	NA	ALL	N.D.	F
NDS02R	Relapse	BM	B-II	97	NA	ALL	N.D.	M

Supplementary-Tab.S1) Clinical and biological characteristics of the leukemia samples used in this study and therapy outcomes.

Supplementary-Tab.S2) List of Bonferroni-corrected *P*-values

Fig.1B)

Comparison:	Bonferroni p-value after one-way ANOVA:
— vs. hJAK2^{R683G}	>0.99999
— vs. hCRLF2	>0.99999
— vs. hJAK2^{R683G} + hCRLF2	0.00160
hJAK2^{R683G} vs. hCRLF2	>0.99999
hJAK2^{R683G} vs. hJAK2^{R683G} + hCRLF2	0.00364
hCRLF2 vs. hJAK2^{R683G} + hCRLF2	0.00347

Fig.2A)

Comparison:	p-value:	Holm-Bonferroni corrected p value:
JAK2 activity uninduced vs. TSLP	0.00043	0.00171
MEK1/2 activity uninduced vs. TSLP	0.00065	0.00195
Pan-Ras activity uninduced vs. TSLP	0.00308	0.00616
PTPN11 activity uninduced vs. TSLP	0.01846	0.01846

Fig.2D)

Comparison:	p-value:	Holm-Bonferroni corrected p value:
KRas activity uninduced vs. TSLP	0.00216	0.00648
NRas activity uninduced vs. TSLP	0.01905	0.03810
HRas activity uninduced vs. TSLP	0.06632	0.06632

Fig.2E)

Comparison:	p-value:	Holm-Bonferroni corrected p value:
AKT2 (@-Ser474) unind. vs. TSLP	0.01657	0.05404
CDKN1A (@-Thr145) unind. vs. TSLP	0.00002	0.00015
cRAF (@-Ser296) unind. vs. TSLP	0.01546	0.05404
ELK1 (@-Thr417) unind. vs. TSLP	0.00016	0.00097
GAB2 (@-Ser159) unind. vs. TSLP	0.01351	0.05404
MYC (@-Ser62) unind. vs. TSLP	0.01025	0.05124
PTPN6 (@-Tyr536) unind. vs. TSLP	0.01570	0.05404

Fig.6B)

Comparison:	Bonferroni p-value after one-way ANOVA:
Uninduced (+DMSO) vs. TSLP (+DMSO)	0.01572
Uninduced (+DMSO) vs. TSLP + Ras inh.	>0.99999
Uninduced (+DMSO) vs. TSLP + JAK inh.	0.20936
Uninduced (+DMSO) vs. PLA negative control	0.04445
TSLP (+DMSO) vs. TSLP + Ras inh.	0.02177
TSLP (+DMSO) vs. TSLP + JAK inh.	0.00214
TSLP (+DMSO) vs. PLA negative control	0.00102
TSLP + Ras inh. vs. TSLP + JAK inh.	0.13163
TSLP + Ras inh. vs. PLA negative control	0.03079
TSLP + JAK inh. vs. PLA negative control	>0.99999

Fig.8C)

Comparison (each mean compared to respective control mean (DMSO))	Dunnett p-value after one-way ANOVA:
DS17	
DMSO vs. RAS comp. inh.	0.32889
DMSO vs. PI3K/mTOR inh.	0.91477
DMSO vs. JAK inh.	0.51257
DMSO vs. RAS comp. inh. + JAK inh.	0.04654
DS16	
DMSO vs. RAS comp. inh.	0.00027
DMSO vs. PI3K/mTOR inh.	<0.0001
DMSO vs. JAK inh.	0.72408
DMSO vs. RAS comp. inh. + JAK inh.	<0.0001
DS20	
DMSO vs. RAS comp. inh.	0.00615
DMSO vs. PI3K/mTOR inh.	0.00588
DMSO vs. JAK inh.	0.69698
DMSO vs. RAS comp. inh. + JAK inh.	0.00643
DS27	
DMSO vs. RAS comp. inh.	0.00036
DMSO vs. PI3K/mTOR inh.	0.00143
DMSO vs. JAK inh.	0.1684
DMSO vs. RAS comp. inh. + JAK inh.	0.00014
DS09	
DMSO vs. RAS comp. inh.	0.02829
DMSO vs. PI3K/mTOR inh.	0.85979
DMSO vs. JAK inh.	0.85979
DMSO vs. RAS comp. inh. + JAK inh.	0.15412
DS23	
DMSO vs. RAS comp. inh.	0.00083
DMSO vs. PI3K/mTOR inh.	0.1601
DMSO vs. JAK inh.	0.12471

Fig.3A)

Comparison:	Bonferroni p-value after one-way ANOVA:
DMSO uninduced vs. DMSO TSLP	>0.99999
DMSO uninduced vs. Ras inh. uninduced	<0.00001
DMSO uninduced vs. Ras inh. TSLP	<0.00001
DMSO uninduced vs. PI3K inh. uninduced	<0.00001
DMSO uninduced vs. PI3K inh. TSLP	<0.00001
DMSO uninduced vs. JAK inh. uninduced	>0.99999
DMSO uninduced vs. JAK inh. TSLP	0.33322
DMSO TSLP vs. Ras inh. uninduced	<0.00001
DMSO TSLP vs. Ras inh. TSLP	<0.00001
DMSO TSLP vs. PI3K inh. uninduced	<0.00001
DMSO TSLP vs. PI3K inh. TSLP	<0.00001
DMSO TSLP vs. JAK inh. uninduced	>0.99999
DMSO TSLP vs. JAK inh. TSLP	0.00589
Ras inh. uninduced vs. Ras inh. TSLP	>0.99999
Ras inh. uninduced vs. PI3K inh. uninduced	0.00111
Ras inh. uninduced vs. PI3K inh. TSLP	>0.99999
Ras inh. uninduced vs. JAK inh. uninduced	<0.00001
Ras inh. uninduced vs. JAK inh. TSLP	0.00006
Ras inh. TSLP vs. PI3K inh. uninduced	<0.00001
Ras inh. TSLP vs. PI3K inh. TSLP	0.31820
Ras inh. TSLP vs. JAK inh. uninduced	<0.00001
Ras inh. TSLP vs. JAK inh. TSLP	0.02665
PI3K inh. uninduced vs. PI3K inh. TSLP	0.00944
PI3K inh. uninduced vs. JAK inh. uninduced	<0.00001
PI3K inh. uninduced vs. JAK inh. TSLP	<0.00001
PI3K inh. TSLP vs. JAK inh. uninduced	<0.00001
PI3K inh. TSLP vs. JAK inh. TSLP	<0.00001
JAK inh. uninduced vs. JAK inh. TSLP	0.11829

Fig.7A

Comparison:	p-value:	Holm-Bonferroni corrected p value:
RAS : p-PTPN11	0.001306	0.002612
NC (rpS6 : p-bRAF) (uninduced vs TSLP)	0.956956	>0.999999

Fig.7C

Comparison:	Bonferroni p-value after one-
DMSO vs. DMSO + TSLP	0.00748
DMSO vs. PTPN11 inh. + TSLP	0.01592
DMSO + TSLP vs. PTPN11 inh. + TSLP	0.00027

Fig.5D)

Comparison:	p-value:	Holm-Bonferroni corrected p value:
Pan-Ras basal activity SR vs HR	0.01315	0.03165
JAK2 basal activity SR vs HR	0.00053	0.00265
STAT5 basal activity SR vs HR	0.55617	0.55617
MEK basal activity SR vs HR	0.00495	0.01980
ERK basal activity SR vs HR	0.00035	0.00209
S6 basal activity SR vs HR	0.01055	0.03165
Pan-Ras TSLP-induced activity SR vs HR	0.00383	0.00766
JAK2 TSLP-induced activity SR vs HR	0.00027	0.00161
STAT5 TSLP-induced activity SR vs HR	0.00241	0.00722
MEK TSLP-induced activity SR vs HR	0.01622	0.01622
ERK TSLP-induced activity SR vs HR	0.00163	0.00653
S6 TSLP-induced activity SR vs HR	0.00032	0.00162

Fig.8B)

Comparison:	Bonferroni p-value after one-way ANOVA:
Pan-Ras activity	
pan-Ras inh. vs. PI3K/mTOR dual inh.	0.023
pan-Ras inh. vs. JAK inh.	0.023
PI3K/mTOR dual inh. vs. JAK inh.	0.800
JAK2 activity	
pan-Ras inh. vs. PI3K/mTOR dual inh.	0.944
pan-Ras inh. vs. JAK inh.	0.944
PI3K/mTOR dual inh. vs. JAK inh.	0.944
STAT5 activity	
pan-Ras inh. vs. PI3K/mTOR dual inh.	0.606
pan-Ras inh. vs. JAK inh.	0.002
PI3K/mTOR dual inh. vs. JAK inh.	0.002
MEK1/2 activity	
pan-Ras inh. vs. PI3K/mTOR dual inh.	0.544
pan-Ras inh. vs. JAK inh.	0.228
PI3K/mTOR dual inh. vs. JAK inh.	0.544
ERK1/2 activity	
pan-Ras inh. vs. PI3K/mTOR dual inh.	0.824
pan-Ras inh. vs. JAK inh.	0.668
PI3K/mTOR dual inh. vs. JAK inh.	0.824
rpS6 activity	
pan-Ras inh. vs. PI3K/mTOR dual inh.	0.066
pan-Ras inh. vs. JAK inh.	0.066
PI3K/mTOR dual inh. vs. JAK inh.	0.808

Supplementary-Fig.S1C)

Comparison:	Bonferroni p-value after one-
JAK2 mRNA levels:	
— vs. hJAK2^{R683G}	0.00415
— vs. hCRLF2	>0.99999
— vs. hJAK2^{R683G} + hCRLF2	0.01031
hJAK2^{R683G} vs. hCRLF2	0.00413
hJAK2^{R683G} vs. hJAK2^{R683G} + hCRLF2	0.69131
hCRLF2 vs. hJAK2^{R683G} + hCRLF2	0.01023

Supplementary-Fig.S1D)

CRLF2 mRNA levels:	Bonferroni p-value after one-way ANOVA:
— vs. hJAK2^{R683G}	>0.99999
— vs. hCRLF2	0.02509
— vs. hJAK2^{R683G} + hCRLF2	0.00020
hJAK2^{R683G} vs. hCRLF2	0.02514
hJAK2^{R683G} vs. hJAK2^{R683G} + hCRLF2	0.00020
hCRLF2 vs. hJAK2^{R683G} + hCRLF2	0.00077

Supplementary-Fig.S1E)

Comparison:	Bonferroni p-value after one-way ANOVA:
Day4:	
— vs. hJAK2^{R683G}	>0.99999
— vs. hCRLF2	0.98323
— vs. hJAK2^{R683G} + hCRLF2	0.00016
hJAK2^{R683G} vs. hCRLF2	0.98323
hJAK2^{R683G} vs. hJAK2^{R683G} + hCRLF2	0.00016
hCRLF2 vs. hJAK2^{R683G} + hCRLF2	0.00022

Supplementary-Fig.S2C,D,E)

Comparison:	p-value:	Holm-Bonferroni corrected p value:
GRB2 : phospho-PTPN11 (uninducedvsTSLP)	4.1E-06	0.000434405
pan-RAS : bRAF (TSLPvsRigo)	8.2E-05	0.006362897
pan-RAS : p110αPI3K (TSLPvsRigo)	0.00016	0.0118114
pan-RAS : phospho-PTPN11 (TSLPvsRigo)	0.10487	0.97912792
pan-RAS : phospho-PTPN11 (uninducedvsTSLP)	1.7E-07	2.19501E-05
pan-RAS : PTPN11 (TSLPvsRuxo)	7E-06	0.000709391
pan-RAS : SOS1 (uninducedvsTSLP)	0.00029	0.019530583
rpS6 : phospho-bRAF (TSLPvsRigo)	3.6E-06	0.00387867
rpS6 : phospho-bRAF (TSLPvsRuxo)	0.0004	0.025484468
rpS6 : phospho-bRAF (uninducedvsTSLP)	0.00148	0.070801112
rpS6 : phospho-rpS6 (TSLPvsRigo)	2E-05	0.001828029
rpS6 : phosoho-rpS6 (TSLPvsRuxo)	9.9E-08	1.30439E-05
rpS6 : phospho-rpS6 (uninducedvsTSLP)	3.4E-07	4.28713E-05
SOS1 : GRB2 (uninducedvsTSLP)	0.00023	0.016345942

Supplementary-Fig.S4B)

Comparison:	p-value:	Holm-Bonferroni corrected p value:
STAT5 activity uninduced vs. TSLP	0.00006	0.00039
JAK2 activity uninduced vs. TSLP	0.00043	0.00256
MEK activity uninduced vs. TSLP	0.00065	0.00325
rpS6 activity uninduced vs. TSLP	0.00067	0.00325
Pan-Ras activity uninduced vs. TSLP	0.00308	0.01053
PTPN11 activity uninduced vs. TSLP	0.01846	0.03692
ERK activity uninduced vs. TSLP	0.02192	0.03692

Supplementary-Fig.S7A)

Comparison:	p-value:	Holm-Bonferroni corrected p value:
Pan-Ras protein expression SR vs. HR	0.00427	0.02564
JAK2 protein expression SR vs. HR	0.07137	0.28547
STAT5 protein expression SR vs. HR	0.14639	0.43916
MEK1/2 protein expression SR vs. HR	0.40022	0.80045
ERK1/2 protein expression SR vs. HR	0.04039	0.20196
rpS6 protein expression SR vs. HR	0.00034	0.00237
CRLF2 protein expression SR vs. HR	0.49585	0.80045

Supplementary-Fig.S7B)

Comparison:	p-value:	Holm-Bonferroni corrected p value:
KRAS mRNA good vs. poor outcome	0.02670	0.18693
JAK2 mRNA good vs. poor outcome	0.03945	0.23670
NRAS/KRAS mRNA good vs. poor outcome	0.04616	0.23670
STAT5B mRNA good vs. poor outcome	0.10881	0.43525
RPS6 mRNA good vs. poor outcome	0.81850	>0.99999
MEK1/2 mRNA good vs. poor outcome	0.87458	>0.99999
ERK1/2 mRNA good vs. poor outcome	0.95096	>0.99999

Comparison:	p-value:	Holm-Bonferroni
STAT5 phosph. (JAK inh. vs. vehicle control)	0.00000	0.00001
Pan-Ras-GTP level (Ras inh. vs. vehicle control)	0.00004	0.00061
rpS6 phosph. (PI3K inh. vs. vehicle control)	0.00062	0.00988
ERK1/2 phosph. (JAK inh. vs. vehicle control)	0.00213	0.03193
rpS6 phosph. (JAK inh. vs. vehicle control)	0.00231	0.03231
rpS6 phosph. (Ras inh. vs. vehicle control)	0.00320	0.04154
MEK1/2 phosph. (JAK inh. vs. vehicle control)	0.00500	0.06004
MEK1/2 phosph. (PI3K inh. vs. vehicle control)	0.00737	0.08112
Pan-Ras-GTP level (JAK inh. vs. vehicle control)	0.01001	0.10007
JAK2 phosph. (Ras inh. vs. vehicle control)	0.03552	0.31971
JAK2 phosph. (PI3K inh. vs. vehicle control)	0.05956	0.47652
JAK2 phosph. (JAK inh. vs. vehicle control)	0.06092	0.47652
ERK1/2 ohosph. (PI3K inh. vs. vehicle control)	0.06835	0.47652
Pan-Ras-GTP level (PI3K inh. vs. vehicle control)	0.28436	>0.99999
MEK1/2 phosph. (Ras inh. vs. vehicle control)	0.46249	>0.99999
STAT5 phosph. (Ras inh. vs. vehicle control)	0.56159	>0.99999
ERK1/2 phosph. (Ras inh. vs. vehicle control)	0.63041	>0.99999
STAT5 phosph. (PI3K inh. vs. vehicle control)	0.84173	>0.99999

Supplementary-Tab.S2) List of Bonferroni-adjusted or Holm-Bonferroni-corrected *P*-values from all statistical tests engaging in multiple comparisons in this article. Original *P*-values before Holm-Bonferroni-correction are also listed; the P-values appearing in figures and supplementary figures are highlighted red. See Materials and Methods for more details about the statistical methods used.

Supplementary-Tab.S3) List of oligonucleotides

human JAK2 sequencing:

Name:	Sequence:
Fwd-JAK2amp1,Seq1	CCACTCTTGCTCTCTCTCACTTT
Fwd-JAK2amp2,Seq2	CCATCCAGAAACACAAACCATGT
Fwd-JAK2amp3,Seq3	CGCCTGTATTCCCAGCTACT
Fwd-JAK2,Seq4	GGAAGTATTTGGCTAGTTGGT
Rev-JAK2amp3,rSeq1	CCTAATGTCTACTTCAACACGGT
Rev-JAK2,rSeq2	GGCAGCTTACCAGCACTGTA
Rev-JAK2amp2,rSeq3	CCTTTACACCACTGCCCAAGTAA
Rev-JAK2amp1,rSeq4	CCTAGCTGTGATCCTGAAACTGA

human KRAS sequencing:

Name:	Sequence:
Fwd KRas amplicon 1	GCGTCGATGGAGGAGTTTGTA
Rev KRas amplicon 1	GCACAGAGAGTGAACATCATGGA
Fwd KRas amplicon 2	CCACCAGCAATGCACAAAGATT
Rev KRas amplicon 2	CCAAAGCCAAAAGCAGTACCATG
Fwd KRas Seq3	GGTGTAGTGGAAACTAGGAATT
Rev KRas Seq4r	GCCACTGTTTATCCAATCCAA
Fwd KRas amplicon 3A	CCAGTTTCTTGACTCACCTTTGAG
Rev KRas amplicon 3A	GGGATAAGAAAGTGCTGTGCTG
Fwd KRas amplicon 3B	GCCTGAAGAGAAACATAAAGAATCC
Rev KRas amplicon 3B	GGGAATACTGGCACTTAGAGGAA

human HRAS sequencing:

Name:	Sequence:
Fwd HRas amplicon	GCTGTGGGTTTGCCCTTCA
Rev HRas amplicon	CCATGTCCTGAGCTTGTGCTG
Fwd HRas Seq2	GCCATCAACAACACCAAGTCTT
Rev HRas Seq3r	CCCATCAATGACCACCTGCTT
Fwd HRas Seq3	GGCACCTGTTGGTTCTGAGTCT
Rev HRas Seq2r	CCCACTAAGACTCAGAACCAACA

human NRAS sequencing:

Name:	Sequence:
Fwd NRas amplicon 1	GGGATTTCCATTGCTTAGGCT
Rev NRas amplicon 1	GGTTGGGAGAGATTCAGTTGCT
Fwd NRas amplicon 2	GGGACAAACCAGATAGGCAGAA
Rev NRas amplicon 2	CCCAAAGCACTGACATTCCAG
Fwd NRas amplicon 3	GGCTAATCTCAAACTCCTGGGTT
Rev NRas amplicon 3	GGTCATTGCCAGGAATAGGGTAT
Fwd NRas Seq4	CCCAGCCTGTTGTTAGGCATTT
Rev NRas Seq2r	GGCTGAGGCAGGAGAATCACTT

qPCR primers:

Name:	Sequence:
qRTPCR CRLF2 F	CCTTCTCCAGGAAGGTCACA
qRTPCR CRLLF2 R	GTCCCATTCCTGATGGAGAA
qRTPCR JAK2 F	CGGATAGATCACATAAAACTTCTGC
qRTPCR JAK2 R	TGCCAGATCCCTGTGGATA
mouse GAPDH qRT PCR fwd	GGTGCTGAGTATGTCGTGGA
mouse GAPDH qRT PCRrev	CGGAGATGATGACCCTTTTG

Supplementary-Tab.S3) List of oligonucleotides used to establish the mutation status of key genes involved in the analyzed pathways in the DS-ALL patients. Forward and reverse strand oligonucleotides were used to amplify genomic regions of interests (named Amp) in PCR and all primers were then used in Sanger sequencing on produced PCR amplicons. DNA of previously(3) whole-exome-sequenced samples was used as control for both wt and mutant sequence detection.

Supplementary Fig.S1

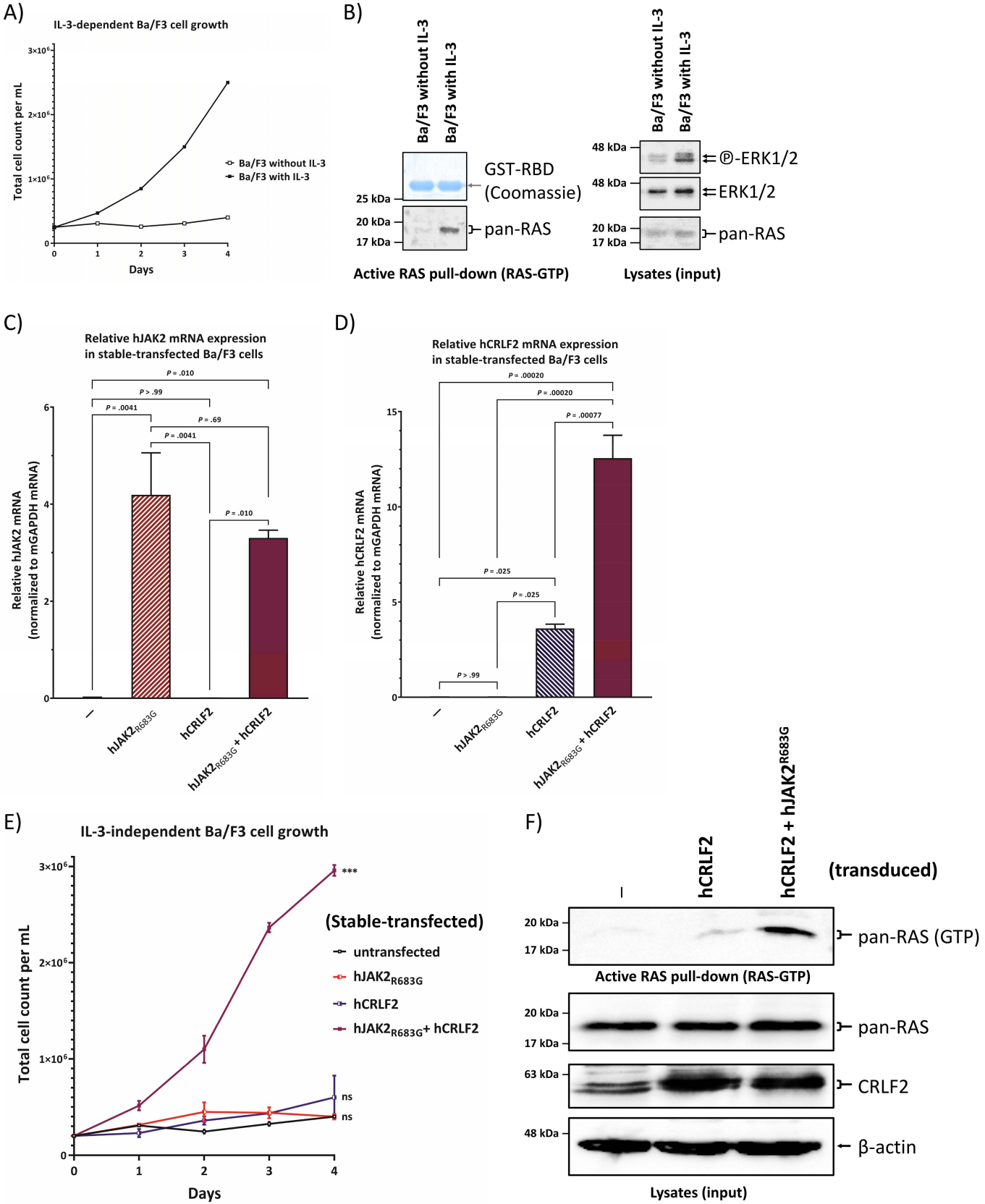

Supplementary-Fig.S1) IL-3 induces wtRAS activity and cell growth in murine pro B cells, but can be substituted by stable overexpression of constitutively active JAK2 and CRLF2. (A) Cell count of Ba/F3 cells (untransfected) over time. Cells were either cultured with 10 ng/mL IL-3 or without.

(B) Ba/F3 cells were cultured in 10 ng/mL IL-3. 17 hrs before lysis, the culture medium was changed to medium containing either 10 ng/mL IL-3 or no IL-3. A RAS-pull-down assay was performed. Lysates of pull-down and input were loaded on separate SDS-PAGE gels followed by Western blotting. Before Western blotting, the top part of the gel loaded with the RAS-GTP pull-down samples was stained with Coomassie dye to visualize the GST-RBD to ensure pull-down samples were loaded equally. To assess the total protein and phosphorylated protein amounts on the same PVDF-membrane, membranes were stripped and reprobed with new antibodies.

(C&D) Ba/F3 cells were stably transfected with hJAK2$_{R683G}$, hCRLF2, or both constructs together. Quantification of qPCR results for human JAK2 mRNA expression (A) and human CRLF2 mRNA expression (B) for the stably transfected Ba/F3 cell lines. All gene expression levels were normalized to murine GAPDH expression. Error bars are SD and *P*-values were determined in one-way ANOVA and post-hoc Bonferroni multiple comparison.

(E) Only the co-expression of human CRLF2 and a constitutively active JAK2$_{R683G}$ mutant construct enabled IL3-independent growth of Ba/F3 cells. The expression of either hCRLF2 or hJAK2$_{R683G}$ alone is not sufficient to promote cell growth over the course of 4 days. Data shown reproduced the experiments already published by Yoda et al.(23) to ensure that the cellular model recreated in our laboratory behaves the same and as evidence of the correlation with the state of RAS activation in these cells (Fig.1). Error bars are SD and *P*-values from a one-way ANOVA with post-hoc Bonferroni multiple comparison for the last timepoint are symbolized as asterisks (***: $P < 0.001$) or ns ($P > 0.05$).

(F) Ba/F3 cells were stably transduced (Lentiviral) with hCRLF2 alone, or followed by hJAK2$_{R683G}$. This second set of Ba/F3 lines was generated independently of the transfected lines used in (A-E) and Fig.1. All cells were then starved from IL-3 and cells were lysed. Each cell lysate was split up for analysis in RAS-GTP pull-down assay and for total proteins. An SDS-PAGE followed by WB was performed.

Supplementary Fig.S2

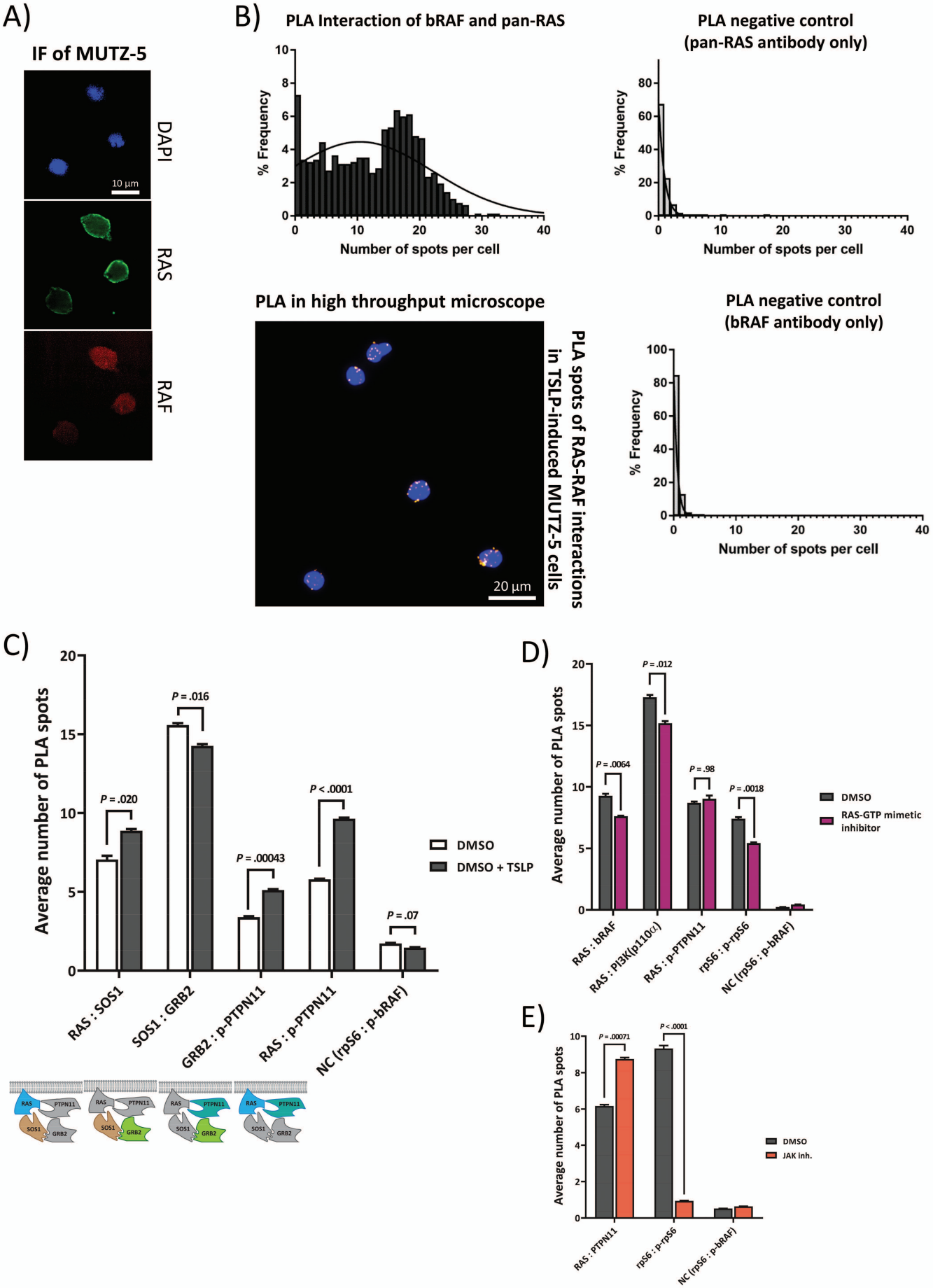

Supplementary-Fig.S2) CRLF2-signaling promotes direct protein-protein binding (quantitated by proximity ligation assays) of multiple components involved in RAS activation in the absence of RAS mutations in human Philadelphia-like (rearranged CRLF2, JAK2$_{R683G}$) B-ALL cells. (A) MUTZ-5 cells were PFA-fixed, permeabilized, and stained with DAPI. Primary antibodies against either pan-RAS or bRAF were used. Secondary antibodies specific to the respective primary antibody species labeled with either Alexa-488 (green) or Alexa-594 (red) were used to visualize the spatial organization of RAS (mostly plasma membrane) and RAF (mostly cytosolic) proteins in confocal microscopy.

(B) Direct interaction between individual RAS proteins and the MAPK pathway protein bRAF was monitored via proximity ligation assay (PLA) in high-throughput microscopy. MUTZ-5 cells were induced with 20 ng/mL TSLP for 5 min. After blocking, antibodies against Pan-RAS and bRAF were used in conjunction with PLA rabbit and mouse probes to allow specific readout of RAS binding to bRAF proteins in single cells in a high-throughput manner. Fluorescent microscope image shows the PLA spots in DAPI-stained cells. Histograms show the distribution of the number of spots in all cells, negative assay controls only received one of the antibodies (PLA for two non-interacting antigens showed higher levels of spots than the assay control, but remained at background levels, not shown). A minimum of 600 cells were analyzed per sample. Non-linear Gaussian fitting curves were plotted.

(C) Direct interaction between protein pairs involved in RAS activation (see cartoon below the graph) was monitored via PLA in high-throughput microscopy. MUTZ-5 cells were either not induced or induced with 20 ng/mL TSLP for 10 min. Cells were fixed and permeabilized in a 96 well plate. After blocking, the indicated antibody pairs were used in conjunction with PLA rabbit and mouse probes to allow the amplification and staining of interaction-specific PLA spots. The negative control (NC) samples used antibodies for two cytosolic proteins (rpS6 and phosphorylated bRAF) that were not expected to directly interact. At least 1900 cells per condition were analyzed in a high-throughput manner. The bar graph shows the averages of 3 technical replicates. Error bars are SD and *P*-values shown are Student's T-test after Bonferroni correction for sequential multiple comparison for all uninduced vs TSLP-induced pairs.

(D) Direct interaction between protein pairs involved in RAS activation and the binding between RAS to RAS effectors was monitored via PLA in high-throughput microscopy. MUTZ-5 cells treated with 20 ng/mL TSLP were pre-treated with either DMSO or the RAS-GTP mimetic inhibitor Rigosertib (30 µM) for 1.5 hrs. Cells were fixed and permeabilized in a 96 well plate. After blocking, the indicated antibody pairs were used in conjunction with PLA rabbit and mouse probes to allow the amplification and staining of interaction-specific PLA spots. The negative control (NC) samples used antibodies for two cytosolic proteins (rpS6 and phosphorylated bRAF) that were not expected to directly interact. At least 700 cells per condition were analyzed in a high-throughput manner. The bar graph shows the averages of 3 technical replicates. Error bars are SD and *P*-values shown are Student's T-test after Bonferroni correction for sequential multiple comparison for all DMSO vs Rigosertib pairs.

(E) Direct interaction between protein pairs between RAS and PTPN11 was measured via PLA in high-throughput microscopy. MUTZ-5 cells treated with 20 ng/mL TSLP were pre-treated with either DMSO or 5 µM Ruxolitinib (JAK inh.) for 1.5 hrs. Cells were handled like in (D). The condition using antibodies for rpS6 and phosphorylated rpS6 verified that the JAK inhibitor was effective in this experiment. At least 20,000 cells per condition were analyzed in a high-throughput manner. The bar graph shows the averages of 3 technical replicates. Error bars are SD and *P*-values shown are Student's T-test after Bonferroni correction for sequential multiple comparison for all DMSO vs Ruxolitinib pairs.

Supplementary Fig.S3

A)

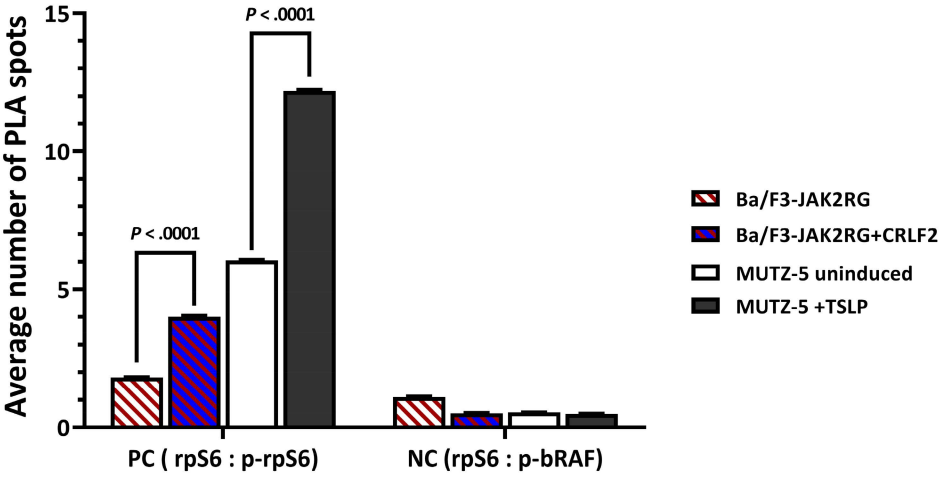

B)

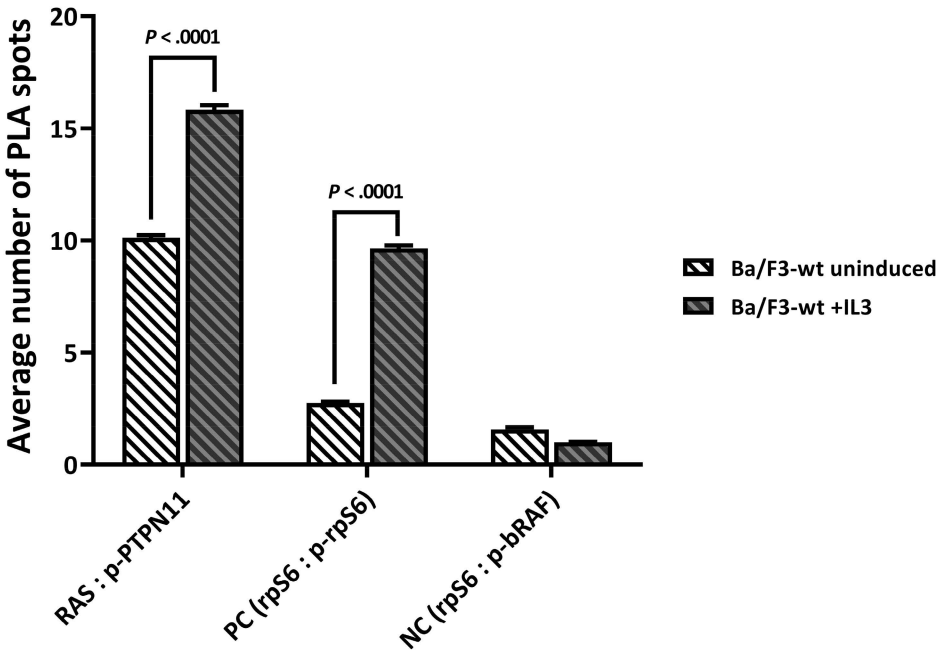

Supplementary-Fig.S3) PLA detects rpS6-phoshporylation and interaction between RAS and p-PTPN11 pattern in Ba/F3 lines comparable to MUTZ-5 cells.

(A) Activation of PI3K/mTOR downstream target rpS6 protein was monitored via PLA in high-throughput microscopy. Ba/F3 cell lines were IL-3 starved for 17 hrs. MUTZ-5 cells were either not induced or induced with 20 ng/mL TSLP for 10 min. Cells were fixed and permeabilized in a 96 well plate. After blocking, antibodies against phosphorylated rpS6 and total rpS6 were used in conjunction with PLA rabbit and mouse probes to allow specific readout of rpS6 activation in single cells in a high-throughput manner. At least 10.000 cells were analyzed per sample. The graph summarizes the average PLA spot counts of 3 technical replicates. Error bars are SD and *P*-values were determined in one-way ANOVA and post-hoc Bonferroni multiple comparison.

(B) Ba/F3 cells were cultured in 10 ng/mL IL-3. 17 hrs before lysis, the culture medium was changed to medium containing either 10 ng/mL IL-3 or no IL-3. PLA protocol was performed like in (A). Direct interaction between RAS and phosphor-PTPN11 was measured via PLA in high-throughput microscopy. At least 2.500 cells were analyzed per sample. The graph summarizes the average PLA spot counts of 3 technical replicates. Error bars are SD and *P*-values were determined in one-way ANOVA and post-hoc Bonferroni multiple comparison.

Supplementary-Fig.S4

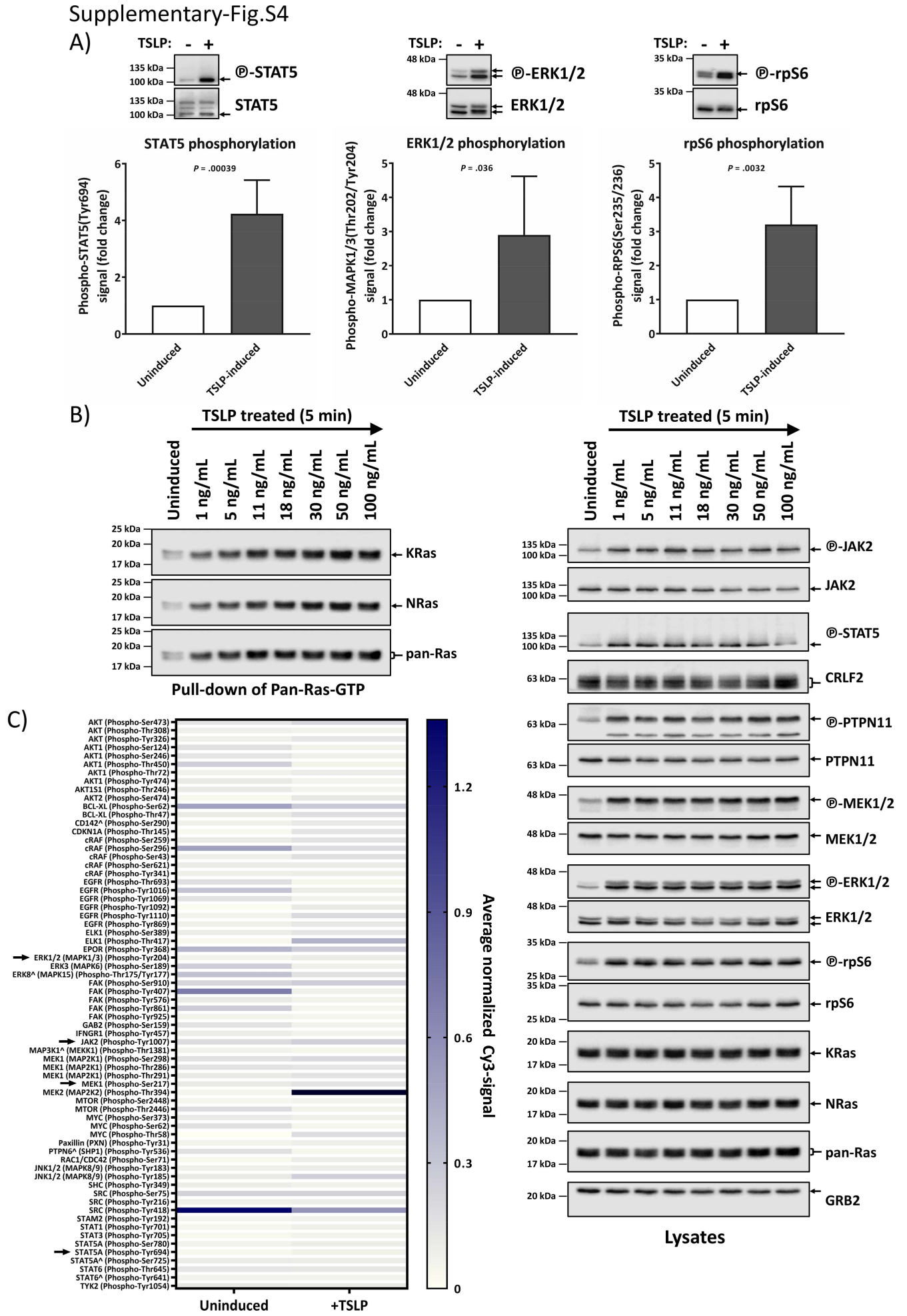

Supplementary-Fig.S4) TSLP-induction actives STAT and PI3K/mTOR signaling in Ph-like B ALL cells. Titration of TSLP concentration in Ph-like B ALL cells. (A) Extension of Fig.2A. MUTZ-5 cells (Human Ph-like B-ALL cells bearing CRLF2-rearranged and spontaneous JAK2R683G mutation) were stimulated (or not) with 20 ng/mL human TSLP for 10 min before cell lysis. Lysates were loaded on an SDS-PAGE gel followed by Western blotting. To assess the total protein and phosphorylated protein amounts on the same PVDF-membrane, membranes were stripped and reprobed with new antibodies. The experiment was repeated 5 times independently and the graphs show the quantification for active STAT5 (phosphorylated STAT5), active ERK1/2 (phosphorylated ERK1/2) and active RPS6 (phosphorylated RPS6). Representative Western blots above the respective graph show the phosphorylated protein form and the total expression of each protein.
(B) Effect of TSLP concentration titration. MUTZ-5 cells were incubated with the indicated amounts of TSLP (0 ng/mL to 100 ng/mL) for 5 min and then the cells were lysed on ice. Each cell lysate was split up for analysis in RAS-GTP pull-down assay and for total protein signal. RAS-GTP pull-down and lysate samples were loaded on separate gels. An SDS-PAGE followed by Western blotting was performed. To assess the total protein and phosphorylated protein amounts on the same PVDF-membrane, membranes were stripped and reprobed with new antibodies. Left-hand side blots show the RAS-GTP pull-down while the right-hand side blots show whole cell lysates of the same samples. Antibody-targets are labeled on the right side of each image with black arrows indicating the respective protein band.
(C) Whole, non-denatured lysate from uninduced or TSLP-induced (20 ng/mL, 10 min) MUTZ-5 cells was subjected to an antibody-microarray. Binding of Cy3-labeled, endogenous proteins was measured. 6 spots per antibody were averaged and normalized to the Cy3-control present on each microarray slide. To exclude changes that are due to epitope-obstruction from bound protein partners, the signal for phosphorylation-site-specific antibodies was normalized to the signal from each corresponding total antibody raised against the same (unphosphorylated) peptide sequence (for phosphorylation-sites marked with ^, no total peptide counterpart was contained on the microarray-slide). Changes in phosphorylation that originated completely from epitope-availability were disregarded from the analysis altogether. BSA-spots (empty) were used to set and subtract background signal. For analysis, minimum signal threshold was set to 3% signal strength of the Cy3-normalization control. Heatmap shows the signal for all normalized phosphorylation-sites on the antibody microarray that passed the mentioned criteria (68/97). Black arrows indicate phosphorylation-sites that were also investigated via Western blot in this work.

Supplementary-Fig.S5

A)

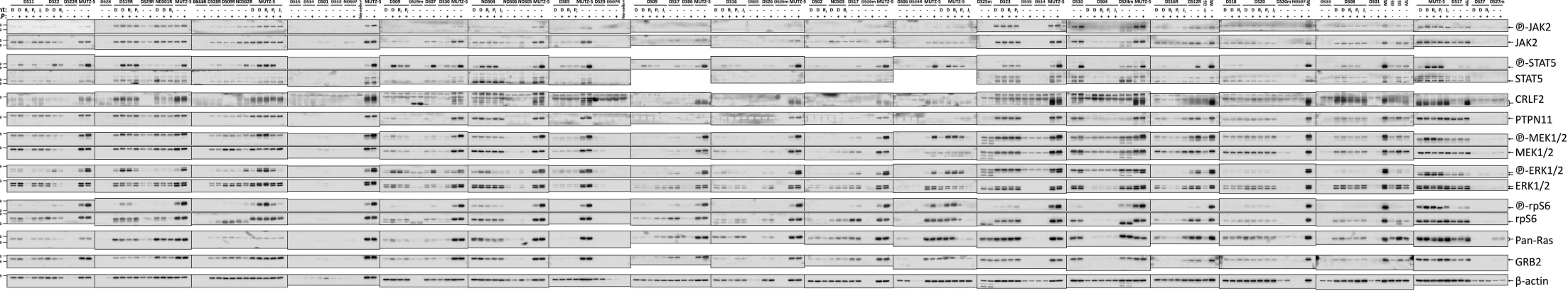

B)

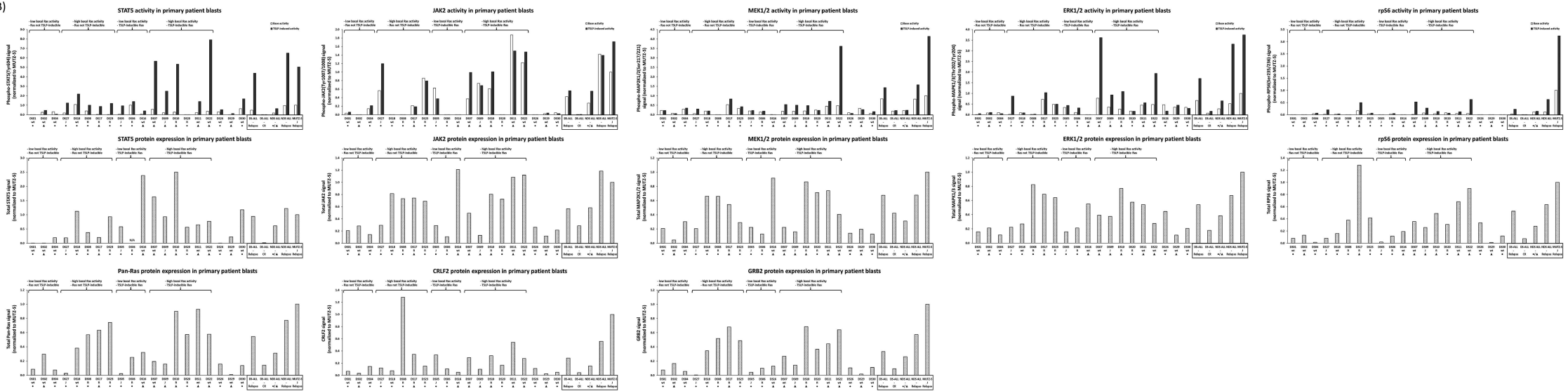

Supplementary-Fig.S5) Western blots for all analyzed patient samples and the resulting quantified data for the sub-stratification of DS-ALL by PCA. (A) Primary samples of DS-ALL patients at presentation, relapse, or remission, as well as MUTZ-5 cells, were thawed and cells were gently recovered in 9 mL RPMI1640 (Cat.#11-875-119; Life Technologies, Carlsbad, US) containing 20% characterized fetal bovine serum (FBS; Cat.#SH30071.03; GE Healthcare, Chicago, US), 20 U/mL Benzonase (Cat.#70746; EMD Millipore), 2 mM L-Glutamine (Cat.#25030081 Life Technologies), and 100 U/mL Penicillin-Streptomycin (Cat.#15140122, Life Technologies). Cells were resuspended in 5 mL fresh medium without Benzonase. Cells were counted using the automated cell-counter NucleoCounter NC-250 (ChemoMetec, Allerod, DK) and viability was assessed via staining with Solution18 (Cat.#910-3018, ChemoMetec). Cells were seeded at 1.5×10^6 cells/mL density in IMDM-complete (IMDM (Cat.#12440053; Life Technologies) with 10% FBS, 2 mM L-Glutamine, 100 U/mL Penicillin-Streptomycin, 200 µg/mL apo-Transferrin (Cat.#11096-37-0; Santa Cruz Biotechnlogy), 0.1% 2-Mercaptoethanol (Cat.#21985023; Life Technologies), 1 µg/mL insulin (Cat.#11061-68-0; Sigma-Aldrich), 10 ng/mL IL-3 (Cat.#200-03; Peprotech, Rocky Hill, US) and 10 ng/mL IL-7 (Cat.#200-07; Peprotech). After 24 hrs, surviving cells were reseeded at 1×10^6 viable cells/mL density in IMDM-complete. After 16 hrs the cells were reseeded at 1×10^6 cells/mL density in 2 mL OptiMEM (Cat.#31985070; Life Technologies) with 5% FBS. After 3 hrs, cells were either left uninduced or induced with 20 ng/mL TSLP (Cat.#1398-TS; R&D Systems) for 10 min at 37 °C before lysis. Where indicated, patient cells were pre-treated during the 3 hrs incubation with DMSO (D), RAS-inhibitor (R_i), PI3K/mTOR inhibitor (P_i), or JAK inhibitor (J_i). For Western blot analysis, cells were lysed and loaded on an SDS-PAGE gel. To assess the total protein and phosphorylated protein amounts on the same PVDF-membrane, membranes were stripped and reprobed with new antibodies. Antibody-targets are labeled on the right side of each image with black arrows indicating the respective protein band. As all lanes are shown for all gels in every specific staining, sample names that are crossed-out were either not part of the analysis, or showed too low loading in all expressed proteins to be used for any quantification. For blot imaging, each PVDF membrane piece was separately incubated with chemiluminescent HRP substrate solution (Cat.#WBKLS0500; EMD Millipore) for 2 min and imaged via the auto-exposure function of the ChemiDoc MP imaging system (Bio-Rad Laboratories) within 100 sec exposure time to standardize the sensitive but otherwise semi-quantifiable enzymatic-based detection.

(B) Quantification of Western blot signals in (A) for all DS-ALL samples at presentation as well as Non-DS (NDS) at presentation, DS complete remission (CR), and DS/NDS at relapse (boxed group at right end of each bar graph). For quantification, the raw images were analyzed in Fiji 1.52n (ImageJ, National Institutes of Health, US) using the subtract background process followed by measuring the signal peaks in the Gel Analyzer function. Microsoft Excel software was used to adjust all samples to either their loading control (β-actin) or the quantitative total protein fluorescent signal (AzureRed, Cat.#AC2124; Azure Biosystems, Dublin, US). All samples' protein activity and total protein signals were normalized to the respective signal from the uninduced MUTZ-5 samples loaded as reference on each membrane. 81% of all analyzed samples showed sufficient signal in loading control and tested proteins to be appropriate for further normalization and analysis. The quantified phosphorylated protein signals were additionally adjusted to the respective quantified total protein loading. Brackets on top indicate the groups of the four RAS activity patterns presented in Fig.3C. White and black bar graphs show the basal and TSLP-induced activation levels, respectively, of STAT5, JAK2, MEK1/2, ERK1/2, and RPS6 while the dotted grey bar graphs show the respective total protein expression levels. Outcome of leukemia is symbolized as circle for good outcome and triangle for poor outcome; RAS pathway mutations (R), JAK2 mutations (J), or neither (wt) are listed for each DS-ALL patient.

Supplementary Fig.S6

A)

Field	PC1	PC2	PC3
Dispers	0.385601	0.049523	0.081659
Overall	0.385601	0.435125	0.516784
Pan-Ras basal activity	0.214594	**0.485179**	0.048106
Pan-Ras activity with TSLP	0.227889	**0.474698**	0.041787
JAK2 basal activity	0.237394	-0.24357	-0.40745
JAK2 activity with TSLP	0.297418	-0.1813	-0.35807
STAT5 basal activity	0.172951	-0.20932	0.065401
STAT5 activity with TSLP	**0.322827**	0.163583	-0.23887
MEK basal activity	0.311386	0.309735	0.091045
MEK activity with TSLP	**0.351922**	0.1494	0.076544
ERK basal activity	0.281839	-0.06334	-0.04313
ERK activity with TSLP	0.287373	-0.22426	-0.26412
S6 basal activity	0.226173	-0.24303	**0.609553**
S6 activity with TSLP	0.280702	-0.32844	**0.303667**
CRLF2 protein expression	0.250139	-0.18761	0.007298

D)

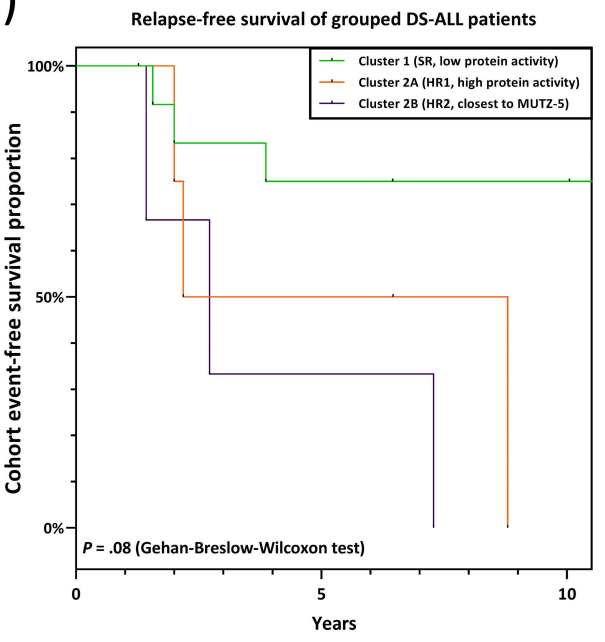

B)

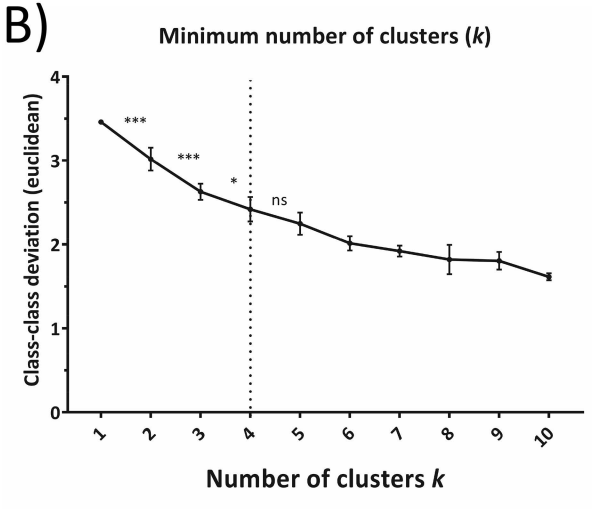

E)

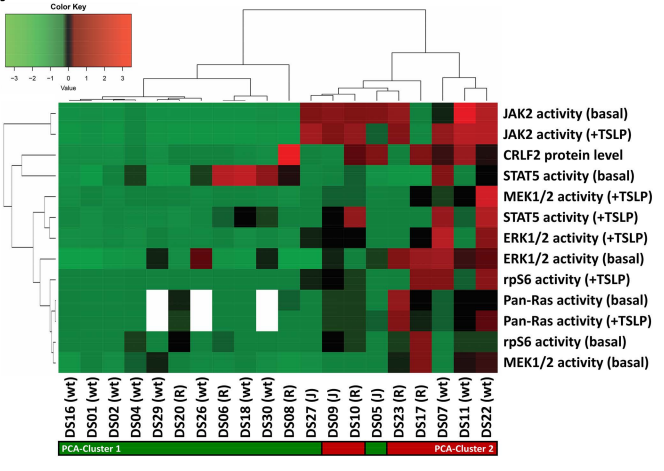

C)

	N =	DS patients with good outcome	DS patients with poor outcome	DS relapse samples	DS Complete remission sample	DS Remission sample with imminent relapse	NDS patients with good outcome	NDS patients with poor outcome	NDS relapse samples	NDS (Ph-like) relapse cell line (MUTZ-5)
Total	**38**	**11**	**9**	**7**	**2**	**2**	**3**	**1**	**2**	**1**
Cluster 1	19	10	3	1	2	0	2	1	0	0
Cluster 2	15	1	6	4	0	2	1	0	1	0
Cluster 3	3	0	0	1	0	0	0	0	1	1
Cluster 4	1	0	0	1	0	0	0	0	0	0

Supplementary-Fig.S6) PCA statistics and PCA cluster counts on primary DS-ALL and NDS-ALL blast cells. (A) Basal and induced activation levels for RAS, JAK2, STAT5, MEK, ERK, and RPS6, as well as CRLF2 protein expression, were fed into ViDaExpert v1.2 to calculate 3 main principal components (PC1-3) in a PCA analysis. Numbers in bold highlight the categories (field) with the greatest correlation within each PC.
(B) Euclidean *k*-means clustering was performed in ViDaExpert v1.2 on the PCA analysis in (A) for $k = 1$ to 10 (6 times each). In order to identify the minimal number of clusters needed for the grouping analysis, class-class deviation was averaged for each k (error bars are SD). Class-class deviation from sequential, increasing number of clusters stopped being statistically significant at $k = 4$ (doted line); * ($P < .05$), *** ($P < .001$), ns (not significant).
(C) Number of samples within each of the four clusters identified in the *k*-means clustering of the PCA data represented in Fig.4A. Count of the different patient sample categories for each cluster.
(D) Kaplan–Meier curves of DS-ALL patients. For this comparison, and cluster 2 (HR = high risk, see Fig.5) was split into two subclusters 2A and 2B (cluster 2B contains the DS-ALL presentation samples that grouped closest to MUTZ-5 in the PCA-based cluster analysis in Fig.5A; DS07, DS11, and DS22). Median survival for subcluster 2A was 5.49 and for 2B 2.72.
(E) Unsupervised hierarchical clustering of all analyzed DS-ALL presentation samples for all 6 measured protein activities (basal and TSLP-induced) as well as CRLF2 protein expression. The clustering results were similar to the independent *K*-means clustering (indicated by the red/green colored bar underneath the sample IDs) of the PCA (Fig.4A), with 90% (18/20) of the samples clustered in the same groups by both methods. Presence of RAS pathway mutations (R), JAK2 mutations (J), or neither (wt) is indicated (no single patient in this cohort was found to have both RAS and JAK2 mutations).

Supplementary-Fig.S7

A) DS-ALL (protein levels)

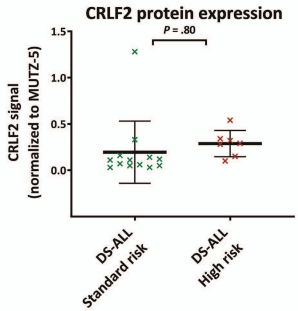

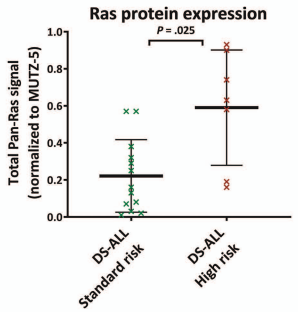

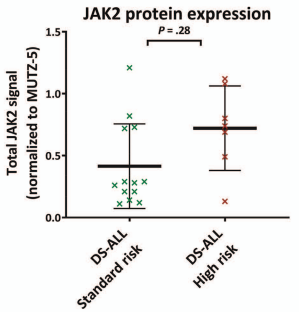

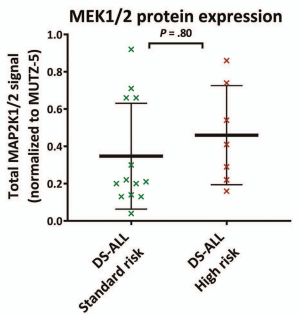

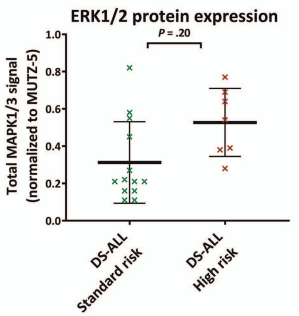

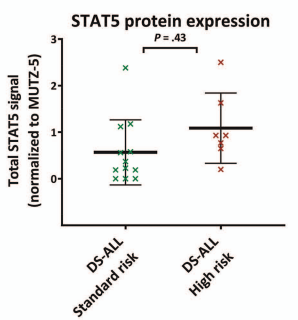

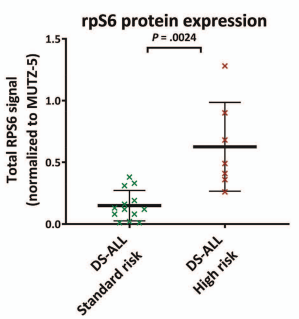

B) non-DS ALL (mRNA levels)

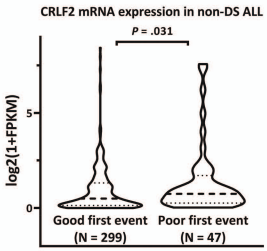

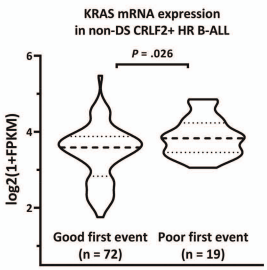

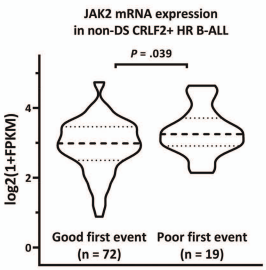

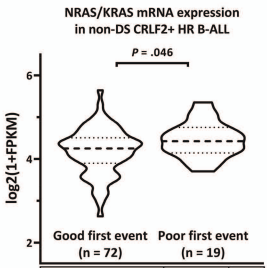

Cox proportional hazards regression variable	Hazard ratio (95% CI)	P
NRAS/KRAS average mRNA expression (in.=1)	3.19 (1.04-9.81)	.040
Sex *Male vs Female*	0.56 (0.19-1.64)	.29
NCI *High vs standard risk*	4.32 (1.30-14.31)	.017
BCR-ABL1 *Positive vs negative*	0.82 (0.18-3.83)	.80

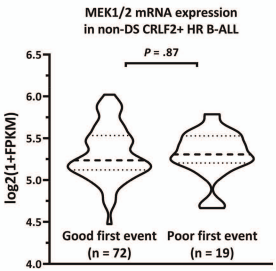

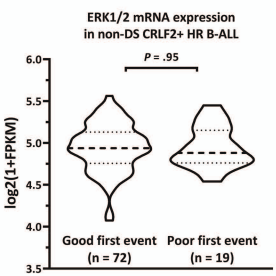

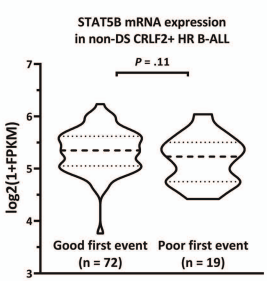

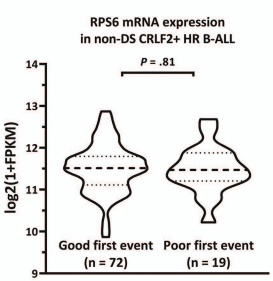

Supplementary-Fig.S7) Disease outcome-correlations with expression levels of components used in RAS-pathway sub-stratification. Protein levels in DS-ALL (A) and mRNA levels in non-DS childhood ALL (MS2003/2010 cohorts) (B)

(A) Average protein expressions of analyzed key pathway components are compared between the SR group (DS-ALL patients at diagnosis in PCA cluster 1) and the HR group (DS-ALL patients at diagnosis in PCA cluster 2) identified in Fig.4. All error bars are SD. *P*-values shown are Student's T-test after Bonferroni correction for sequential multiple comparison for all proteins analyzed.

(B) Violin blots of the mRNA levels based on whole transcriptome RNAseq of the MS2003/2010 cohorts at diagnosis are shown for gene(s) equivalents to proteins analyzed in the DS-ALL cohort. The dashed line represents the median while the dotted lines above and below the median mark the respective quartiles. *CRLF2* was analyzed for outcome on the total non-DS ALL cohort (N = 346). Subsequently, all other shown mRNA expression levels (*KRAS*, *KRAS*&*NRAS* combined, *STAT5B*, *JAK2*, *MEK1*&*2* combined, *ERK1*&*2* combined, *RPS6*) were compared in B-ALL samples positive for *CRLF2*-mRNA expression (log2(1+FPKM) > 0.7) for the first event outcome. Poor first event for the MS2003/2010 cohort was defined as resistance, death or relapse; good first event means complete remission. Subtypes that are known to favor a good outcome were excluded from the analysis (ETV6-RUNX1, hyperdiploid, DUX4 and ZNF384). The resulting n=91 subcohort harbored 13 *RAS* mutations (4/19 poor outcome samples) and 6 *JAK*2 mutations (0/19 poor outcome patients) but never both together. For *KRAS*&*NRAS* combined, table details results of Cox proportional hazards regression. All error bars are SD. *P*-values shown were calculated using Student's T-test. Bonferroni-*P*-values adjusted for sequential multiple comparison were not ≤ α (0.05) and are listed in Supplementary-Tab.S2.

Supplementary-Fig.S8

A) Non-DS ALL mRNA levels (full MS2003/2010 cohort)

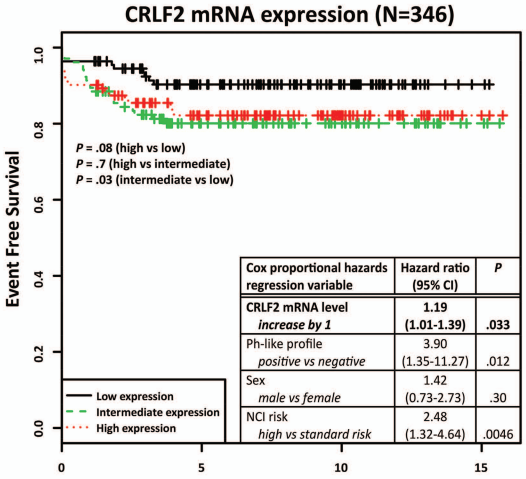

Cox proportional hazards regression variable	Hazard ratio (95% CI)	P
CRLF2 mRNA level *increase by 1*	**1.19 (1.01-1.39)**	**.033**
Ph-like profile *positive vs negative*	3.90 (1.35-11.27)	.012
Sex *male vs female*	1.42 (0.73-2.73)	.30
NCI risk *high vs standard risk*	2.48 (1.32-4.64)	.0046

Number at risk:

Low expression	111	107	98	89	83	71	65	58	47	40	33	24	14	6	4	2
Interm. expression	104	94	84	78	63	55	51	44	37	30	26	16	15	10	5	3
High expression	112	101	92	84	76	70	66	57	47	44	31	23	18	12	4	2

B) Non-DS ALL mRNA levels (CRLF2+, high-risk genetics subcohort)

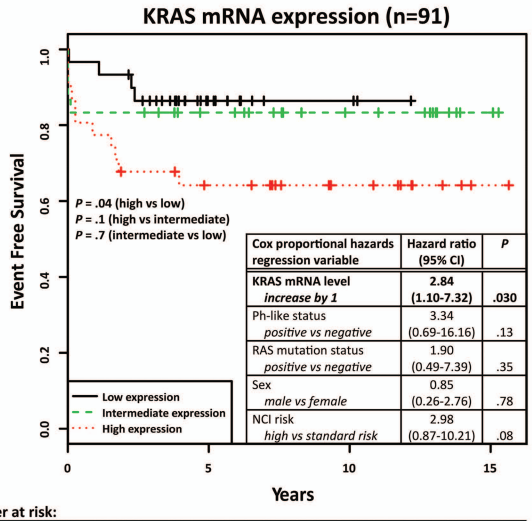

Cox proportional hazards regression variable	Hazard ratio (95% CI)	P
KRAS mRNA level *increase by 1*	**2.84 (1.10-7.32)**	**.030**
Ph-like status *positive vs negative*	3.34 (0.69-16.16)	.13
RAS mutation status *positive vs negative*	1.90 (0.49-7.39)	.35
Sex *male vs female*	0.85 (0.26-2.76)	.78
NCI risk *high vs standard risk*	2.98 (0.87-10.21)	.08

Number at risk:

Low expression	30	29	28	23	17	11	7	3	3	3	3	1	1	0	0	0
Interm. expression	30	25	25	24	20	19	18	16	13	12	11	11	10	7	2	2
High expression	31	24	20	20	18	17	17	16	12	12	9	8	6	4	2	1

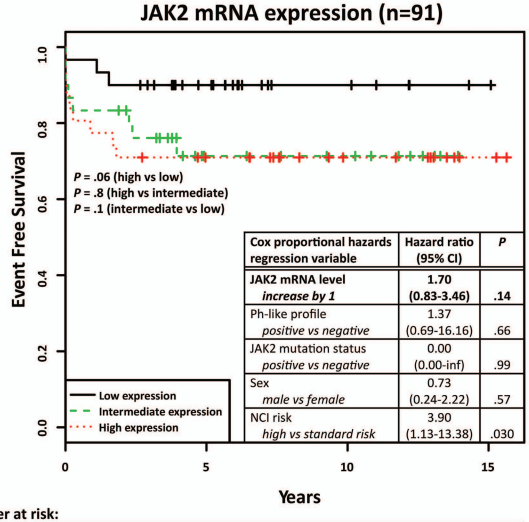

Cox proportional hazards regression variable	Hazard ratio (95% CI)	P
JAK2 mRNA level *increase by 1*	**1.70 (0.83-3.46)**	**.14**
Ph-like profile *positive vs negative*	1.37 (0.69-16.16)	.66
JAK2 mutation status *positive vs negative*	0.00 (0.00-inf)	.99
Sex *male vs female*	0.73 (0.24-2.22)	.57
NCI risk *high vs standard risk*	3.90 (1.13-13.38)	.030

Number at risk:

Low expression	30	29	27	25	19	17	12	8	6	6	6	5	4	2	2	1
Interm. expression	30	25	24	21	15	11	11	10	9	9	8	6	5	3	0	0
High expression	31	24	22	21	21	19	19	17	13	12	9	9	8	6	2	2

Supplementary-Fig.S8) Disease outcome-correlations and multivariate analysis for mRNA expression levels in non-DS childhood ALL (MS2003/2010 cohorts) of key components emanating from RAS-pathway sub-stratification in primary samples at diagnosis (A) Kaplan–Meier estimates of event-free survival of all non-DS ALL patients (N=346) according to *CRLF2*-mRNA expression. Low, intermediate, and high curves for *CRLF2*-mRNA expression levels (overall P = .09) each represent one third of the cohort (bottom, mid, and top third, respectively). Table within the graph shows multivariate analysis using Cox proportional-hazards model for *CRLF2*-mRNA levels together with the prognostic factors Ph-like status, sex, and NCI risk groups. Patient numbers at risk for each year are given in the table below the survival curve.
(B) Subsequently, all other mRNA expression levels (*KRAS*, JAK2, *KRAS*&*NRAS* combined, *STAT5B*, *MEK1*&*2* combined, *ERK1*&*2* combined, *RPS6*) were compared in B-ALL samples positive for *CRLF2*-mRNA expression (log2(1+FPKM) > 0.7) for the first event outcome (Supplementary-Fig.S7B). Subtypes that are known to favor a good outcome were excluded from the analysis (ETV6-RUNX1, hyperdiploid, TCF3-PBX1, DUX4, and ZNF384). The resulting n=91 subcohort harbored 13 *RAS* mutations (4/19 poor outcome samples) and 6 *JAK2* mutations (0/19 poor outcome patients), but never both together. Kaplan–Meier curves show estimates of event-free survival of the HR non-DS ALL subcohort (n=91) grouped by *RAS* (overall P = .08) or *JAK2*-mRNA (overall P = .2) expression levels. The tables within the graphs show multivariate analysis using Cox proportional-hazards model for either *RAS*-mRNA or *JAK2*-mRNA levels respectively, together with *KRAS/NRAS* or *JAK2* activating mutations respectively, and the prognostic factors Ph-like status, sex, and NCI risk groups.

Supplementary-Fig.S9

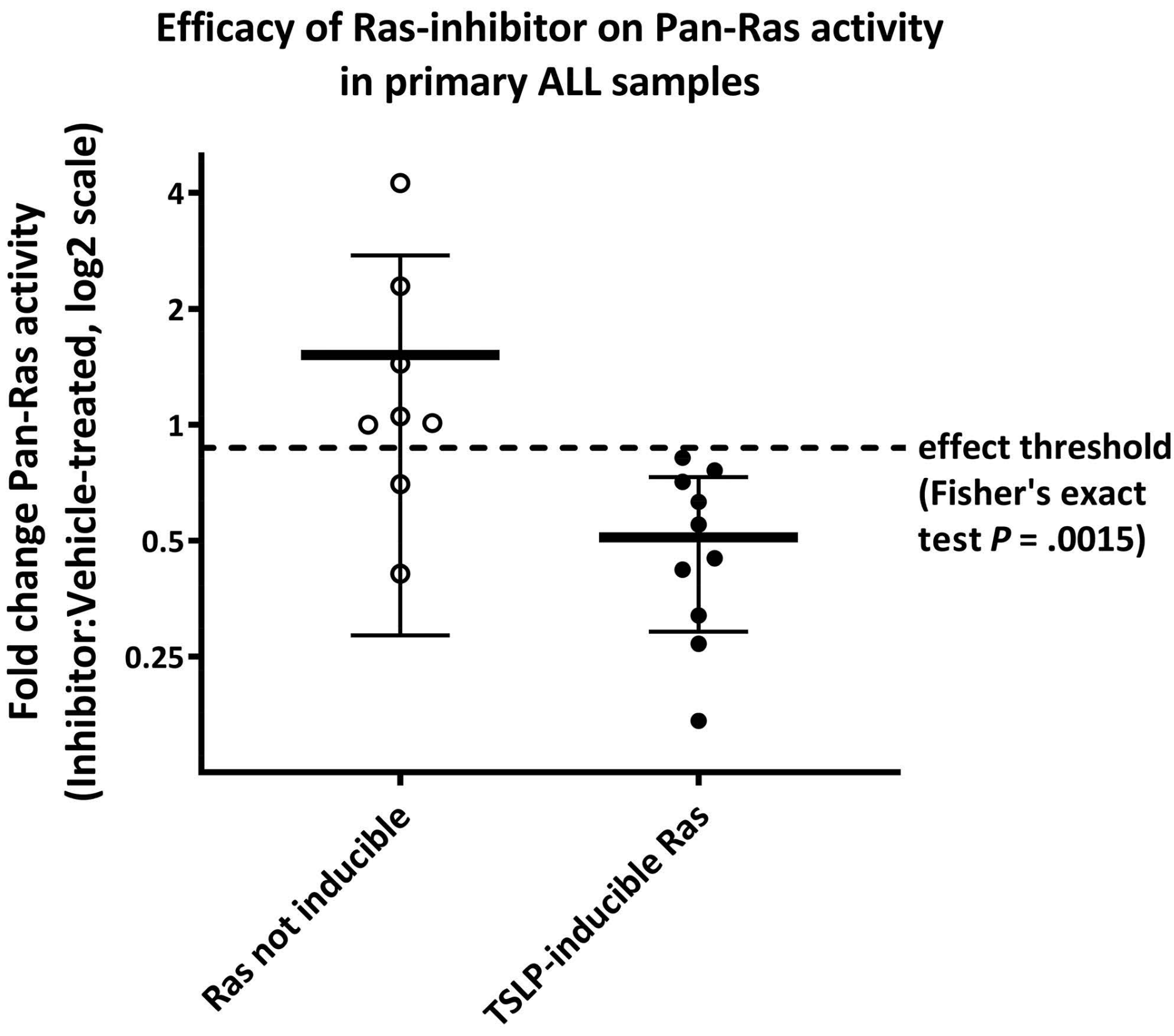

Supplementary-Fig.S9) Efficacy of the RAS inhibitor stratified by patient sample inducibility. Primary presentation samples of DS-ALL and non-DS ALL patients (characterized in Supplementary-Tab.S1) were cultured for 2 days (see Supplementary-Fig.S5A for details). Samples with sufficient cell count were treated with either 0.5% DMSO (vehicle control) or 50 µM Salirasib (indirect pan-RAS inh.) for 3 hrs after which the cells were induced for 10 min with 20 ng/mL TSLP in serum-reduced medium. Cells were lysed and a RAS-GTP ELISA pull-down assay was performed. The efficacy of the RAS inhibitor (expressed as RAS activity of inhibitor-treated divided by RAS activity of DMSO-treated) on ELISA-measured RAS activity in patient samples that were defined in Fig.3B as not TSLP-inducible for RAS is compared to those in which RAS activity was inducible by TSLP. If inhibitor treatment reduced the RAS activity by over 10% compared to vehicle-control (dashed line in plot), the sample was tallied as successful RAS blocking. A Fisher's exact test was performed between the groups.